TU Delft Delft University of Technology

Master's Thesis

Mechanical Engineering:
Energy & Process Technology

Influence of rheology on the motility of microorganisms

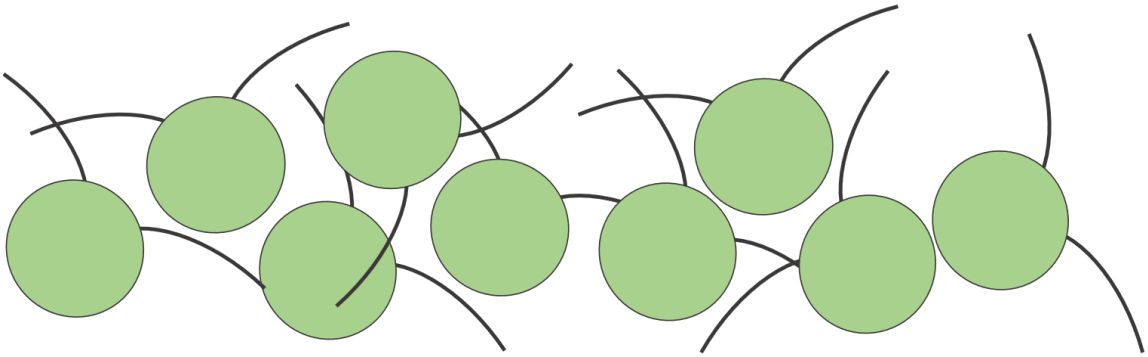

Author:
Stefan Dankelman

Supervisors:
Dr. Daniel Tam
Junaid Mehmood
Bob Mulder

Influence of rheology on the motility of microorganisms

An experimental study on the motility of Chlamydomonas reinhardtii in viscoelastic fluids.

by

Stefan Dankelman

to obtain the degree of:

Master of Science
in Mechanical Engineering

at the **Delft University of Technology**

to be publicly defended on th 27th of July, 2021.

Student number:	4463587	
Thesis committee:	Dr. Daniel Tam	TU Delft
	Dr. Remco Hartkamp	TU Delft
	Dr. Abel-John Buchner	TU Delft
	Ir. Junaid Mehmood	TU Delft

Acknowledgement

Hereby I would like to express my gratitude to all who have contributed to this Master's thesis, whom without I would not have been able to succeed.

Firstly, I would like to express my sincere gratitude to my daily supervisor and mentor Junaid Mehmood. I would like to thank him for the countless long days of introducing me to new topics, teaching me the used protocols in the laboratory and explaining how to perform experiments with microorganisms. Working together on improving the experimental setup and tackling the many problems that arose has been very enjoyable and has taught me very valuable lessons.

I would like to express my appreciation to my supervisor Dr. Daniel Tam, for providing me the opportunity to dive headfirst into a very interesting topic. By getting me out of my comfort zone with this project, I learned a lot, not only about rheology and motility, but I have also grown as a person. His weekly check-ins, useful feedback and words of wisdom helped me to regain motivation whenever needed. I would like to thank him for all the patience and freedom he has given me during my master's thesis.

I would like to thank Koen Muller for allowing me to use the Lagrangian tracking algorithm which he has put so much effort into, and his support and feedback while working with it. I would like to thank Parviz Ghoddoosi Dehnavi for the useful discussions on cell cultures and his help on performing the 2D recordings of the motile cells. I would like to thank Haike Ruijters (Anton Paar), Yavuz Emre Kamış and Bob Mulder for their useful suggestions and discussions on how to tackle the rheological problems of this thesis.

I am grateful to my parents, Jenny and Freek, whom without I would not have been able to succeed. I would like to thank them for the many discussions regarding my thesis and their unconditional support during my master's thesis. I would like to thank my friends, as they made it easier to write this thesis during the COVID-19 pandemic. They provided a healthy balance between working and good distractions by reminding me that implementing breaks is important too. Working from home on a topic that is very challenging might be hard, but less difficult when having the right people around you.

Stefan Dankelman
Delft, July 2021

Abstract

Flagellar locomotion is one of the first forms of locomotion on our planet. Microorganisms use their flagella to reorientate or generate movement in search for nutrients or gradients in light intensity. These microscopic swimmers are able to adapt their swimming gait to the circumstances they encounter. Motile microorganisms such as the *Chlamydomonas reinhardtii* are used as a source of inspiration in biomimetics and used in biological, pharmaceutical and industrial applications to produce for example biofuels or medication. The fluids in which these microscopic cells swim are often of complex rheology, containing macromolecules such as synthetic polymers of proteins, which influences the motile behaviour of these cells. The motile behaviour is mostly studied in a quasi 2D environment which might be different from the behavior in a more natural 3D environment. Therefore, our aim is to analyse the motility of microorganisms in a 3D environment in fluids with different rheological properties.

To gain more insight in the influence of rheology on the motility of microorganisms, the model microorganism *Chlamydomonas reinhardtii* is observed in fluids of various levels of elasticity. An in-house 3D microscopic setup, consisting of 4 LaVision sCMOS cameras, is used to observe the motility of the cells. A Lagrangian tracking algorithm is used to detect and follow many individual motile cells simultaneously. We focused on the velocity of the cells, their helical motions (radius and pitch) which they use to scan their surroundings, and their flagellar beating frequency.

We observed a velocity and pitch independent of the Deborah number, whereas decreasing values for these metrics were found in Newtonian fluids of equal viscosity. The radius of the helical motion showed to be independent of elasticity or viscosity. The beating frequency of the cells shows to be constant in a viscoelastic fluid independent on the viscosity or elasticity, whereas it tends to decrease in Newtonian fluids of increasing viscosity.

Chlamydomonas reinhardtii might have developed a more efficient swimming gait to propel themselves in a viscoelastic fluid compared to a Newtonian fluid, especially in high viscosities. Moreover, we argued that motile microorganisms that are allowed to swim freely in a 3D confinement, show a different motile behaviour than when their motility is constricted by a quasi 2D plane. To validate these findings we recommend to perform experiments both in quasi 2D and 3D, while using the same cell culture.

Keywords: *Rheology, viscoelasticity, flagellar motility, cell kinematics, particle tracking*

Contents

1 | Motivation

The behaviour of microorganisms is determined by their urge to survive. To do so, microscopic cells have developed mechanisms to sense and adjust to changes in their environment to stay viable [1]. One of these mechanisms is their capacity to move to more favourable environments, by exerting mechanical work on the surrounding fluids. For example, the green alga *Chlamydomonas reinhardtii* (*C. reinhardtii*) adjusts its motility and direction by reorientating themselves with respect to unidirectional light, to enhance their ability to photosynthesize [2]. The motility of these kind of microorganisms is an active area of research, as motility plays an important role in various biological processes, such as biofilm formation [3], development of diseases by pathogens [4] and swimming spermatozoa within the female reproductive tract [5, 6].

Besides biological processes, the motility of microorganisms is of interest for industrial applications as well. Within the field of biomimetics, flagellated motile microorganisms have been a source of inspiration for the design of microswimmers [7–9] for applications at low Reynolds number. These microscopic swimmers can be used for targeted drug delivery for biomedical purposes within the human body, or aid in minimally invasive procedures [10]. Motile microorganisms such as *C. reinhardtii* (Figure 1.1), could also aid in manufacturing processes of proteins (antibodies) for pharmaceutical and chemical industries [11, 12] or of biofuels such as hydrogen [13] for the energy sector. Many of the fluids within these environments, such as bioreactors or the human body, contain particles, polymers (synthetic or proteins), and other macromolecules [14, 15], causing non-Newtonian effects and a complex rheology. These properties have influence on the motility of motile microorganism. As flagellated microorganisms adapt their kinematics and behaviour to their local environment [8, 16–19], understanding this adaptation mechanism for different rheological properties can be crucial to the design of more efficient bioreactors or microscopic swimmers.

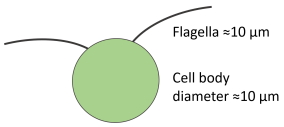

Figure 1.1: Sketch of *Chlamydomonas reinhardtii*.

1.1 Goal & Thesis outline

Motility of microorganisms has mostly been studied in Newtonian fluids using 2D experimental settings [20–23]. However, it has been shown that the motile microorganisms show 3D motile behaviour [24]. Also, due to concentrations of for example synthetic polymers and proteins, the ambient fluid in which the microorganisms find themselves is not always Newtonian [17]. The influence of these complex rheological properties on motility remains a topic which is not fully understood yet. The goal of this master thesis is to experimentally characterise the rheological properties of a fluid containing macromolecules and to create a better understanding of how the rheological properties of fluids influence the motility of *C. reinhardtii* in 3D.

In the first part of the thesis, a literature review on motile microorganisms in Newtonian fluids and viscoelastic fluids is presented. Thereafter, rheological properties of polymer solution are characterized using an Anton Paar Rheometer. We are interested in the elastic properties of viscoelastic fluids and aim to characterise them via the dimensionless Deborah Number $De = \lambda\omega$, where λ is the relaxation time of the fluid and ω the relevant frequency of the proposed experiment. The rheological results found are used in the final part of this thesis, which is to analyse the motility of motile *C. reinhardtii*. The motility and trajectories of these microorganisms in a 2D and a 3D setting are experimentally investigated for Newtonian and viscoelastic fluids with an emphasis on the single cell kinematics.

2 | Motility of motile microorganisms: Literature review

2.1 Introduction into motility

Motility is the ability of a living system to produce mechanical work and move independently [25]. Flagellated motile microorganisms are microscopic cells that have filaments attached to the cell body (see example in Figure 1.1). Flagella, which is Latin for whip, are used for cell-cell recognition during mating [26] or to generate the movement of the cell. Due to the low velocities and small length scales, the movement of these microorganisms is governed by low Reynolds number hydrodynamics. The Reynolds number is defined as the ratio between inertial forces to the viscous forces that act on the fluid element. $\mathrm{Re} = \frac{\rho\, U\, L}{\mu}$, where ρ is the fluid density, U the characteristic velocity, L the length scale, and μ the dynamic viscosity of the fluid. Motile microorganisms interact with fluids at low Reynolds numbers. For example, bi-flagellated puller motile microorganism *C. reinhardtii* interacts with the fluid at Reynolds number of $\mathrm{Re} \approx 10^{-4} - 10^{-3}$ [20–23]. Other examples, such as *spermatozoa* (pusher) at $\mathrm{Re} \approx 10^{-2}$ [27] and *Escherichia coli* (pusher) at $\mathrm{Re} \approx 10^{-5} - 10^{-4}$ [14]. At these low Reynolds numbers, viscous effects dominate and inertial effects are negligible, causing extra limitations on effective methods for locomotion of microorganisms [27]. As this study focuses on motility of microorganisms in Newtonian and viscoelastic fluids, this literature review aims to cover research previously done on these topics.

2.2 Motility in Newtonian fluids

In 1977, Purcell described kinematic reversibility for swimmers in Newtonian fluids [28]. He explains that swimmers cannot achieve a net displacement by exerting a time-reversible motion, indicated as the Scallop Theorem. Scallops are swimmers that deform their body to propel forward (power stroke), and undergo the same exact deformation in reverse to return to their initial configuration (recovery stroke). Kinematic reversibility means that any instantaneous reversal of the forces acting on the body will not change the nature of the fluid flow around it, but simply change the direction of the flow [27]. This makes it is impossible for a microscopic swimmer to generate a net displacement while exhibiting a time-reversible motion, as the displacement forwards during the power stroke would be equal and opposite to the displacement backwards during the recovery stroke. Because of this, motile microorganisms have developed asymmetric power and recovery strokes, to break free from the kinematic reversibility [22].

Microorganisms exist in different configurations. The three morphologies that are considered are pusher (extensile) cells, puller cells (contractile) and neutral swimmers (potential). *Spermatozoa* and *E. coli* are pusher cells that have a flagellum behind the cell

body, exerting forces on the fluid located behind the cell to generate forward movement. *C. reinhardtii* are puller cells that have two flagella on the front of the cell body, pulling fluid located in front of the cells backwards. These puller cells propel themselves in a way that resembles the human breaststroke. This motion contains a power stroke, in which the flagella move backwards and the cell body forward, and a recovery stroke, in which the flagella return to their initial configuration, moving the cell body slightly backwards. If these strokes are performed with both flagella beating synchronously, the cell moves forward. Asynchronous beating of the two flagella, leads to reorientation of the cell body. This is called 'run and tumble' which on average, motile organism do for 70% and 30% of the time, respectively [29]. A third variant of motile microorganisms, the neutral swimmers, are ciliated swimmers, which use hairlike structures on their cell body, called cilia, to propel themselves forward [30].

A very well-studied puller microorganism is *C. reinhardtii*, which is widely used as a model organism for motility research [2]. The mean swimming speed of *C. reinhardtii* in Newtonian fluids is found to be in the range of 10-100 μm/s [20–22], whereas Guasto et al. found a higher mean swimming velocity of 100-200 μm/s [23]. The flagella of the Chlamydomonas beat with a frequency of about 50 Hz [17, 23], resulting in a net displacement between 2 to 4 μm per beating sequence. The motility of *C. reinhardtii* is further characterised by complex 3D dynamics, which has been reported by Crenshaw [24]. This motion consists of a rotating and translating behaviour which forms a helical motion in the trajectories of the cells. The motile microorganisms use this helical motion to scan a large 3D domain for favourable environments, such as areas of high light intensity, nutrients, specific pH levels or temperature. Crenshaw describes these helical trajectories in a more quantified way by its velocity, curvature and torsion [31].

2.3 Motility in viscoelastic fluids

Viscoelastic materials contain both viscous and elastic properties, causing a time dependency when a stress is applied. This time dependency can break down the time reversibility described by Purcell, and opens the door to more swimming gait possibilities [17, 28]. The level of elasticity of a fluid under specific flow conditions is described with the dimensionless Deborah number. This number describes the ratio between the fluid relaxation time, the time the material takes to adjust to an applied stress, and the characteristic time scale of the experiment. For motile microorganisms, the Deborah number is defined as $\mathrm{De} = \lambda\omega$, where λ is the fluid relaxation time and ω the beating frequency of the microorganism.

In the experimental work of Qin et al. [17], puller microorganisms *C. reinhardtii* are observed in a thin film of $\pm 20\mu$m. The film limits the cell motility to a quasi 2D plane, as the film thickness is approximately two cell body diameters. This work focuses on the kinematics of a motile cells in a viscoelastic fluid and compares this to the kinematics in a Newtonian fluid. They found that *C. reinhardtii* cells alter their flagellar swimming gait when submerged in a viscoelastic fluid. Furthermore, they observed differences in motility

of the motile cells. One metric used for comparison was the traveling velocity of the cells. A velocity difference of around 50% is reported for Deborah number of 2.5 (Figure 2.1 right), and remains roughly constant at a 40% for Deborah numbers larger than 2.5. This plateau is consistent with theoretical predictions [19]. According to Qin et al., this constant value without further decrease could originates from a limited maximum in the generated elastic stress at tips of the flagella [17]. In figure 2.1 (right), U_{VE} is the velocity of the motile *C. reinhardtii* in a viscoelastic fluid, and U_N the velocity in a Newtonian fluid.

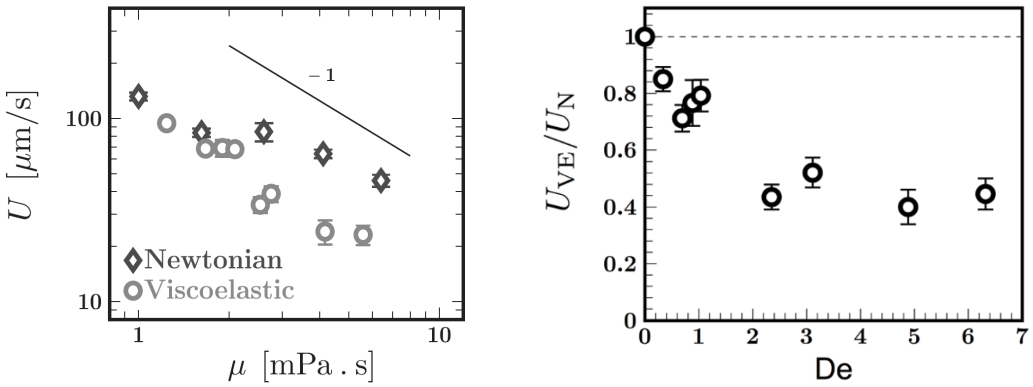

Figure 2.1: Velocity of motile *C. reinhardtii* cells in a quasi 2D plane of Newtonian and viscoelastic fluids. Source: Qin et al. 2015 [17].

Qin et al. also found that beating frequency of the cells remains constant in fluids with increasing fluid elasticity (Figure 2.2 left). The measured beating frequency showed to be lower in a Newtonian fluid than in viscoelastic fluid of equal viscosity. This results in a normalized beating frequency that increases with increasing Deborah number (Figure 2.2 right). λ indicates the relaxation time of the fluid, which is linked to the Deborah number. The increase in normalized beating frequency is more apparent for Deborah numbers larger than 2, where the beating frequency in a viscoelastic fluid can be up to 50% higher for a Deborah number of 6. However, for Deborah numbers lower than 2, the beating frequency shows no change with respect to the beating frequency in a Newtonian fluid. In figure 2.2 (right), ω_{VE} stands for the beating frequency of the motile *C. reinhardtii* in a viscoelastic fluid, and ω_N stands for the beating frequency in a Newtonian fluid.

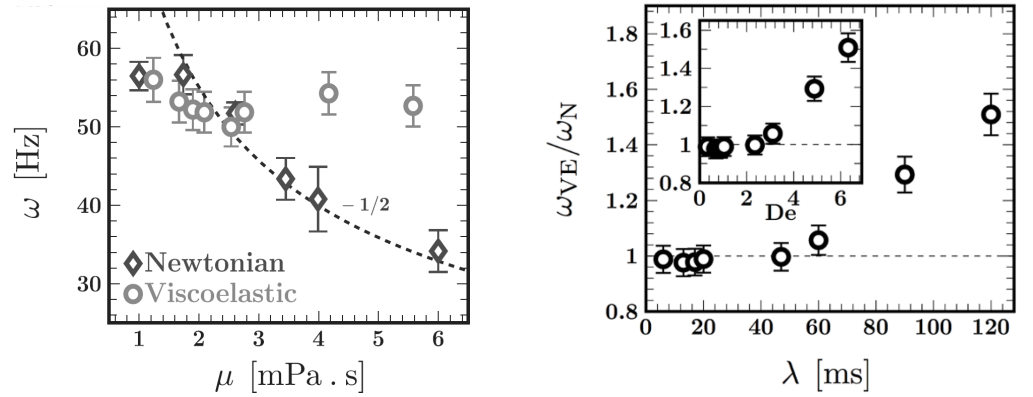

Figure 2.2: Beating frequency of motile *C. reinhardtii* cells in a quasi 2D plane of Newtonian and viscoelastic fluids. Source: Qin et al. 2015 [17].

The motile *C. reinhardtii* propel themselves similar to human breaststrokes, consisting of a power stroke (forwards movement) and a recovery stroke (backwards movement). Qin et al. found that the normalized velocity of *C. reinhardtii* during a single power stroke decreases at Deborah numbers smaller than 5, whereas it slightly increases for higher Deborah numbers. For the recovery stroke however, increasing velocities were found for Deborah numbers larger than 2. For Deborah numbers lower than 2, the recovery stroke showed to be slightly hindered in its velocity, as a reduction in backwards velocity was observed. As one motility sequence consists of both the power and the recovery stroke, this results in a lower net displacement at higher Deborah numbers. The increase in beating frequency does not compensate for the decrease in displacement per 'beat', however, as the swimming velocities were found to decrease with increasing Deborah number (Figure 2.1 left).

A follow up 3D numerical study was performed by Li et al. [32] to corroborate the experimental results from Qin et al. [17] and is co-authored by the original authors. In this numerical work, the swimming gait used by the *C. reinhardtii* cells in viscoelastic fluids is compared to the swimming gait of the cells in a Newtonian fluid. The experimentally derived swimming gaits are obtained from Newtonian and viscoelastic fluid samples with a viscosity of 2.5e−3 Pa s and a Deborah number of 2 for the viscoelastic fluid. The same protocol is used as in the experimental work by Qin et al., as they simulated a viscoelastic and a Newtonian fluid of the equal viscosity. Both the viscoelastic and Newtonian swimming gaits were tested in Newtonian and viscoelastic fluids to observe the performance. The numerical study shows the efficiency of the swimming gaits for a range of Deborah numbers. It was found that velocity of the Newtonian swimming gait is up to 60% higher than the viscoelastic swimming gait. However, it was found that the power output required for this velocity for Newtonian swimming gait is significantly higher than the required power output of the viscoelastic swimming gait. The power required by both gaits were compared when in a Newtonian fluid (De = 0) and a viscoelastic fluid with a Deborah number of 2. The power consumption of the Newtonian swimming gait increases 150%, whereas the viscoelastic swimming gait had only an increase of roughly 50% (Figure 2.3 left). They found that the viscoelastic swimming gait is more efficient than the Newtonian gait, indicated by the travelled distance per unit of energy (Figure 2.3 right). Furthermore, this study elaborates on the results found by Qin et al. [17], that the forward and backwards velocity during a motility sequence is enhanced due to the fluid elasticity. They also found that the recovery stroke is more enhanced than the displacement during the power stroke, resulting in a lower net displacement per motion sequence [32].

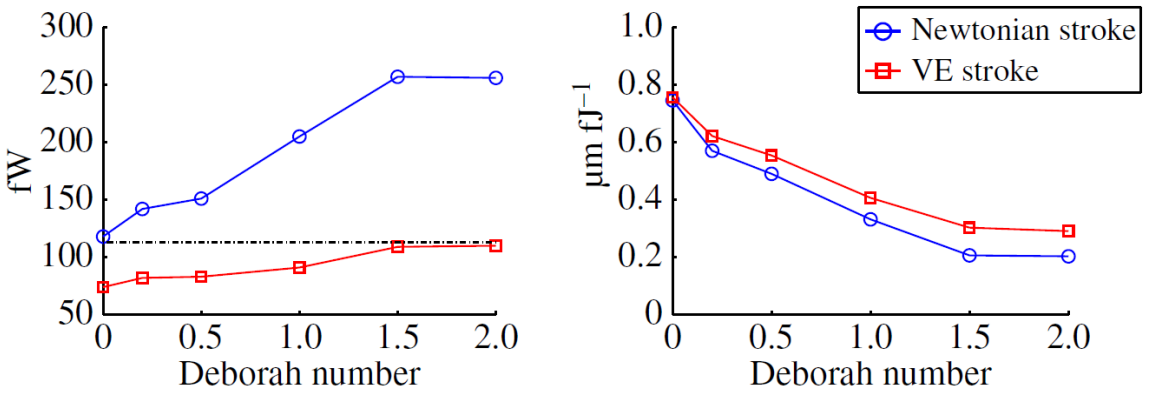

Figure 2.3: The power output of the cell for both the viscoelastic and the Newtonian swimming gait, as function of the Deborah number (left). The energy efficiency of the viscoelastic and the Newtonian swimming gait (right). Source: Li et al. 2017 [32].

In the experimental study of Patteson, an *E. Coli* cell is observed in a polymeric solution to investigate the run and tumble dynamics [14]. They found that even small amounts of polymer concentrations, and thus small elastic effects, can cause significant changes in the dynamics of the pusher cell. In line with other papers, an increase in the velocity of the pusher cells is observed, which is argued to be due to the build-up of elastic stresses in the fluid. Another observation made by Patteson et al. is that the cells tend to 'run' more and 'tumble' less. The results show that this is mainly due to the increased viscosity levels of the solutions and not due to the elastic stresses.

2.4 Previous work

Previous experimental work at the 3mE faculty on the 3D motility of *C. reinhardtii* are conducted by Muller [33] and Sudha [34]. Muller focused on characterising the collective swimming behaviour of motile microorganisms in Newtonian fluids. Sudha continued on his work by introducing viscoelastic mediums in which the motility of individual microorganisms was observed. During his thesis, he aimed to characterise the viscoelasticity of specific fluids and investigate the influence of viscoelasticity on the motility of microorganisms. Due to limitations of available measuring equipment, no clear results were found for the rheological part of his thesis. With new insights, a different viscoelastic material and new rheological equipment, we aim to tackle the question: What is the influence of rheology on the motility of micro-organisms.

3 | Characterising rheology of fluids

3.1 Introduction into rheology

The field of rheology studies the deformation and flow of materials [35]. The word 'rheology' originates from the Greek word "rhei", which means "to flow" and the Greek suffix "logia", which translates to "the study of something". This branch of physics covers the deformations of materials with both liquid and solid characteristics. This chapter aims to provide an introduction into the field of rheology as well as explaining the experimental methodology for characterising the rheological properties of the selected fluids.

3.1.1 Newtonian fluids

All fluids have a certain resistance to the rate of deformation, which is in part represented by the viscosity. The viscosity links the deformation rate within the fluid to the stresses within the fluid. For incompressible and isotropic Newtonian fluids, this relation is linear and indicated by Newton's law of viscosity:

$$\tau = \mu \frac{du}{dy}, \quad or \quad \tau = \mu \dot{\gamma} \tag{3.1}$$

where τ is the shear stress and $\frac{du}{dy}$ or $\dot{\gamma}$ the shear rate. For Newtonian fluids, the relation between stress and deformation rate at a certain temperature is given by a constant value, which is called the viscosity of that fluid.

3.1.2 Non-Newtonian fluids: Viscoelastic fluid

Viscoelastic fluids are a special type of non-Newtonian fluids. Fluids that do not follow Newton's law of viscosity are indicated as a non-Newtonian fluids [36]. These fluids have a nonlinear relation between stress and rate of deformation and show a dependency of the viscosity on the applied shear rates, regularly written as $\mu(\dot{\gamma})$. In non-Newtonian fluids, viscosity changes when under stress creating shear thickening, shear thinning or time dependent behaviours. These non-Newtonian fluids do not necessarily contain an elastic component.

Viscoelastic fluids are fluids that show both viscous behaviour as well as elastic behaviour, as applied stresses are both stored and dissipated. These kinds of fluids contain for example biological molecules and cells, and cannot be fit using classical models of either elasticity or viscosity. Perfect solid materials have an infinite memory to applied stresses, where perfect liquids do not have any memory at all. The fact that viscoelastic fluids contain both elastic and viscous characteristics, gives them a time-dependent property and a finite memory. For viscoelastic fluids, this memory aspect dissipates on some characteristic time scale, which is indicated by the relaxation time of a fluid [32].

Deborah number
The Deborah number describes the level of elasticity of a fluid under specific conditions, based on the relaxation time of the fluid and the characteristic time scale of the experiment. If the characteristic time is relatively long or the fluid relaxation time scale is short, a low Deborah number is expected, indicating that the response of the fluid will have predominantly fluid-like characteristics. If it is the other way around, with a high Deborah number, elastic effects are more significant and the material behaves more like an elastic material at the given application [37]. For the application of motility of microorganisms, the characteristic time scale is indicated as one divided by the beating frequency of the flagella. $De = \lambda / T_{experiment}$ or $De = \lambda\,\omega$, where, λ is the fluid relaxation time and ω is the beating frequency of the microorganism.

Polymer physics
Concentrations of large polymer chains of high molecular weight or large protein chains are the origin of a viscoelastic effect. At rest, these long polymer chains form spherical coils in the solution, creating a structure within the solution. On the edges of these coils, polymer chains start to become entangled with the polymers of other coils. This entanglement phenomenon increases substantially if a certain critical concentration is reached. This concentration is indicated as the overlap concentration, or entanglement concentration. As shear stresses are applied to the fluid, the coils deform from a spherical shape into an ellipsoidal shape, as shown in Figure 3.1.

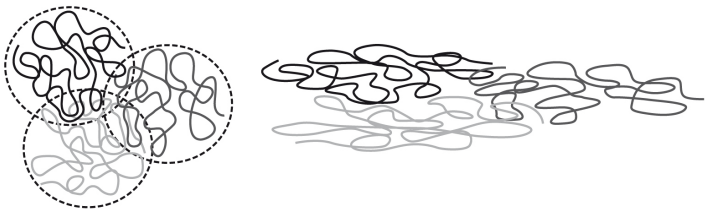

Figure 3.1: Polymer coils. Left: At rest with coiled and entangled molecules. Right: In motion under shear, stretched and partly disentangled molecules. Source: Anton Paar [38].

Deformation of these coils requires a certain energy because these coils act like springs. This deformation stores some of the energy applied to deform the sample and provide the solution with elastic properties [39]. Besides providing the fluid with an elastic property, the coils in the fluid deform to ellipsoids, which causes more polymer chains to align, reducing the entanglement of the internal structure. Individual molecules have lower resistance to flow than the entangled superstructures [40], resulting in lower viscosity values at higher shear rates, i.e. a shear thinning effect.

3.2 Methods to characterize rheology of fluids

This part of the thesis aims to characterise the rheological properties of the fluids used for motility experiments. First, the viscosity levels and shear rate dependency of the viscosities are determined using rotational measurements of the Anton Paar Rheometer MCR302 (Figure 3.2 left). With the results of the viscosity measurements, it is possible to match specific concentrations of the viscoelastic fluid with concentrations of a Newtonian fluid such that both samples have equal viscosity. To be able to make qualitative conclusions on how the viscoelasticity influences the motility of the microorganism, the elastic effects of the fluid is isolated. As viscoelastic materials have a time dependency, the rheological properties of the viscoelastic sample are investigated with dynamic (oscillatory) tests. The goal of these dynamic tests is to obtain the relaxation time λ, the time a fluid sample takes to return to equilibrium after a stress is applied, for different levels of concentration. This relaxation time is used to determine the Deborah number for motility experiments with a specific viscoelastic sample.

The viscoelastic fluid is prepared by adding polymers of high molecular weight to a Tris minimal medium. Tris minimal is a solution containing nutrients which algae use to remain viable (see Section 5.1.2). The dynamic viscosity of Tris is similar to water (10^{-3} Pa s). The polymer used is Polyacrylamide (PAM), which is a long-chained molecule that provides viscoelastic properties when in a solution [41]. PAM has a molecular weight (MW) of 1.8e7 g/mol and is also used in the study of Qin et al. [17]. Adding polymer to the solution increases the viscosity and the shear thinning properties become more prominent. Ficoll400 (MW = 400 g/mol) is used to obtain Newtonian fluids with different levels of viscosity.

All rheological measurements are performed with the Anton Paar rheometer MCR 302 (Figure 3.2 left) at the 3mE High-tech Engineering lab. The temperature is set to 23°C. The measurement tools (Figure 3.2 right) used are the parallel plate tool of 50 mm in diameter (PP50) or the Cone plate tool of 25 mm in diameter (CP25). To reduce the influence of experimental errors or inhomogeneity of the prepared fluid, each rheologically distinct fluid sample is measured 6 times. The rheometer is calibrated for system inertia and tool inertia using the Anton Paar Rheocompass software.

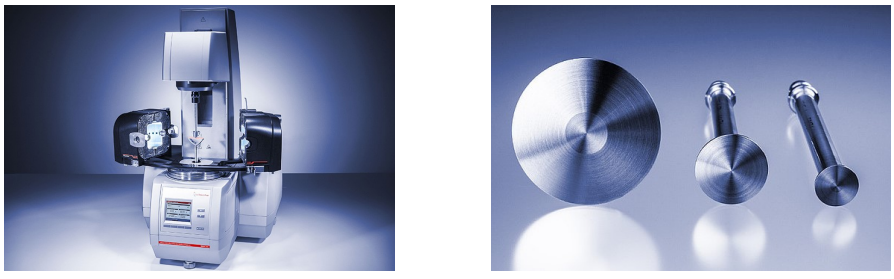

Figure 3.2: The Anton Paar rheometer MCR302 (left) and the rheological tools (right). Source: Anton Paar [42].

The Anton Paar MCR302 rheometer consists of two parallel plates. The material sample of interest is placed in between these two plates. The bottom plate remains stationary and regulates the temperature settings of the measurement. The top plate is actuated by the Anton Paar Rheocompass software to apply deformations onto the material sample. The rheometer is able to measure the relation between the applied stresses and the resulting deformation of the material. The relation between these variables provides insights into the material properties of the measured sample.

3.2.1 Rotational measurements: Viscosity

To determine the Ficoll concentrations required to match the viscosity of the PAM solutions, viscosity curves of both materials are made with the Anton Paar MCR302 and the Cone plate tool. The Anton Paar can be set to a mode of Controlled Rate (CR) or Controlled Stress (CS). Both result in a viscosity curve where the viscosity is a function of the shear rate. As for the application of this study, the movement of *C. reinhardtii*, it is easier to determine the shear rates produced by their motion than to determine the stresses generated by the algae. A second reason to choose for CR settings is the higher accuracy for the shear rates of interest (10^0-10^2 1/s) [36]. Hence, the rheometer is set to a controlled rate, meaning the rheometer actuates such that a certain shear rate is achieved. The rheometer measures the shear stress required to achieve the set shear rate and calculates the viscosity using:

$$\mu(\dot{\gamma}) = \tau/\dot{\gamma} \tag{3.2}$$

where $\mu(\dot{\gamma})$ is the dynamic viscosity, τ the applied shear stress and $\dot{\gamma}$ the shear rate. For the cone plate, the shear rate is linked to the angular velocity according to:

$$\dot{\gamma} = \frac{\Omega\ r}{H(r)} = \frac{\Omega}{tan\ \alpha} \tag{3.3}$$

where Ω is the angular velocity, r the radius, $H(r)$ the gap height between the parallel plates, and α the cone angle. The benefit of the cone plate tool is that the shear rate is independent of r. For the parallel plate, $\dot{\gamma}(r) = \Omega\ r/H$, where H is independent of the radius. For the viscosity measurements, the cone plate tool of 25mm diameter is chosen.

The presence of long chained polymers provides the fluid with a shear thinning effect. To reduce the effect of shear thinning, low polymer concentrations ranging from 20 to 80 ppm are chosen, remaining below the overlap concentration of 350 ppm [43]. The viscosity value for a specific level of concentration is selected according to the relevant shear rate characteristics of *C. reinhardtii*. The lower bound of the relevant shear rates are caused by the forward movement of the body ($\dot{\gamma} = |U|\ /D \approx 15s^{-1}$), with U the mean velocity of the *C. reinhardtii* and D the diameter of the cell body. The upper bound is caused by the beating frequency of the flagella ($\dot{\gamma} \approx 50s^{-1}$) [17]. To obtain an estimate of the viscosity experienced by the motile cell, the viscosity values linked to shear rates between 15-50 s^{-1} are averaged. The resulting viscosity is used to determine the required concentration of polymer for the Newtonian samples.

3.2.2 Oscillatory measurements: Viscoelasticity

To determine the level of viscoelasticity, small amplitude oscillatory shear (SAOS) measurements are conducted. During SAOS measurements, the Anton Paar rheometer applies small periodically varying strain to the sample given by Equation 3.4 [36], with γ_0 the maximum amplitude of the oscillation and ω the angular velocity. A graphic example given in Figure 3.3.

$$\gamma = \gamma_0 \sin(\omega t), \quad with \quad \omega = 2\pi f \tag{3.4}$$

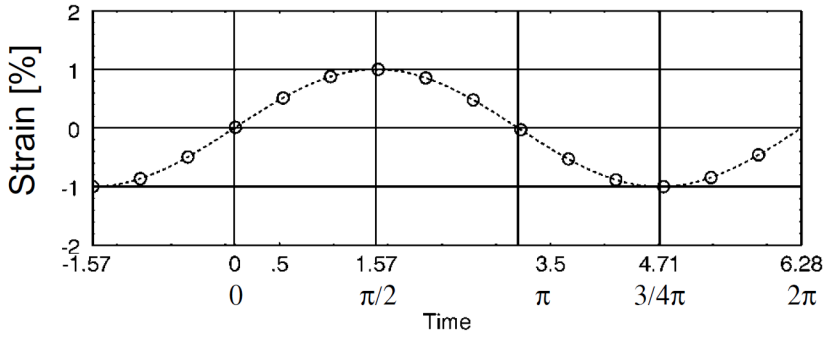

Figure 3.3: The oscillatory strain during an SOAS measurement.
Source: A practical approach to rheology and rheometry [36].

The required shear stress to achieve these strains is given by Equation 3.5, with τ_0 the maximum stress and δ the phase angle [36].

$$\tau = \tau_0 \sin(\omega t + \delta) \tag{3.5}$$

Viscoelastic materials contain both elastic and viscous characteristics. The level of viscoelasticity can be described by the phase angle δ, which indicates the phase shift between the applied strain and resulting stresses. An ideal solid is described by $\delta = 0°$, as the stress is in phase with the oscillatory deformation of a oscillatory measurements. A Newtonian liquid is described by $\delta = 90°$, as stress and strain are completely out of phase. Materials with $0° < \delta < 90°$ are considered viscoelastic materials. A graphic overview of the phase shift for different types of materials is given in Figure 3.4.

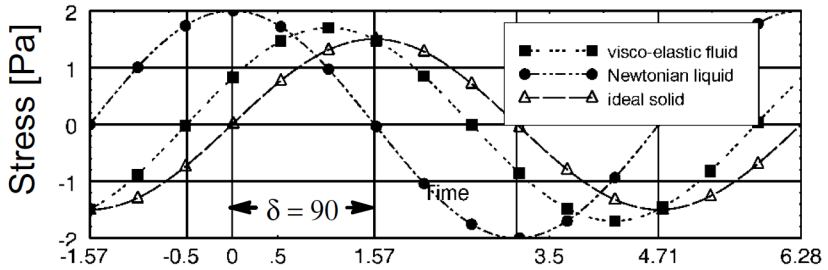

Figure 3.4: The stress profile of an viscoelastic liquid, a Newtonian liquid and an ideal solid when subjected to the oscillatory strain of a SAOS measurement.
Source: A practical approach to rheology and rheometry [36].

Now, we introduce the complex modulus G*, which represents the total resistance of the material against the applied strain [36]. The complex modulus G* is derived from the phase angle δ and defined as:

$$\mathrm{G}^* = G' + iG" \quad \text{or} \quad |\mathrm{G}^*| = \tau_0(t)/\gamma_0 \tag{3.6}$$

where G' is the storage modulus defined as G' = |G*|cos(δ), and the loss modulus G" defined as G" = |G*|sin(δ). The storage modulus G' represents the stress energy that temporarily stored, and the loss modulus G" represents the stress energy that is lost.

From the SAOS measurements, we can also distinguish if the material sample behaves as a viscoelastic solid or a viscoelastic liquid. If the value for the storage modulus is higher than the loss modulus (Figure 3.5a), the sample shows more the behaviour of a solid structure and is considered a viscoelastic solid. If the storage modulus is lower than the loss modulus however (Figure 3.5b), the sample shows more liquid-like behaviour and is considered a viscoelastic liquid.

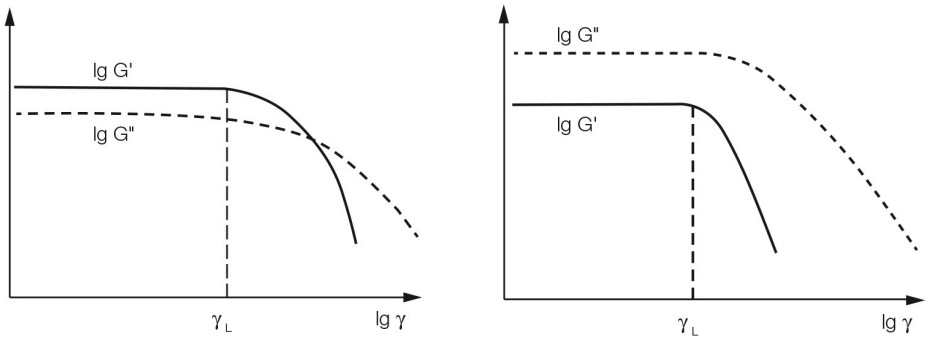

(a) Viscoelastic solid (b) Viscoelastic liquid

Figure 3.5: Linear viscoelastic range of a viscoelastic solid and a viscoelastic liquid. Source: https://wiki.anton-paar.com/en/amplitude-sweeps/.

Linear viscoelastic range

Polymer coils within the solution create resistance to deformation, as deforming from spherical to ellipsoidal shapes requires energy. The energy used to deform these polymer coils is partially stored, creating an elastic component in the solution. When these coils deform into flat ellipsoids, polymer chains start to align, and the polymer chains start to 'flow' past each other without storing any elastic energy. When this happens, the internal structure of the polymer breaks up, and the linear viscoelastic range (LVR) is exceeded. Within the LVR, the complex modulus G* has a constant value, i.e. the internal structure is stable. As soon as the shear strain exceeds this limit, the internal structure breaks up resulting in a decreasing complex modulus. Figure 3.6 shows a sudden decrease in storage modulus, indicating that the LVR has been exceeded. To gain insights in the relaxation characteristics of the polymer solution, the LVR has to be determined, as experiments are

conducted on a stable internal structure. This LVR is obtained from SAOS measurements at constant frequency for a range of shear strains, i.e. an amplitude sweep. The amplitude sweeps are performed at a constant frequency of 10 rad/s, as is common practice [44].

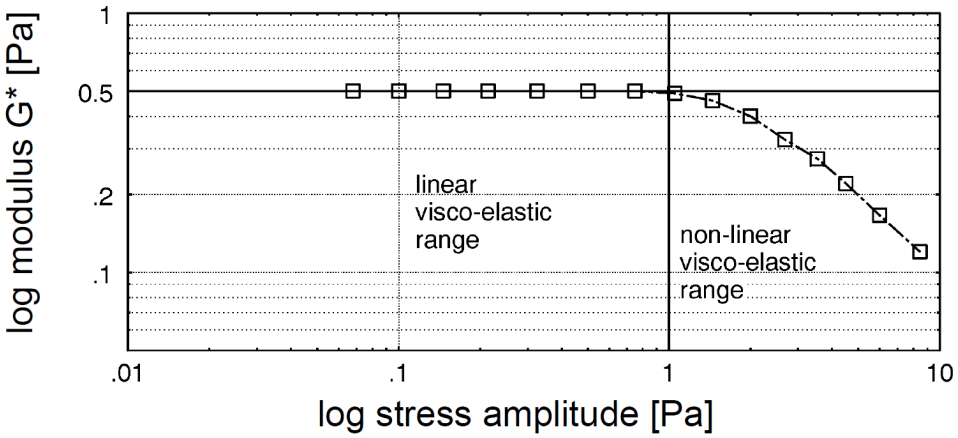

Figure 3.6: The linear viscoelastic range (LVR).
Source: A practical approach to rheology and rheometry [36].

Frequency sweep

The linear viscoelastic range (LVR) is used to select the amplitude or shear strain to be used during a frequency sweep measurement. The Anton Paar is set to a constant shear strain of approximately 10-40% of the LVR limit, to ensure stability of the internal structure during the measurement. The frequency at which the stress is applied, will be the changing variable. The internal structure of the polymer coils comes to rest as soon as the strain is removed. The time the polymer solution takes to come back to a complete equilibrium, is called the relaxation time. An example of a frequency sweep measurement can be seen in Figure 3.7. Here, the relaxation frequency is indicated as the cross over point between the storage and the loss moduli. To clarify, this should be the highest frequency at which the two curves of the moduli intersect, as multiple intersections are possible. For concentrations below the overlap concentration, i.e. dilute polymer solutions, only one crossover frequency is expected. From this crossover point, the relaxation time is obtained simply by taking the inverse of the relaxation frequency, which is then used to determine the Deborah number. The relaxation frequency acts as a separation point between regions of viscoelastic solids and liquids. At frequencies higher than the relaxation frequency, the response is more elastic whereas at lower frequencies, the solution behaves as a viscous liquid.

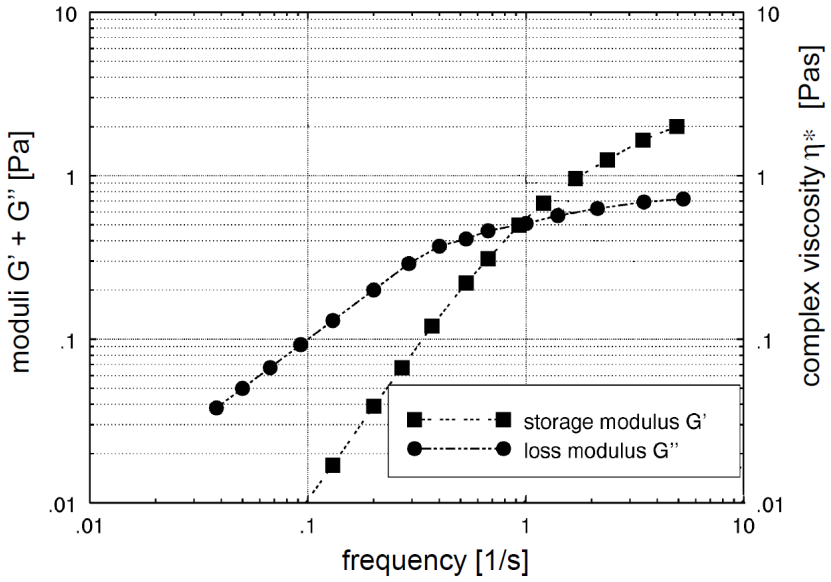

Figure 3.7: Example of a frequency sweep measurement with crossover frequency at the intersection of the lines, indicating the relaxation frequency.
Source: A practical approach to rheology and rheometry [36].

3.2.3 Rotational measurements: Viscoelasticity

Carreau Yasuda

Besides analysis via frequency dependent stresses, another method of determining the relaxation time is proposed. The Carreau Yasuda method determines the viscosity as a function of the shear rate, $\mu(\dot{\gamma})$, via the following formula [45]:

$$\frac{\mu(\dot{\gamma}) - \mu_\infty}{\mu_0 - \mu_\infty} = \frac{1}{\left(1 + (\lambda\dot{\gamma})^{p_1}\right)^{\frac{1-p}{p_1}}} \tag{3.7}$$

where, μ_0 is the viscosity at zero shear rate, μ_∞ the viscosity at theoretical infinite shear rate, λ the relaxation time of the fluid, p1 the "Yasuda Exponent" and p the power-law-index [45]. For the power-law-index of Carreau Yasuda fluids, $p < 1$ indicates shear-thinning fluids, $p > 1$ shear-thickening fluids, and $p = 1$ ideally viscous flow behaviour. As the Anton Paar rheometer has built-in curve fitting tools, rotational viscosity measurements can be used to extract the relaxation time. The apparatus uses the fact that the shear thinning behaviour is inherently linked to the relaxation time of the fluid. Measurements of the relaxation time with the Carreau Yasuda method have been conducted at the rheology lab of Anton Paar in Oosterhout, and only the resulting relaxation times are obtained.

4 Results rheological measurements

This chapter describes the results of the rheological experiments which aims to characterise the fluids used during the experiments for motility analysis. First, the viscosity curves for both PAM and Ficoll400 in Tris minimal are shown. Second, the characterisation of the relaxation time of PAM is provided. An overview is given of the rheological results used during the motility experiments in the second part of this thesis.

4.1 Viscosity measurements

Figure 4.1 shows the measured viscosity for different concentrations of PAM, on a double logarithmic scale. Each experiment is performed 6 times of which the resulting average and standard deviation of the viscosity value are plotted as function of the shear rate. As seen in Figure 4.1, the polymer shows shear thinning effects for all measurements, with increasing shear thinning effects at higher concentrations. The measurements show small values for standard deviation. However, at lower viscosity values in combination with low shear rates, somewhat larger standard deviations are observed which originate from lower signal-to-noise ratios. The characteristic shear rates of 15 1/s and 50 1/s have been indicated with a vertical dashed line. As explained in Section 3.2, the viscosity values between shear rates of 15 1/s and 50 1/s will be averaged to approximate the viscosity experienced by the *C. reinhardtii*.

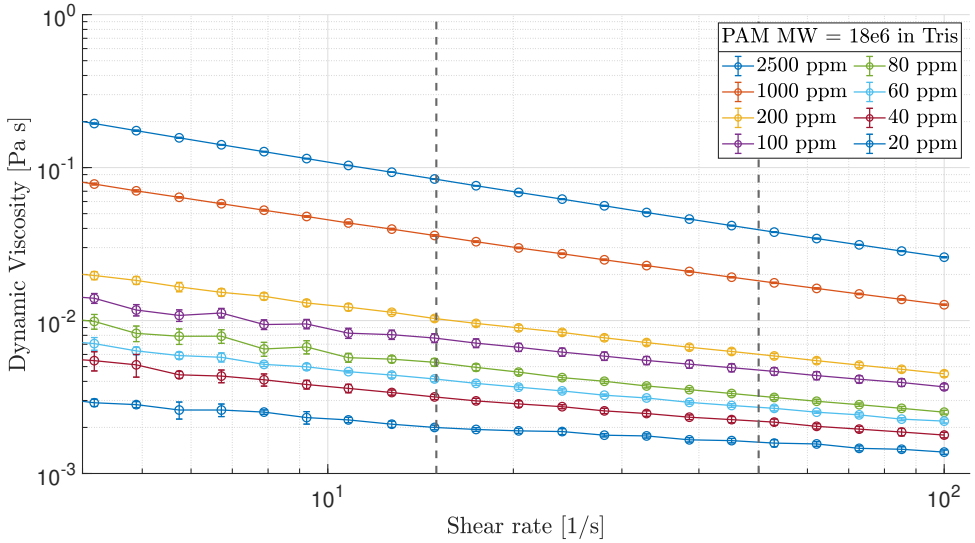

Figure 4.1: Dynamic viscosity as function of shear rate for different PAM concentrations. Note: error bars are shown, but most of them are smaller than the dimension of the marker and therefore not visible.

In Figure 4.2, the dynamic viscosity is plotted as function of the PAM concentration on a double logarithmic scale. The viscosity values originate from averaging the viscosity values found for shear rates between 15-50 1/s. The resulting viscosities show a linear correlation in the double logarithmic plot, indicating a power-law relation between the viscosity and the concentration of PAM. The viscosity value at 100ppm deviates slightly

from the trend of the other data points. In Figure 4.2, the horizontal dashed lines indicate the viscosity levels that belong to the concentrations of PAM that will be used during motility experiments, and are labelled as 'Data sets'. In this thesis, data sets will refer to a combination of a viscoelastic and a Newtonian sample of equal viscosity.

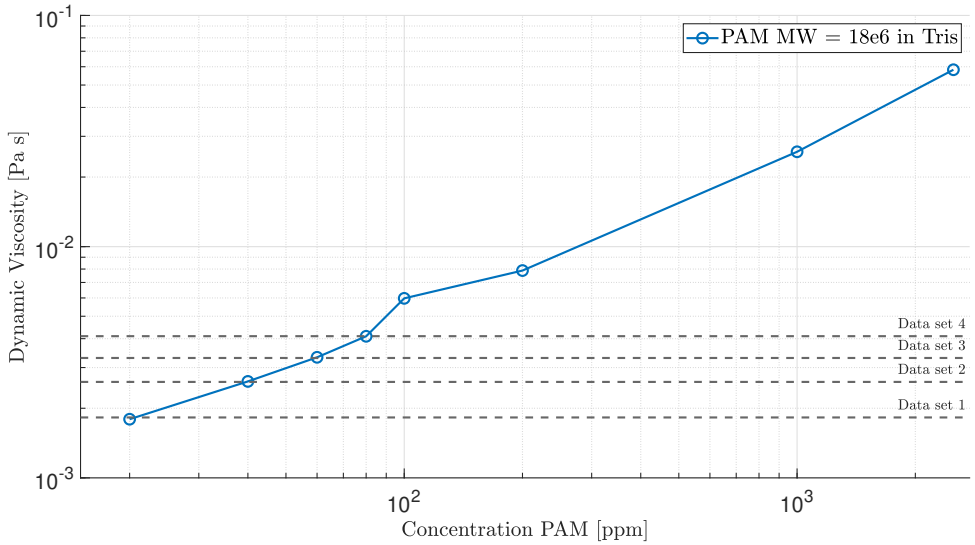

Figure 4.2: Dynamic viscosity for relevant shear rates as function of PAM concentration.

Figure 4.3 shows the results of the viscosity measurements for different Ficoll400 concentrations, plotted on a double logarithmic scale. The measurements show close to constant viscosity values, independent on shear rate, as expected for a Newtonian fluid. However, at low shear rates and especially in combination with low viscosity values, the results have somewhat larger standard deviations, again originating from a low signal-to-noise ratio. It must be noted that for the concentration of 10% wt, only one measurement has been conducted, and therefore no standard deviation could be provided.

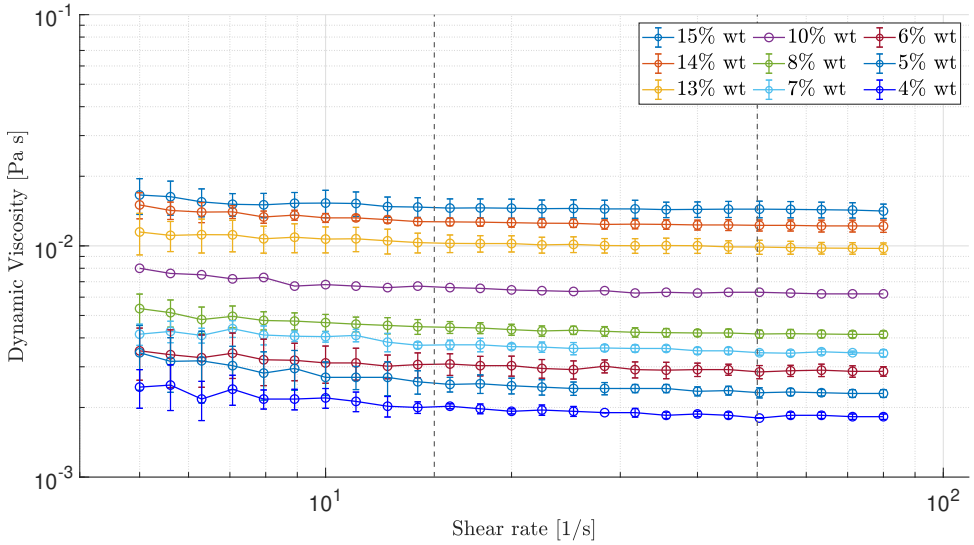

Figure 4.3: Dynamic viscosity as function of shear rate for different Ficoll400 concentrations.

Figure 4.4 shows the viscosity values belonging to the different concentrations of Ficoll400, plotted on a double logarithmic scale. Similar to the results of the viscosity measurements for PAM, the viscosity measurements for Ficoll show a linear regression in the double logarithmic plot for viscosity as function of concentration. This also indicates power-law relation between the viscosity and concentration of Ficoll400.

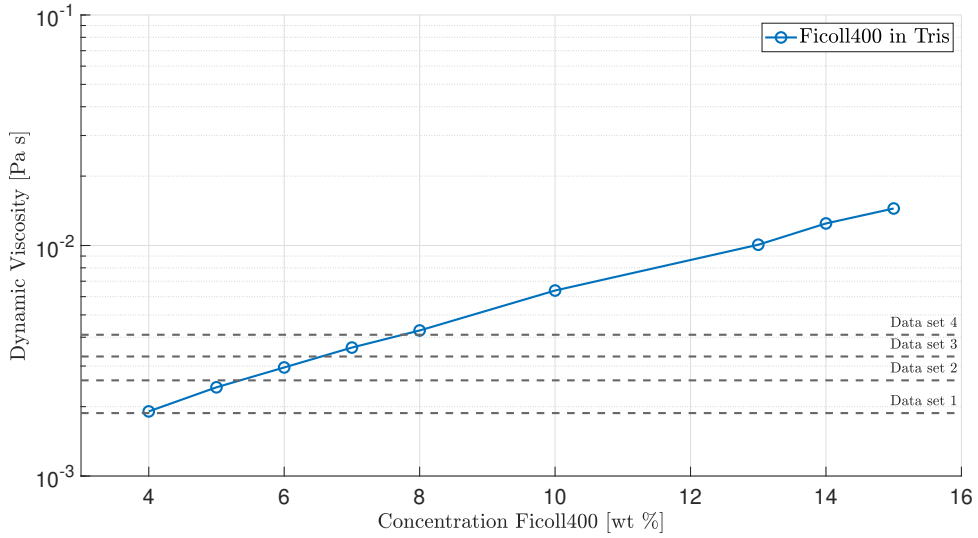

Figure 4.4: Dynamic viscosity at relevant shear rates as function of Ficoll400 concentration.

The horizontal dashed lines in Figure 4.4 indicate the viscosities of the selected PAM concentrations that are used for the experiments. As the goal is to match this viscosity of the viscoelastic and Newtonian samples, the dashed lines in both Figures 4.2 and 4.4 help to pinpoint the required Ficoll400 concentrations. The resulting concentrations of Ficoll400 are summarized in Table 4.1. The baseline consists of only Tris minimal.

Data set	PAM [ppm]	Ficoll [wt%]	μ [Pa s]
Baseline	0	0	1e−3
1	20	4	1.8e−3
2	40	5.5	2.6e−3
3	60	6.5	3.3e−3
4	80	8	4.1e−3

Table 4.1: Overview of viscosity values extracted from Figures 4.2 and 4.4.
These PAM and Ficoll concentrations are used in the experiments of the next chapter.

4.2 Viscoelasticity measurements

4.2.1 Linear viscoelastic regime

As explained in Section 3.2.2, a rough estimate of the linear viscoelastic regime is required to determine the shear strain settings for the frequency sweeps. Figure 4.5 shows the results of an amplitude sweep (constant frequency of 10 rad/s, varying strain) conducted using high concentrations of PAM in Tris minimal. Only the results for high concentrations of PAM are shown, as results for low concentrations showed too large variations and are therefore unreliable. The circular markers show the values for the storage modulus G' and the triangular markers show the loss modulus G". For 2500 ppm as well as for 1000 ppm of PAM, a constant value for both the storage and loss modulus can be observed (constant complex modulus $G^* = G' + iG"$) for values of strain lower than 30%, indicating the linear viscoelastic range (LVR). A drop in complex modulus can be observed for values higher than 30% strain, indicating a break-up of the internal structure. During the frequency sweeps, this internal structure has to remain intact, thus an amplitude lower than the limit of 30% is chosen for the frequency sweeps. A strain of 10% is chosen to be used during frequency sweep measurements. It should be noted that the storage modulus is higher than the loss modulus within the LVR, indicating that under these conditions the sample show the characteristics of a viscoelastic solid.

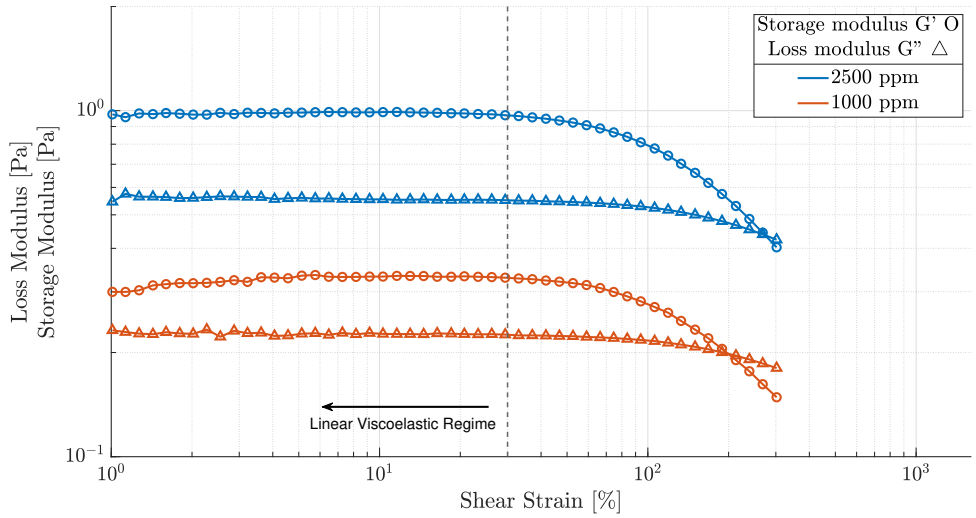

Figure 4.5: Results of amplitude sweep measurements at 2 different high PAM concentrations.

4.2.2 Relaxation time

Figure 4.6 shows the result of the frequency sweep for a solution of PAM at 2500 ppm. The cross-over frequency shows the relaxation frequency, which separates the regimes of viscoelastic solids and viscoelastic liquids. Two cross-over frequencies can be observed, one at 10 Hz and one at 0.03 Hz. For frequency values lower than 0.03Hz, the value for loss modulus is higher than the value for the storage modulus, whereas for values between 0.03 Hz and 10 Hz, the value for storage modulus is higher than the value of the loss

modulus. A sudden increase in loss modulus G" for frequency values higher than 3.5 Hz is observed.

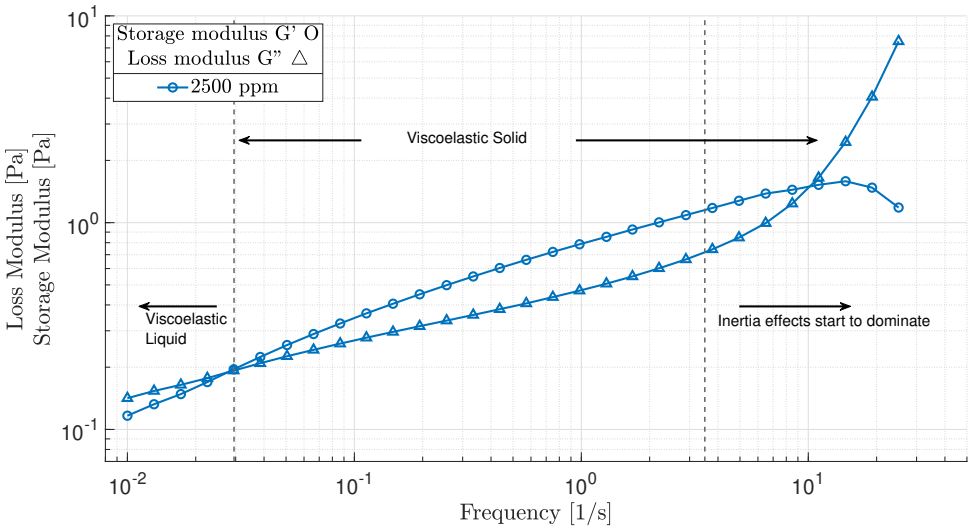

Figure 4.6: Storage and loss modulus during the frequency sweep for 2500ppm of PAM.

Figure 4.7 shows the results of the frequency sweep for a solution of PAM at 1000 ppm, plotted on a double logarithmic scale. The storage modulus is observed to be higher than the loss modulus for all frequency values lower than 10 Hz. Similarly to the results found for PAM at 2500 ppm, a sudden increase of loss modulus is observed for frequencies higher than 3.5 Hz. A sudden increase in storage modulus G' as well as loss modulus G" for a frequency values of approximately 0.04 Hz is observed. However, different from the results for 2500 ppm PAM, no cross-over frequency is observed at lower frequencies, not resulting in an evident relaxation time.

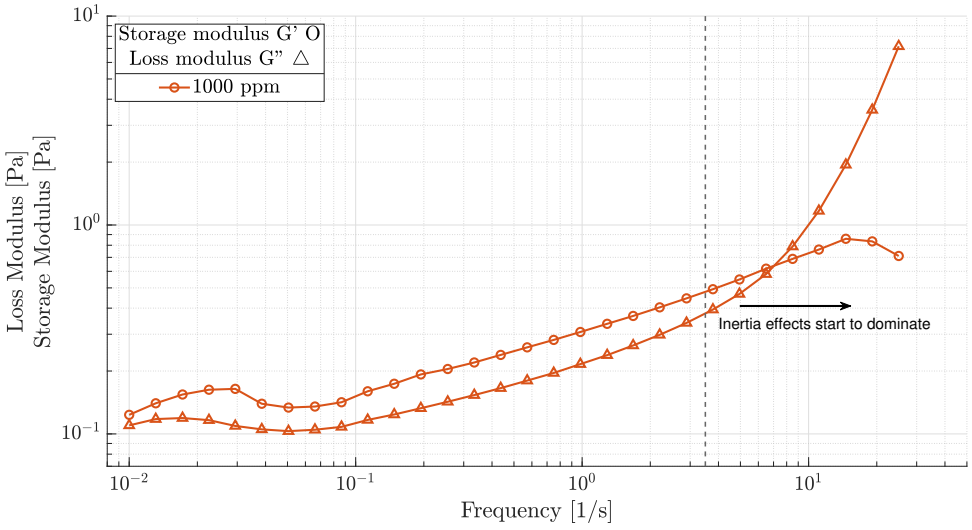

Figure 4.7: Storage and loss modulus during the frequency sweep for 1000ppm of PAM.

In Figure 4.8, the relaxation times of different concentrations of PAM have been plotted on a double logarithmic scale. The graph combines the results found in this study for high concentrations of PAM with the frequency sweep, the results from the Carreau Yasuda method for lower concentrations and the results found by Qin et al. [17] for concentrations which were not able to be measured by the available equipment. Different colors indicate different methods. A trend is observed showing that the relaxation time of the fluid increases for higher levels of concentration. The results found in this study by the means of the frequency sweep, as well as the Carreau Yasuda method, are roughly in line with the results found by Qin et al. [17].

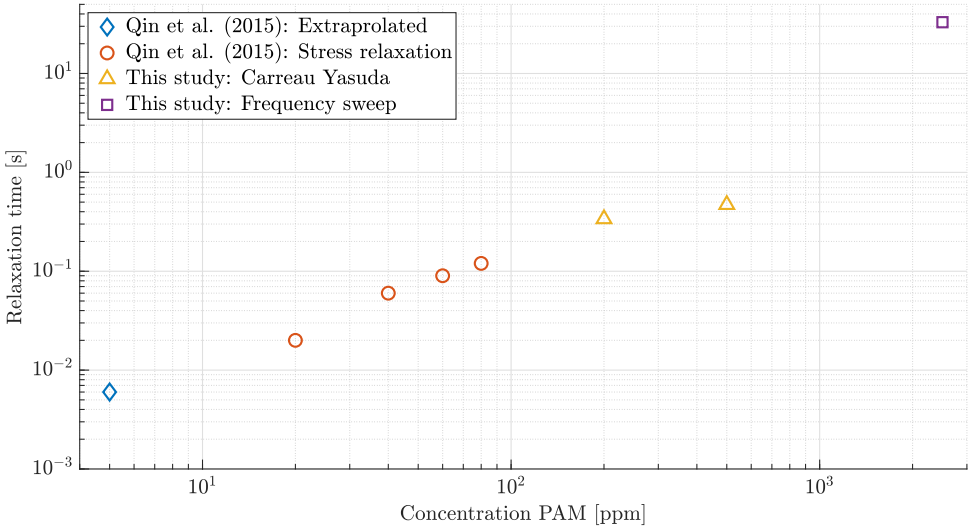

Figure 4.8: Relaxation time λ as function of PAM Concentration.

Table 4.2 provides an overview of the rheology results to be used for the motility experiments, the second part of this thesis. The Deborah number is calculated with $De = \lambda\omega$, with λ the relaxation time of the medium (Figure 4.8) and ω the beating frequency of the *C. reinhardtii* ($\approx$ 50 Hz [17, 23]).

Data set	PAM [ppm]	λ [s]	De [-]	μ [Pa s]	Ficoll [wt%]
Baseline	0	0	0	1e−3	0
1	20	0.02	1	1.8e−3	4
2	40	0.06	3	2.6e−3	5.5
3	60	0.09	4.5	3.3e−3	6.5
4	80	0.12	6	4.1e−3	8

Table 4.2: Overview of the rheological parameters.
These PAM and Ficoll concentrations are used in the experiments of the next chapter.

4.3 Discussion Rheology

The rheological properties of PAM and Ficoll400 dissolved in a Tris minimal medium are determined. From the resulting viscosities for different concentration of PAM, the required concentrations of Ficoll400 are obtained such that the viscosity matches the viscosity of the selected PAM concentrations. The assumption here is that by matching the viscosities of both fluid samples, the influence of the elastic properties of PAM on the motility of motile *C. reinhardtii* cells can be isolated. The rheological properties of the PAM samples are determined using multiple methods and a reference paper which uses the same viscoelastic material [17]. The relaxation times found for different concentrations of PAM are used to determine the Deborah number for different motility experiments.

Viscosity measurements
The viscoelastic samples of PAM show a clear shear thinning property for all levels of concentrations. The polymer coils, originating from the long polymer chains of PAM (high MW), tend to deform into a more ellipsoidal shape when sheared resulting in more aligned chains which reduces the internal friction, i.e. the viscosity of the material. As the molecular weight of Ficoll400 is relatively low, this phenomenon does not occur, resulting in a Newtonian fluid with a viscosity independent of the shear rate. The shear rates generated by the *C. reinhardtii* cells are assumed to be within the range of 15Hz (movement of the cell body $|U|/D$) and 50Hz (the beating frequency of the flagella). The resulting viscosities within this range are averaged, as it is assumed that these are the levels of viscosities to be experienced by the body and the flagella of the algal cells. This results in one characteristic viscosity value for each level of concentration.

Viscoelasticity measurements
To determine the Deborah number, the relaxation time of the viscoelastic fluid for different levels of concentration is determined. Multiple methods are used to determine the relaxation time. With the first method, dynamic tests are performed on the fluid by varying the frequency at which the applied stresses oscillate at a constant strain, and measuring the fluid responds. Due to limiting factors of the Anton Paar rheometer, values for relaxation time could only be accurately measured at high levels of concentration, as the inertia of the system and the used rheological tool largely influence the results at low concentrations. At low concentrations of PAM, the resistance to deformation is low. This resulted in a low stresses required to achieve the oscillating amplitude. The moduli are governed by the fluid stress and strain which are both low for low concentrations ($|G^*| = \tau_0(t)/\gamma_0$), resulting in a low signal-to-noise ratio, resulting in unreliable results. After discussions with Haike Ruiters (Anton Paar Engineer), it became clear that the relaxation times of fluids with a combination of low levels of viscosity and elasticity cannot be measured with frequency sweeps on the MCR302. The frequency sweep method was therefore only used at higher concentrations, where a distinct relaxation time could be observed.

For lower concentrations, the Carreau Yasuda method is used. Limitations to the Carreau Yasuda method are apparent, as approaching the 'zero shear rate' μ_0 required for this method is difficult. The Rheometer cannot measure any relation between stress and shear rate when no deformation is present. In practice, this viscosity value is taken at relatively low shear rates, where inaccuracies in measurements arise as result of a low signal-to-noise ratio. When approaching μ_∞ other limitations arise. The accuracy of the measurement is influenced by the inertia of the used tool. As seen in Equation (3.7), only a rough estimate of μ_∞ is needed to determine the relaxation time, because the formula uses this parameter only by means of subtraction.

The obtained result of the relaxation time of the fluid at various concentrations is a combination of various methods. The results found in this study at high concentrations of PAM are compared to the results found by Qin et al. [17] at low concentrations by the means of extrapolation. Figure 4.8 provides the relaxation times of this study as well as the results found by Qin et al. using the same viscoelastic materials. It shows that our results are roughly in line with results they obtained from stress relaxation measurements. The relaxation times for low concentration found by Qin et al. are used to determine the Deborah numbers for the motility experiments in the next part of this thesis.

5 | Methodology to measure the motility of microorganisms

5.1 Algae culture conditions

For this research, the bi-flagellated green alga *C. reinhardtii* wild-type *CC-125* strain is used. This model organism is often used for research and is classified as a puller motile microorganism. *C. reinhardtii* has a cell body of 10 μm and two flagella of 10 μm (Figure 1.1). The *C. reinhardtii* culture is grown in a custom growth chamber in the MicroLab at the TU Delft 3mE faculty. The following steps in the protocol are used for growing the algae culture which follows established methods by Quaranta et al. [46] and the TU Delft Wetlab Procedures Handbook.

5.1.1 Solid algae culture

C. reinhardtii are originally obtained from *Chlamydomonas* Resource Center growing on solid agar slants. Agar is a colourless gel that contains nutrients to support the growth of microorganisms. The surface of the solid substance is slanted within glass tubes to enhance the surface area that is exposed to light. The tubes are maintained in a growth box under a constant broad spectrum light with an intensity of ± 30 μmol/m^{2}s. From these solid cultures, liquid algal cultures can be made when needed in batches of 100 mL.

Figure 5.1: Solid algae culture on an agar slant (left). Growth box (right).

5.1.2 Liquid algae culture

From the agar slant, algal cells are inoculated into Tris minimal medium to create a liquid algal culture. Tris (Tris(hydroxymethyl)amino methane) is a buffer solution which contains various organic salts. Tris minimal consists of TAP salts solution (NH_4Cl, $MgSO_47H_2O$ and $CaCl_22H2O$), Tris salts ($C_4H_{11}NO_3$ obtained from www.carlroth.com), phosphate solution (K_2HPO_4 and KH_2PO_4) and Hutner's trace element (Obtained from *Chlamy* Resource Center). These salts are essential to the growth and sustainability of

the algae cells. They serve as nutrients and create a buffer solution to maintain a desired pH level [47]. The algal cells consume these nutrients which causes a depletion of phosphates resulting a shift in pH level that can have negative influence on the viability of the cells.

An Erlenmeyer flask with Tris is inoculated, and is placed under 180 μmol/m^{2}s of light intensity. The culture is subjected to light/dark (14/10 h) cycles such that the algal cells are exposed to night and day. This so called Zeitgeheber time schedule aids in syncing the cycle of mitosis of the algal cells. A side effects of these light bulbs is the increase in temperature of the culture when turned on. A graph of the measured temperature fluctuations inside the growth box are shown in Figure 5.2. The average temperature during the day is $\pm$21°C with a temperature of $\pm$19°C at night. A small supply of sterile air is added via a tube, which provides air bubbles to the liquid culture. This serves as a slow stirring mechanism as well as aerating the culture with CO_2.

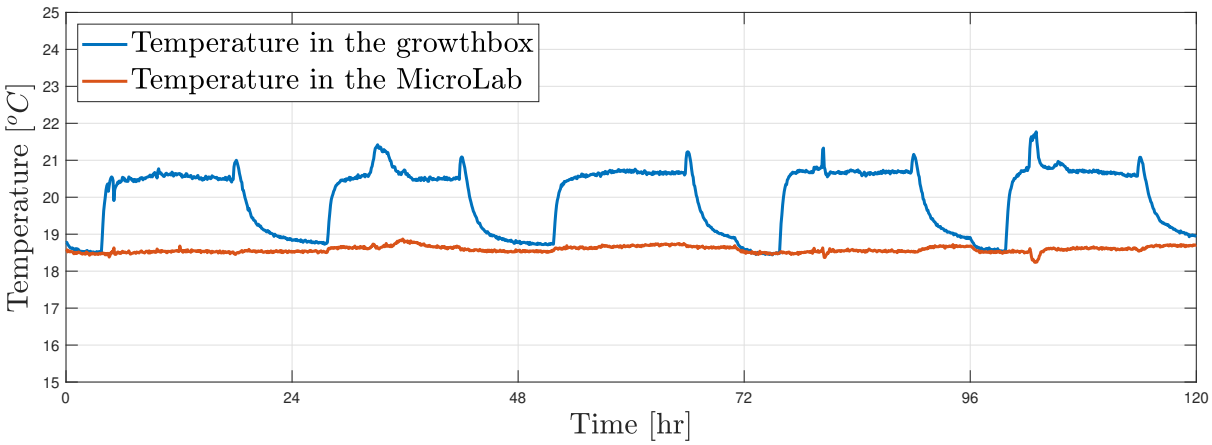

Figure 5.2: Temperature fluctuations due to the light/dark cycle of the lights.

5.1.3 Cell count of algae culture

Following protocols set by Quaranta et al. [46], the experiments on *C. reinhardtii* should be conducted while in the exponential growth phase. This phase is reached on the 4th day after inoculation, on which the algae concentration of the liquid culture is $\mathcal{O}$1e6 cells/mL. After harvesting the cells from the culture, a rough estimate of the cell concentration within the algae culture is made using a haemocytometer. The counting device and its grid layout of four quadrants. Of the liquid culture, a total of 900 μl is extracted from the culture to which 100 μl of iodine solution is added to kill the algal cells, making the counting process more convenient. A few droplets of liquid culture are placed on the counting grid and the cells are counted manually. With this cell count, a rough estimate of the cell concentration per mL in the liquid culture is made, following the formula: *Average cell count per grid quadrant* $\cdot \frac{10^4}{0.9} =$ [cells/mL]. Cell concentrations above 5e5 cells/mL can lead to errors in detecting and tracking of individual cells. To prevent this, cell culture is diluted with Tris(-polymer) solutions to obtain the desired culture densities. Used cell concentrations during experiments range from 2.5e4-1e5 cells/mL.

5.2 Tracking of motile microorganisms in 3D

5.2.1 Experimental setup: the 3D Microscopic setup

A 3D microscopic setup is used (Figure 5.3) to track the 3D dynamics of the *C. reinhardtii*, using dark field microscopy. The location of the flow chamber, containing the polymeric liquids and motile cells, has been highlighted. This section aims to elaborate on the individual parts of the microscopic setup, of which a overview can be seen in Figure 5.4. This setup has been previously used for flow measurements in a thin immersion droplet [48] using passive tracer particles and used to track the behaviour of motile microorganisms such as *C. reinhardtii* [33, 34, 49]. In contrary to previous research using this setup [33, 34, 49, 50], the flow chamber is orientated in vertical direction as seen in Figure 5.3.

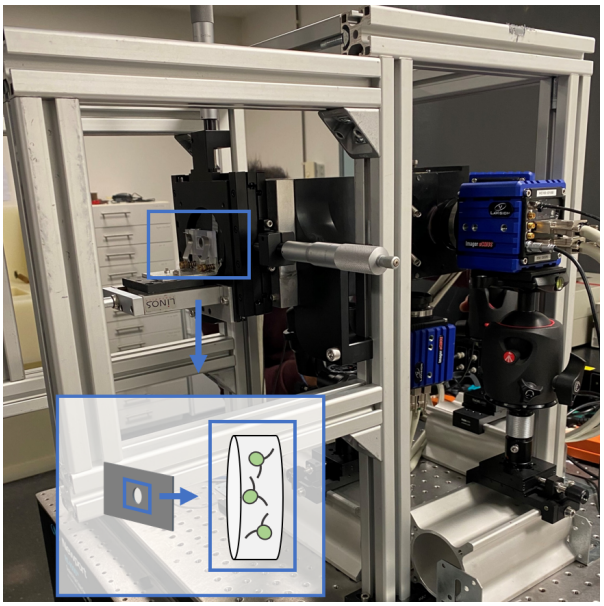

Figure 5.3: The 3D microscopic setup

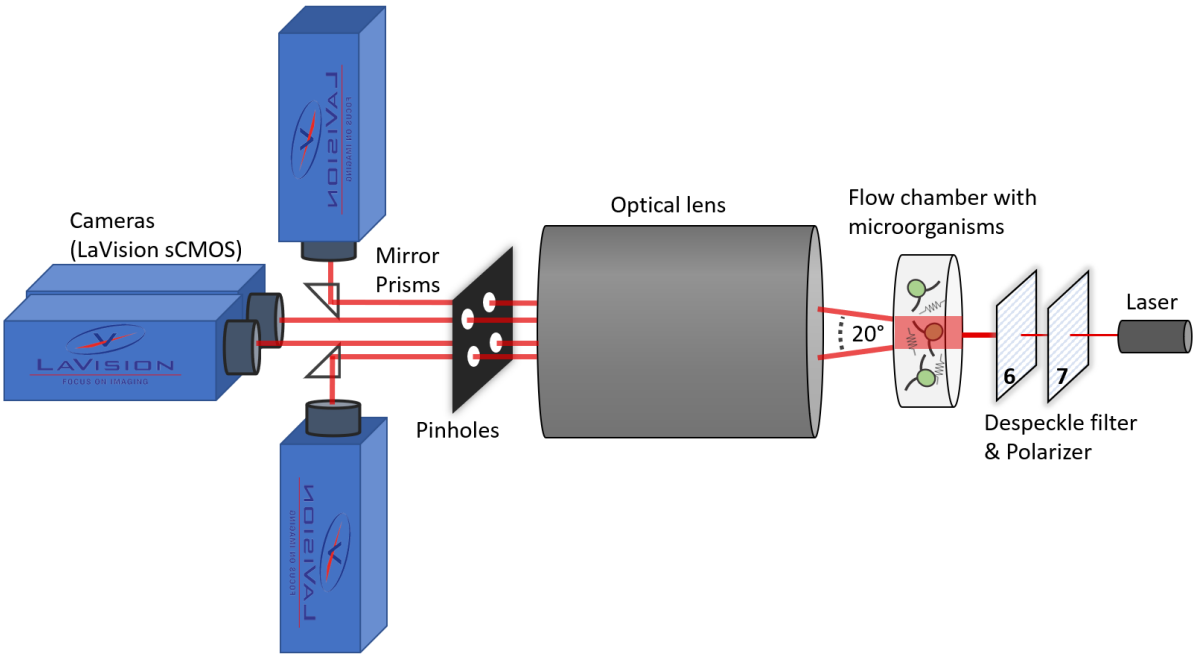

Figure 5.4: A schematic overview of the 3D microscopic setup.

Flow chamber
The flow chamber is made from an acrylic sheet with a thickness of 2 mm. Small rectangles (60x25x2 mm) with a ⌀8 mm hole in the middle (Figure 5.5 left) are laser-cut at the 3mE student workshop. During experiments, this cylindrical gap is filled with a sample of the diluted algae culture. Glass coverslips (20x40x0.1 mm) are used to the seal the bottom and the top of the flow chamber.

The optical path passes through the coverslips, and therefore it is crucial that these are extremely clean. Precleaning is done by immersing the coverslips in a surfactant solution of 0.5% Hellmanex III. The coverslips and surfactant solution are placed in an ultrasonic cleaner for 25 minutes and rinsed with Deionized (DI) water. Afterwards, the surfactant solution is replaced with DI water for another 25 minutes in the ultrasonic cleaner. The coverslips are rinsed again and dried with pressurized air to remove any cleaning residue. The coverslips are treated by immersing them in a protein solution of bovine serum albumin (BSA) and Phosphate Buffered Saline (PBS) based on the saturation of the contact line [51]. The protein solution creates a small layer on the coverslips which prevents surface adhesion of the cells [49]. The coverslips are stored in the protein solution for 20 hours, after which the coverslips are rinsed with DI water to remove any excess BSA-PBS solution, dried with pressurized air, and stored in sterile test tubes.

The bottom coverslip is glued to the flow chamber with Norland Optical Adhesive, which is cured using a UV lamp. The cylindrical gap is loaded with the selected algae sample using a micropipette. The tips of the micropipette are cut to reduce the outflowing shear rates, which reduces the chance of de-flagellation of the cells. The top of the flow chamber is sealed with another treated coverslip, which is held in place using clear nail polish. The algae in the flow chamber are given 5-10 minutes to acclimatize to the conditions of the flow chamber and the lab. The flow chamber is placed on an x-y-z linear stage (Figure 5.3) that can be adjusted by rotating the micrometer. A benefit of the vertical orientation is that non-motile microorganisms are less likely to remain in the camera view, as they are likely to sink due to their slightly negative buoyancy. A downside is that the size of the domain in direction of gravity has increased. As a result of that, temperature gradients can now have larger effects on the recordings, as thermal convection currents (back ground flow) arises.

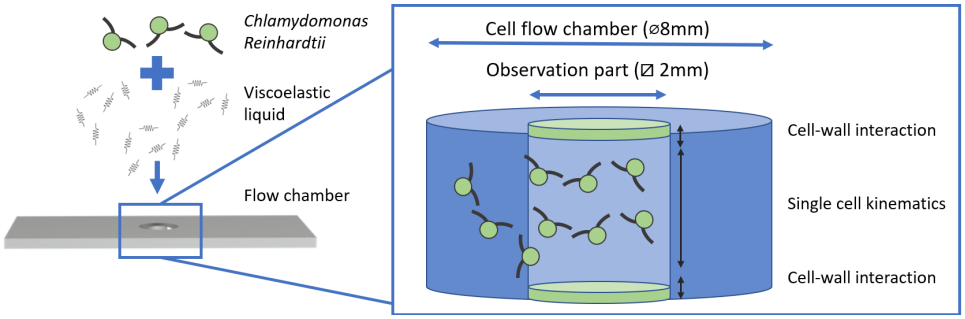

Figure 5.5: Schematic of the cell flow chamber.
Note: The flow chamber is orientated vertically in the experimental setup of Figure 5.3.

LaVision sCMOS cameras (Imager Pro M)

The experimental setup consists of four LaVision imager scientific Complementary Metal Oxide Semiconductor (sCMOS) cameras. By using multiple camera views of the same physical space, a 3D reconstruction can be made. This principle is explained more in depth in Section 5.2.3. The cameras are mounted on adjustable standards which can be seen in Figure 5.3 (bottom right). These standards provide degrees of freedom to position the cameras such that all cameras are in focus and view the same physical space. DaVis 10.1 is used to trigger and capture the images of the cameras at the given frame rate. Each frame, containing the image plan of all four cameras, occupies roughly 1.8 MB of storage capacity. Each experiment is set to be 300 seconds of recording, which could lead to large datafiles. Hence, the track quality and the data storage are the two variables to consider. Lower frame rates can cause inaccuracies in the trajectories and mismatches among cells in the 3D plane, whereas higher frame rates do not necessarily provide more insight into the motility of the microorganisms. To determine the appropriate frame rate, the relevant characteristics of the experiment need to be taken into account.

The beating frequency of *C. reinhardtii* is roughly 50 Hz [17, 23]. To do analysis on the beating frequency, a minimal frame rate of roughly 100 fps is needed to meet the aliasing criteria of $f_{sampling} \geq 2f_{experiment}$. The cameras have a maximum frame rate of 50 fps, meaning the aliasing criteria for beating frequency analysis cannot be reached with the current setup. As the main goal of the first series of experiments is to observe and analyze the trajectories of *C. reinhardtii*, 100 Hz will not be required. The decision is made to set all cameras to a frame rate of 20 fps which is inherently linked to an exposure time of 42000 μs. This frame rate is high enough to capture trajectories such that we can analyze the general motility and behaviour of the cells.

Optical path

The optical paths are converged towards the flow chamber by the lens resulting in a 20° angle between optical paths (see Figure 5.4). The used objective lens has a magnification factor of $M = 1.5$. Figure 5.6 shows the absolute angle of the optical paths with the centerline, which is 10°. Mirror prisms are used to redirect the light rays by 90° towards the cameras. In the current configuration, this is done for 3 out of 4 of the cameras, as one camera is directly aligned towards the lens. Because of these mirrors, the images of 3 cameras are mirrored, which is taken into account during calibration. For simplicity, the sketch shown in Figure 5.4 indicates two cameras directly aligned. In reality, one of these cameras is located from behind with a mirror prism redirecting the optical path.

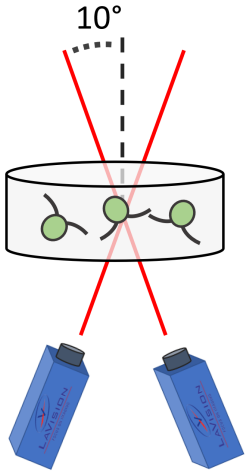

Figure 5.6: Optical paths of 2 of the 4 cameras with respect to the centerline.

Illumination conditions
The flow chamber is illuminated with a red dot laser module. The laser light has a wavelength of $\lambda = 650$ nm and is powered by a dc Power Supply ES 030-5 (3V and 1A). This wavelength of light minimizes phototaxis, which is the tendency of the algal cells to move towards or away from the light. *C. reinhardtii* are sensitive to blue and green light [2]. The light of the laser is scattered from the microorganisms and the forward scattering light passes through the objective lens into the cameras. Since only scattered light is captured by the cameras, the background of the image remains dark with small dots of light indicating the locations of the cells. This principle of excluding the directly transmitted light is called dark-field microscopy. One limitation of dark-field microscopy is the low light intensity values in the image, as a limited amount of light is captured. This means that the sample requires strong illumination, which is achieved using the laser module. Two filters are placed between the laser and the flow chamber (Figure 5.4 right). A Despeckle filter removes speckle from the images whereas the polarizer is used to reduce the light intensity provided by the laser.

Pinholes
A laser-cut card with pinholes is used to increase the depth of field. The depth of field is the depth in space within which an object is sufficiently in focus of the camera view. Pinholes function as an aperture which only lets light at shallow angles pass through, blocking the diverging light rays. As the remaining light rays are more parallel to each other, a sharp image can be captured at a larger depth in space. According to Kim et al., the depth of field Δz_0 scales with $f^{\#^2}$ [48]. Here $f^{\#}$ is the f-number of the lens, which scales inversely with the diameter of the aperture. Hence, Δz_0 scales with d^{-2}, where d is the aperture diameter. The added pinholes reduce the aperture $\mathrm{d_o}$ from 7 mm of the original setup [33] to an aperture $\mathrm{d_{pinholes}}$ of 2 mm. From the scaling analysis $(\mathrm{d_o}/\mathrm{d_{pinholes}})^2 \approx 10$. This results in a depth of field that is extended from 200 μm to 2 mm [33], which covers the depth of the flow chamber. This increase in depth of field however, comes at the cost of a lower light intensity, which is resolved by using the laser for illumination.

5.2.2 Calibration of the 3D microscopic setup

Calibrating the system provides a relation between the coordinates in the 2D image planes $\mathbf{x}= [x, y]^T \in \mathbb{R}^2$, and the coordinates in 3D physical space $\mathbf{X}= [X, Y, Z]^T \in \mathbb{R}^3$. Since the camera images are all angled with respect to each other, a 3D reconstruction can be made to include depth. The system is calibrated using the calibration code written by Muller [33], which is based on a pin-hole model. During calibration, we solve the projection matrix P in $\mathbf{x} = P\mathbf{X}$.

To calculate the projection matrix P, a Lavision Calibration grid (Figure 5.7 left) is used. The calibration grid has equally spaced grid points of 100 μm. The calibration grid is placed in the microscopic setup on the location of the flow chamber during experiments. Before calibration, the pinhole card is removed such that the depth of field is shallow.

This helps with focusing all cameras to the same depth of the domain. The focus plane of the cameras is made co-planar, reducing possible Scheimpflug effects [52]. The pinhole card is placed back into the system during calibration. The calibration grid is placed at 13 different depths with respect to the cameras, all with an equidistant spacing of 0.2 mm. For each of these 13 depths, all four cameras capture an image of the dotted calibration grid. A LED light is used to illuminate the calibration grid during this process. DaVis 8.2.1 detects the dots of the calibration grid on the captured images, and generates tables of the locations on the image $\mathbf{x}$ with corresponding location in the physical space $\mathbf{X}$. With $\mathbf{x}$ and $\mathbf{X}$, an optimization algorithm is used to compute the projection matrix P for each camera individually.

The result is a calibrated domain of 2.7x2.7x2.4 mm (Figure 5.7 middle), which covers the depth of the flow chamber. The domain in the image plane is 640x640 px, resulting in a scaling of 1 px $\approx$ 4 μm. The system is calibrated for a depth of 2.4 mm, to leave room for optical distortion errors or possible misalignment of the flow chamber. By re-projecting algae location back into the image plane, the calibration can be checked (Figure 5.7 right).

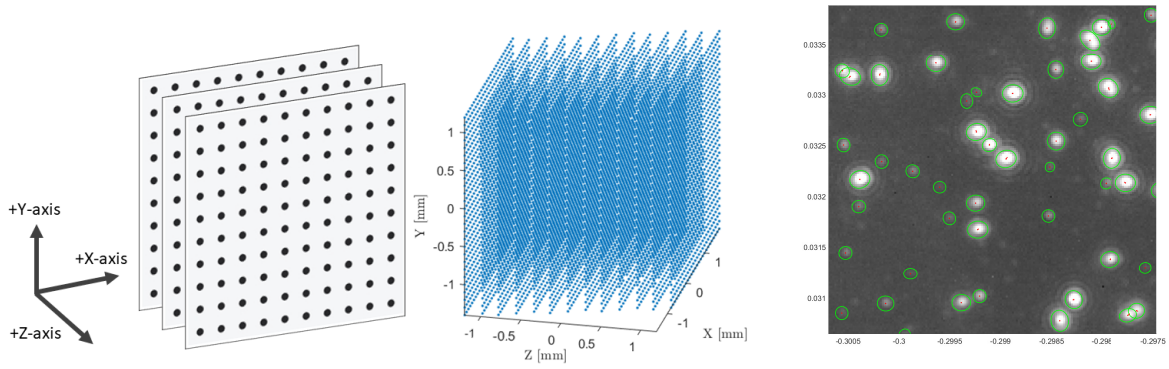

Figure 5.7: Lavision calibration target (left). Resulting calibrated domain (middle). Calibration check by reprojecting the algae location on the image (right).

5.2.3 3D Lagrangian particle tracking algorithm

After an experimental recording, the captured images are extracted in the *.im7* format from the DaVis LaVision software. These images are read with the *readimx* function from the MATLAB library. As described, each file contain 4 images of bright dots (cells) of approximately 7 pixels against a dark background. However, as the cells move and rotate, the surface from which the laser reflects, changes orientation continuously. This results in non-constant light intensity values of the bright spots. To improve on image quality, we process the images using a Mexican hat filter. This filter enhances the local maxima on the image from which the cell midpoints are estimated. The 2D locations of these cells on the image are stored for all four camera views and will be used in the tracking algorithm.

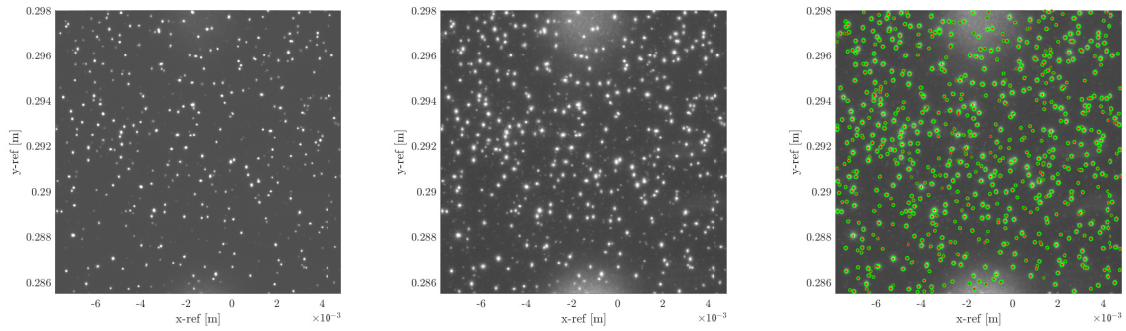

(a) Raw image (b) Pre-processed image (c) Detected algae on image

Figure 5.8: Pre-processing of the images to detect *C. reinhardtii.*

The next step is to use the detected objects in the images, and translate it to cell motility. Instead of using the commercial LaVision DaVis imaging software, an in-house developed tracking algorithm designed by Muller [33] is used. This 3D Lagrangian particle tracking algorithm works as follows:

On the pre-processed 2D images (Figure 5.8), cells are detected using local maxima of intensity values. These cell are tracked in 2D in the image plane of each camera separately using the nearest neighbour method. This method compares two consecutive images and uses a proximity search to pinpoint which cells are most likely to be the same cell on consecutive images of which 2D trajectories are created. These trajectories are compared to trajectories found in other camera views and by matching their epipolar lines, 2D motion can be translated to 3D motion. With the use of epipolar geometry, matches are found in as many camera views as possible, as it is not required to be found in all four cameras. The matching method is optimized by using a recursive divide and conquer method. This method divides the large task of matching all trajectories in different camera views into smaller tasks. This is done by first matching the long tracks, i.e. tracks that are successfully detected for many consecutive frames in the image plane. Having the trajectory of individual cells in multiple camera views, triangulation is used to translate the 2D movement into a 3D trajectory.

Kinematics

The tracking algorithm provides information on the 3D location for each detected cell on consecutive time steps. From this, 3D trajectories for all cells within the observation domain of the flow chamber are extracted. As the raw tracks can contain noise, the tracking algorithm applies a Savitsky-Golay filter and a 3^{rd} order polynomial to smoothen the trajectories. From trajectories of individual cells, the algorithm does a statistical analysis on general behaviour of the motile cells.

The Frenet-serret framework [31, 53] is used to define their local frame of reference. The Frenet-Serret framework defines a local frame at the cell by use of the local tangent vector $\mathbf{t}$, normal vector $\mathbf{n}$, and bi-normal vector $\mathbf{b}$ to the trajectory position vector $\mathbf{r}(t)$ known

as the *Frenet trihedron* **t**, **n**, **b** [31, 53]. From this frame of reference and the *Frenet trihedron*, the curvature κ and torsion τ of the trajectories are calculated [33].
From the torsion and curvature, other metrics that describe the helical motion of the *C. reinhardtii* are determined. With Equations 5.1, the radius R and pitch P of the helical motion are calculated:

$$R = \frac{\kappa}{\kappa^2 + \tau^2}, \quad P = \frac{2\pi\tau}{\kappa^2 + \tau^2} \tag{5.1}$$

Figure 5.9 shows the radius and pitch of the helical motion. Here, the red arrow indicates the net displacement by the *C. reinhardtii*, for which these variables are of interest.

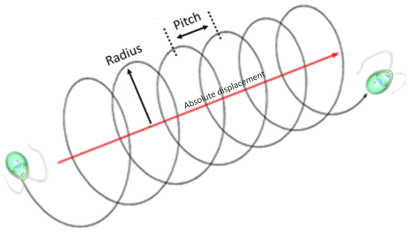

Figure 5.9: Metrics used for analysis of the helical motion.

Domain scaling
The system is calibrated with an air-air interface, whereas experiments are conducted with an air-liquid interface. Due to the differences in refractive index, a slight difference in the dimensions of the z-direction of the flow chamber can be noticed. As this has influence on not only the location of the algae, but also the velocities of the cells, this has to be taken into account. Moreover, cells are found that get stuck on the surface of the domain, which indicates the exact location of the coverslips in the domain. The dimension of the z-direction is scaled such that the reconstructed domain and the flow chamber match in size.

5.2.4 Experimental protocol

In Table 4.2, the different data sets that are used for motility experiments are provided. Each data set consists of a Newtonian and a viscoelastic sample of equal viscosity. On the day of experiments, *C. reinhardtii* cells are submerged in the fluid samples and their motility is recorded with the 3D microscopic setup. First the baseline experimental recordings are conducted in Tris minimal, followed by alternating viscoelastic and Newtonian fluid samples with increasing concentrations of PAM. This is done to limit any possible changes in conditions during the experiments.

To make sure that mostly motile cells are analyzed, some segmentation criteria are implemented to separate the healthy and motile algae from non-motile algae that move along with the background flow. The effect of different levels of segmentation are investigated. Trajectories with a median velocity higher than 25 μm/s, and a minimum track length of 200 frames (10 s) are further analyzed.

5.3 Beating Frequency analysis in 2D

To analyze the beating frequency of the *C. reinhardtii*, the relevant time scale must be considered. From literature, a beating frequency of approximately 50 Hz is expected [17, 23]. With this beating frequency, the 3D microscopic setup is not capable of meeting the aliasing requirement of $f_{sampling} \geq 2f_{experiment}$. Therefore, to analyze the beating frequency, a different microscopic setup is used. This setup consists of a single sCMOS LaVision Camera with an adjustable shutter, mounted on an inverted microscope. A limited image size is chosen (2560x432 px), which presents the opportunity to capture images at a higher frame rate. An example of a captured image of the *C. reinhardtii* is shown in Figure 5.10. By capturing more narrow images, the shutter of the camera has less distance to cover. This extends the mechanical limitation to the maximum frame rate. For these recordings, the sCMOS LaVision camera is set to a frame rate of 500 fps. Not only does this meet the aliasing requirement for frequency, but also the aliasing requirement for amplitude $f_{sampling} \geq 10f_{experiment}$, which could provide extra insights. The motile microorganisms are submerged in Newtonian and viscoelastic samples and given some time to acclimatize before a recording is made. A droplet of the selected sample with *C. reinhardtii* cells is placed on a glass slide and placed in the inverted microscope. The motile cells are extracted from Culture 1 (February 23$^{\text{rd}}$. For each different fluid sample, as indicated in Table 4.2, 3 recordings of at least 500 frames are made of multiple motile algae. For each rheologically distinct fluid, roughly 10 motile cells are analysed.

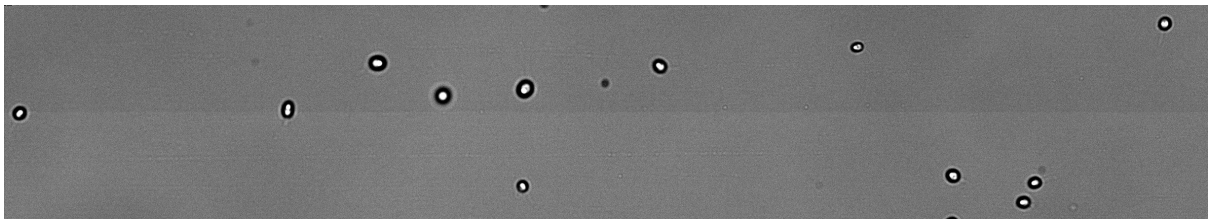

Figure 5.10: An example of an image captured by the inverted microscope.

From the cameras, images are extracted in the *jpg* format and processed with the use of MATLAB. The tracking algorithm of Muller [33] has been modified such that the cells are only detected and tracked in 2D. From the modified tracking algorithm, we obtain the trajectories of the detected algae on the 2D image. Since the frame rate is 25 times higher than the frame rate used in the 3D microscope, additional information is obtained such as the forward and backward motion of the cell. From this forward and backward motion, formally known as the power and recovery stroke, we can extract the characteristic beating frequency of the *C. reinhardtii*. As the frame rate of the cameras is known, and the displacement of the cells in between frames measured, the magnitude of the velocity vector is easily calculated. To extract the beating frequency, we analyze the velocity profile and in particular its periodicity. By using MATLAB's Fourier transformation, the dominant frequencies can be obtained.

6 | Results of motility measurements

This chapter describes the results of the motility experiments with *C. reinhardtii* in Newtonian and viscoelastic fluids. During this experimental thesis, a total of eight cultures have been made. Three of the cultures were used to get acquainted with the protocol for tracking experiments in the 3mE MicroLab. One culture was discarded as the polymer did not have the correct rheological characteristics. Two cultures were prematurely discarded due to low motility or cell cluttering. Two cultures were used to perform the analyses on, based on the overall culture motility. The cultures that have been used for analysis originate from the 23$^{\text{rd}}$ of February (Culture 1) and 26$^{\text{th}}$ of February 2021 (Culture 2).

6.1 Motile and non-motile cells

To statistically analyse the data obtained from the tracking algorithm, motile and non-motile cells should be separated. As we wish to do our analysis only on the motile and healthy microorganism, two segmentation criteria is applied. First, a minimum track length is chosen. The upper bound is governed by the size of the observed domain (2700x2700 μm) and an estimate on the highest observed velocities of approximately 200 μm/s. If one highly motile cell swims straight between both edges of the domain, it would take roughly 13.5 s or 270 frames to pass the field of view. If the minimum track length higher than 270 frames, these trajectories would be excluded from the analysis. By analysing the overall velocities of the culture (Figure 6.2a-f) and analysing individual trajectories (Figure 6.4), a minimum track length of 10 seconds or 200 frames is chosen.

Small temperature gradients in the flow chamber generate natural convection, which creates a background flow. Due to this background flow, even non-motile cells suggest motility, indicated by their median velocity equal to this background flow. The velocity histogram shows a clear peak at median track velocities lower than 25 μm/s, indicated with the dashed line in Figure 6.2e. For median track velocities higher than 25 μm/s, roughly a normal distribution is found. As the data from the tracking algorithm did not show a normal distributed result for all data sets (Appendix A.1), an approach of median values in combination with 25$^{\text{th}}$ and 75$^{\text{th}}$ percentiles is used to characterise the data.

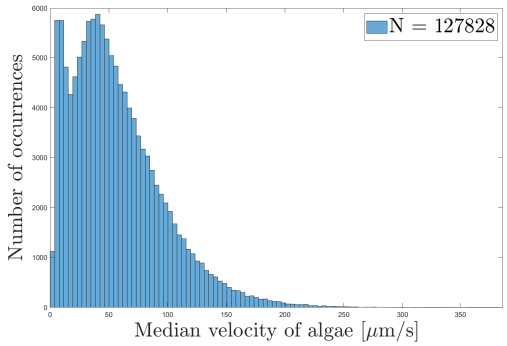

6.2 (a) Raw data:
No segmentation criteria.

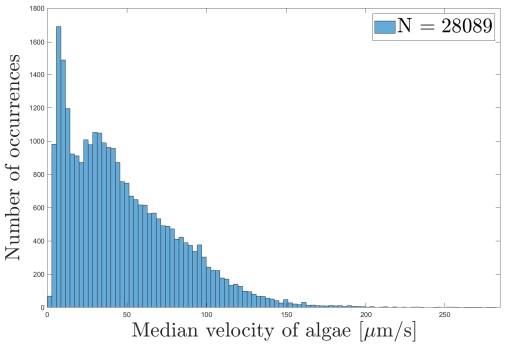

6.2 (b) Minimum track length:
25 frames, (1.25 s).

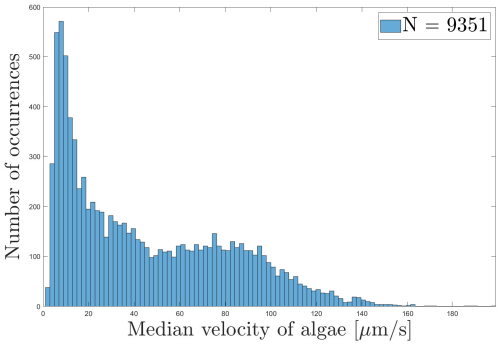

(c) Minimum track length: 50 frames, (2.5 s).

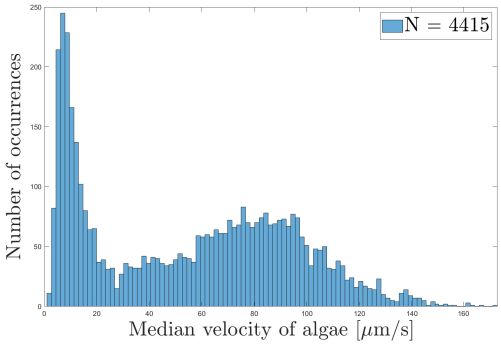

(d) Minimum track length: 100 frames, (4 s).

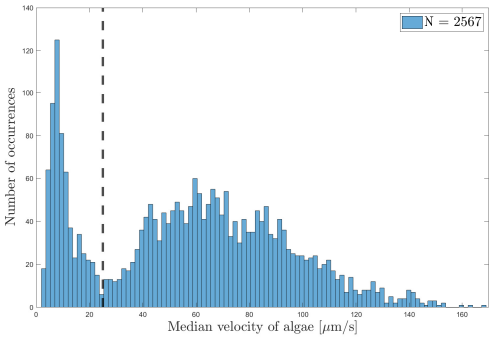

(e) Minimum track length: 200 frames, (10 s).

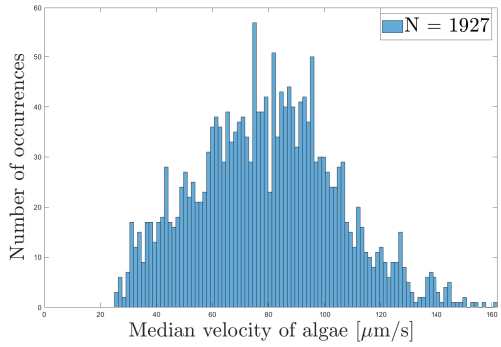

(f) Minimum track length and velocity: 200 frames (10 s) and median velocity 25 μm/s.

Figure 6.2: Velocity histograms with step wise increase of segmentation criteria to separate motile and non-motile cells. Minimum track length increase from Figure a to f.

Figure 6.3 shows the resulting velocities of Culture 2 in Tris minimal, in which the segmentation criteria are applied.

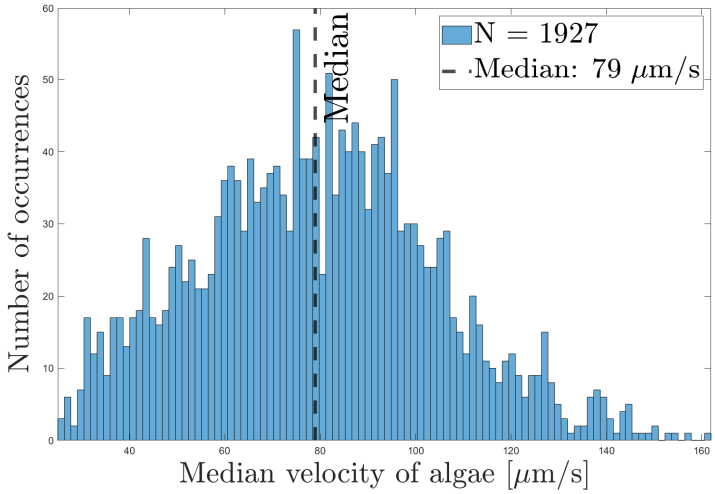

Figure 6.3: Velocity histogram of motile cells in the baseline Tris of Culture 2.

To provide more insights in motile and non-motile cells, the velocity histogram of a typical motile cell (Figure 6.4 left) and of a typical non-motile cell (Figure 6.4 right) are shown with their respective trajectories in Figure 6.5. Figure 6.4 (left) shows the distribution around the median velocity for this specific trajectory of a motile cell. This median velocity is selected as the characteristic velocity of this trajectory for further analysis. Figure 6.5 shows the trajectory of the motile cell, showing both run and tumble behaviours [14]. Figure 6.4 (right) shows a velocity profile of a non-motile cell, that has a non-zero median velocity as it moves along with the background flow. In the trajectory of this non-motile cell (Figure 6.5 right), a straight line is observed with outliers due to small errors when detecting and matching the algae in different image planes.

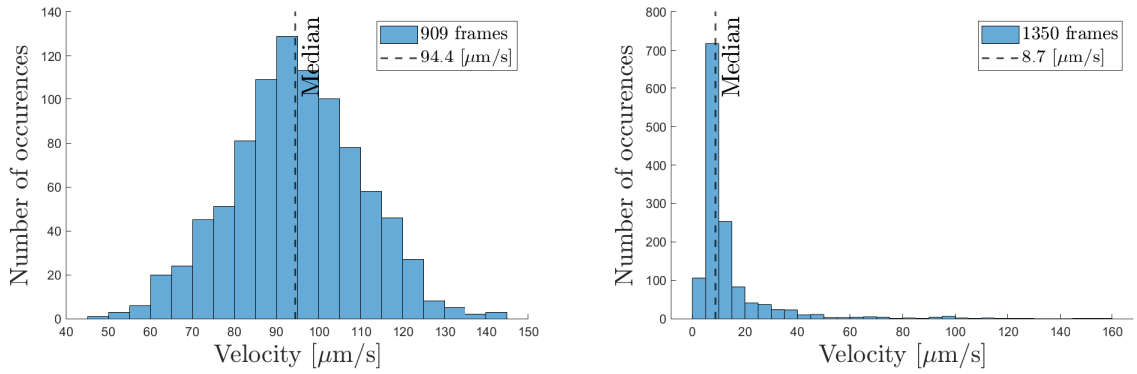

Figure 6.4: The velocity histogram of a motile cell (left) and the velocity histogram of a non-motile cell (right).

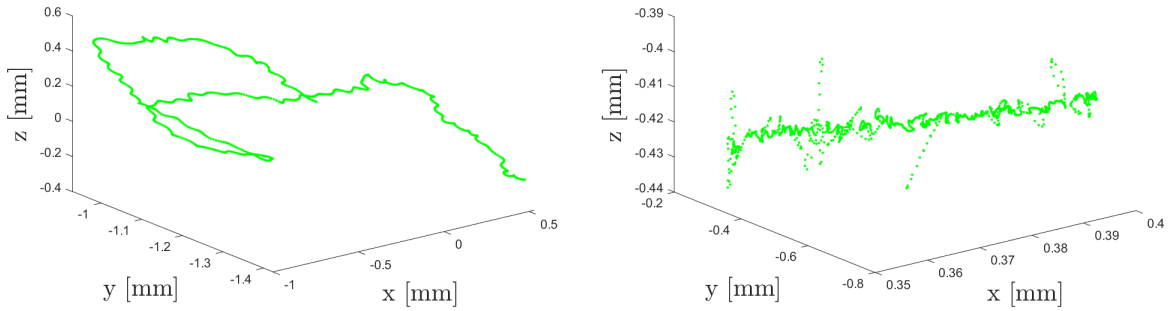

Figure 6.5: A trajectory of a motile cell (left) and a trajectory of a non-motile cell (right).

6.2 Velocity analysis

The first metric considered is the velocity of the cells. The data from the tracking algorithm originates from the images captured by the 3D microscopic setup. In these 3D analysis, the forward and backward motion of the cells are not considered, because the frame rate is not high enough to observe this phenomenon. The cell velocity over multiple motility sequences are averaged. Each experimental recording consists of many individual trajectories of which the median characteristic velocities are determined. The characteristic velocities of the trajectories of Culture 1 are plotted in a histogram in Figure 6.6. The same is done for all experimental conditions, of which the velocity histograms are provided in Appendix A.1.

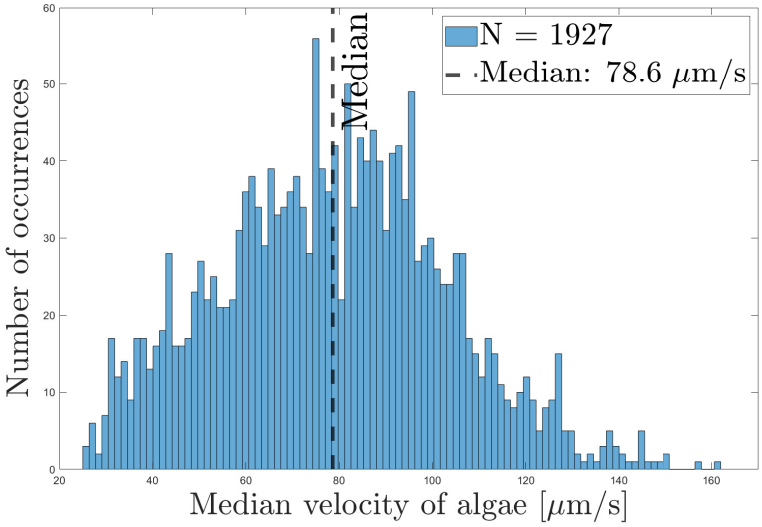

Figure 6.6: Velocity histogram of trajectories in Baseline Tris of Culture 1.

Figure 6.7 shows the median velocity of all cells for a given time step (frame). The mean velocity over all time steps (5 minutes, 6000 time steps) is highlighted in red. The difference in mean velocity values in Figure 6.7 in comparison with the median velocity per trajectory in Figure 6.6 originates from the fact that not all trajectories are equally long, but weigh equally in the velocity histogram. However, with the method of taking the median velocity for each trajectory individually, all tracks are considered equally important. In the method of analysing per time step, long trajectories have more influence on the final result than short trajectories. The second method shows that the average velocity within the cell culture is maintained during the recording and not influenced by the experimental conditions.

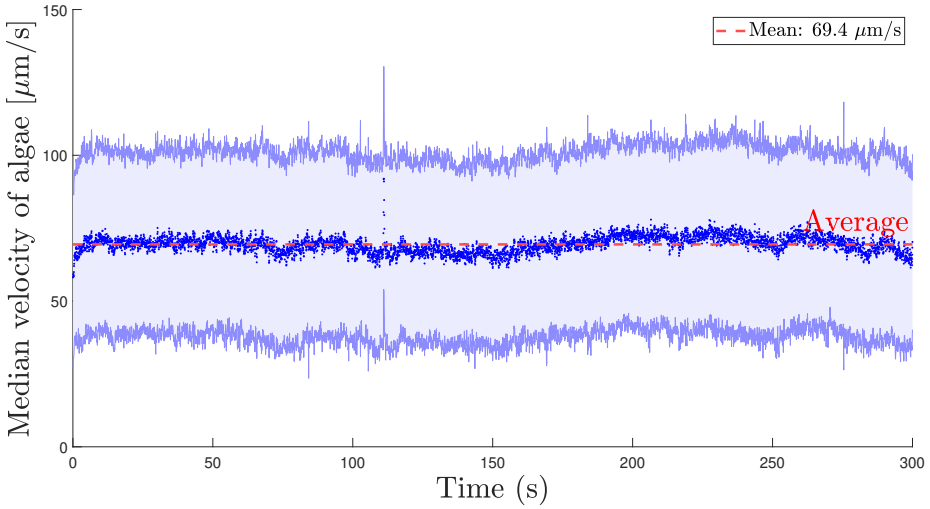

Figure 6.7: Median velocities per time step for full recording (6000 frames/300 s) in Baseline Tris of Culture 1.

Figures 6.8 and 6.9 show boxplots of the velocities of *C. reinhardtii* cells, found in the experiments with Culture 1 and Culture 2 respectively. The red line indicates the median velocity, whereas the blue box indicates the 25^{th} and 75^{th} percentiles for the data sets of the cultures. The black dashed lines indicate the range of the velocities with the red crosses indicating outliers of the data set. First, the cell velocities in the baseline fluid of Tris minimal are shown, followed by the velocities found in a viscoelastic and a Newtonian fluid. In the resulting boxplots for both cultures, it is apparent that velocities in a Newtonian fluid tends to decrease at higher concentrations. This phenomenon is not visible for the velocities found in viscoelastic samples.

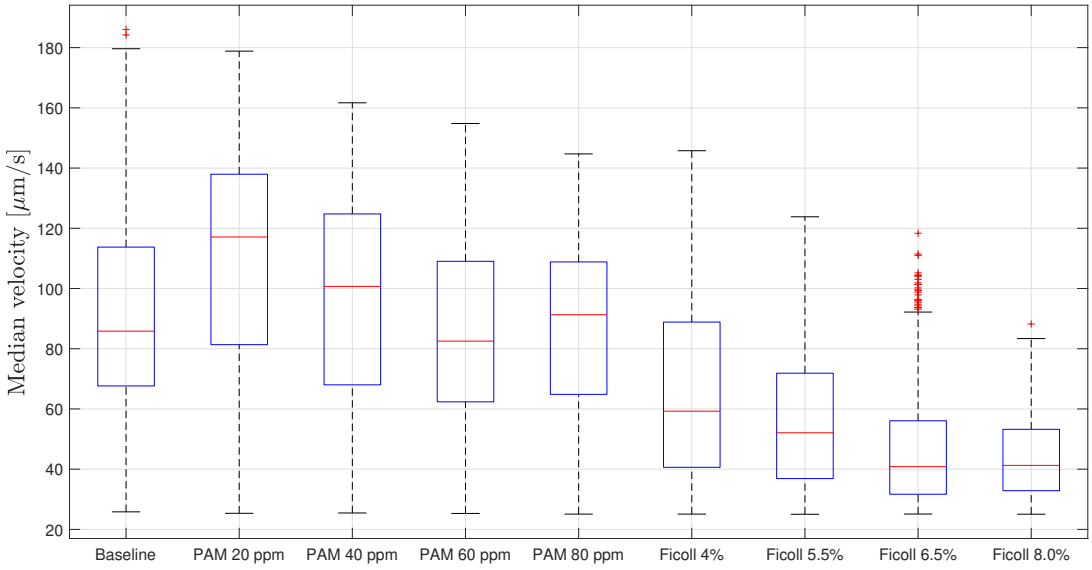

Figure 6.8: Boxplot with the median velocity, and 25^{th} and 75^{th} percentiles, respectively for the different data sets of Culture 1.

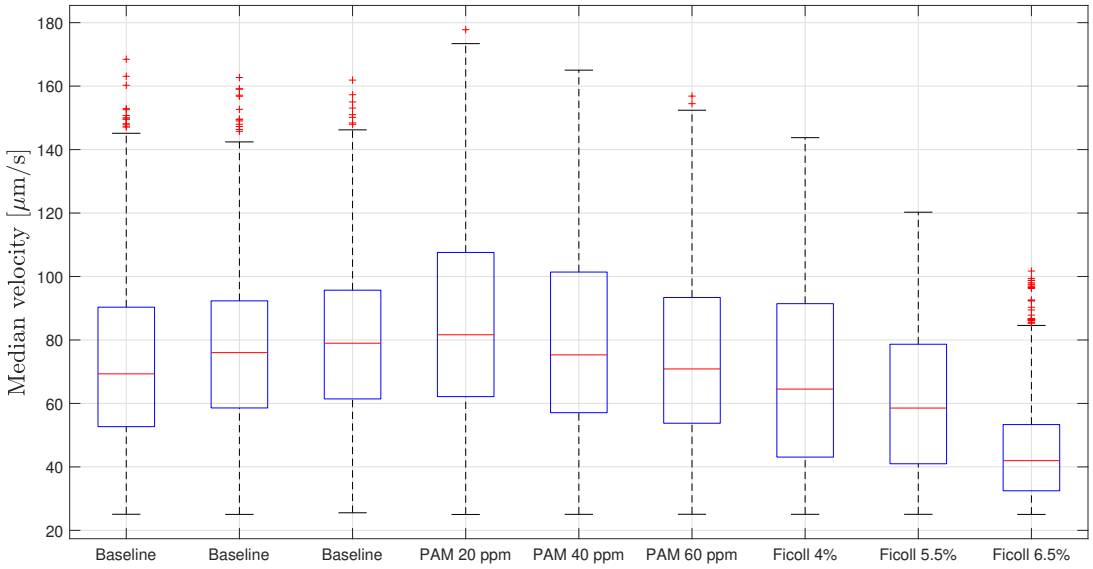

Figure 6.9: Boxplot with the median velocity, and 25$^{\text{th}}$ and 75$^{\text{th}}$ percentiles, respectively for the different data sets of Culture 2.

Figure 6.10 shows the resulting median velocities as a function of the viscosity for both the motility in viscoelastic and Newtonian fluids. The vertical bars indicate the 25$^{\text{th}}$ and 75$^{\text{th}}$ percentiles of the velocities found. It shows a steady decline in viscosity values for motility in Newtonian fluids, up to 50%. The resulting velocities observed for motility in viscoelastic fluids remain rather constant over the range of viscosities. The median velocities as a function of the updated Deborah number will be provided in Section 6.5.

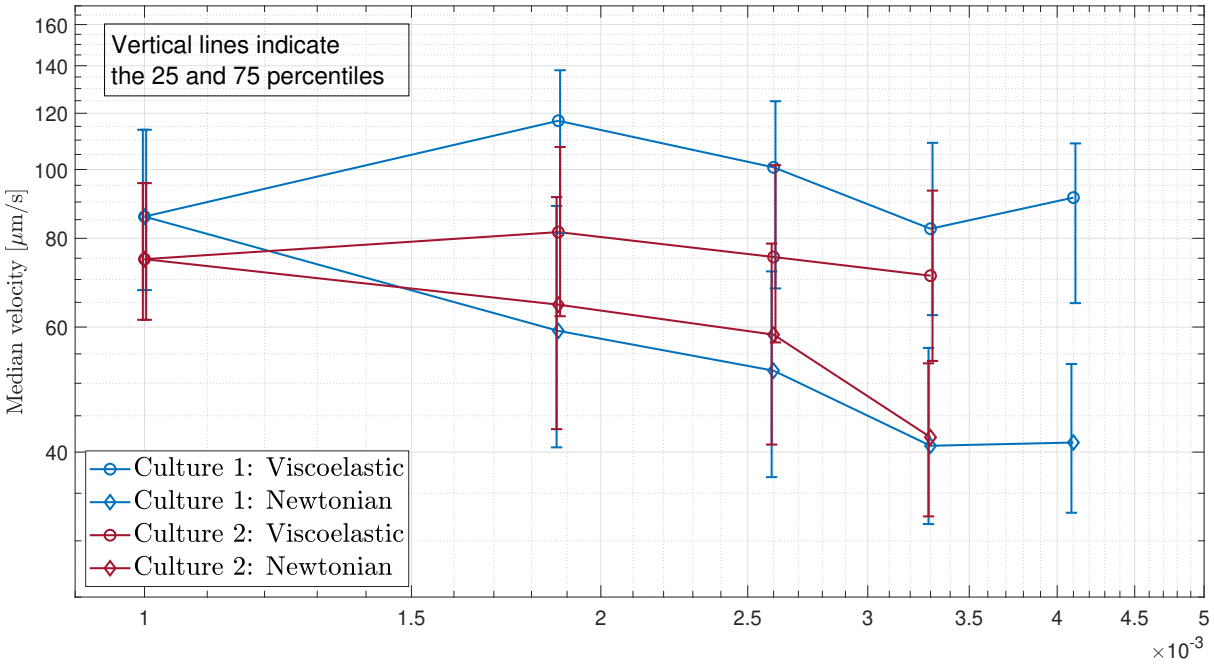

Figure 6.10: Median velocities in Newtonian and viscoelastic fluid as a function of viscosity with 25$^{\text{th}}$ and 75$^{\text{th}}$ percentiles.

6.3 Helical motion analysis

Figure 6.11 shows two typical examples of trajectories of motile microorganisms executing helical motions.

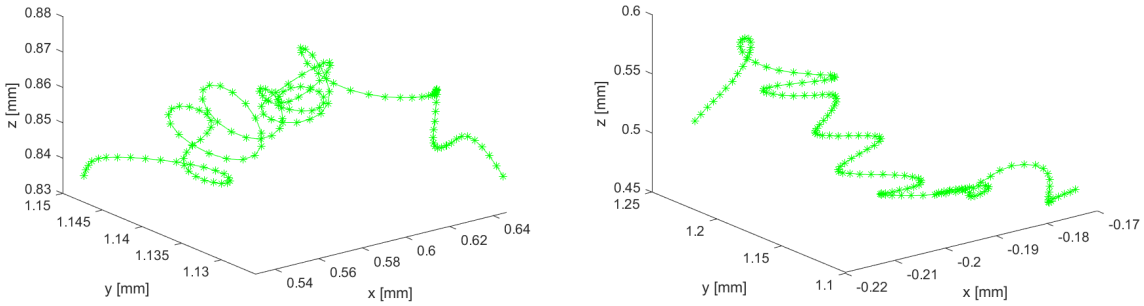

Figure 6.11: Examples of helical motion of *C. reinhardtii*.

The helical motion of *C. reinhardtii* cells is analysed according to the metrics: cell velocity V, pitch P and radius R (Figure 5.9) as described in Section 5.2.3. To describe the behaviour of these cells, the joint distributions of the metrics are plotted (Figure 6.12). The plots of joint distributions for all data sets are shown in Appendix A.2.

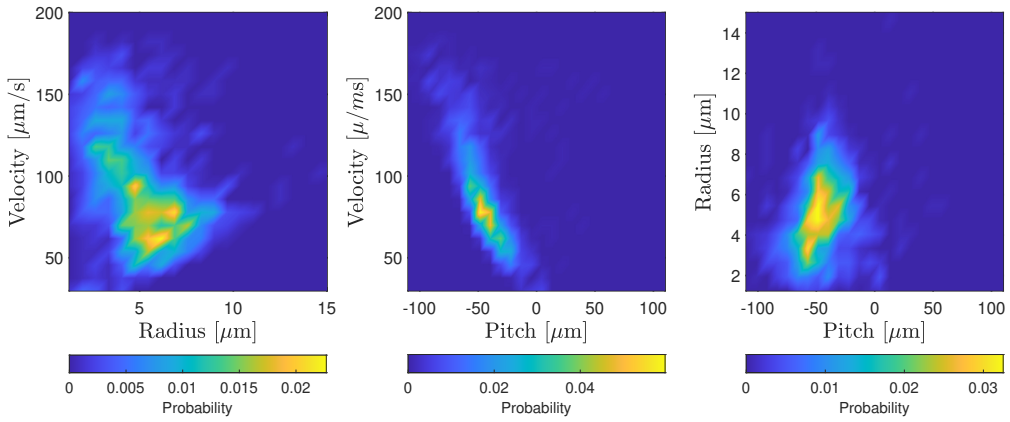

Figure 6.12: Example of joint histograms to analyse the helical motion.
Velocity & radius (left), velocity & pitch (middle), radius & pitch (right).

The median values for the considered metrics for all data sets are given in Table 6.1, with the 25^{th} and 75^{th} percentiles. The median values for radius of the helical motion shows to be consistent for all data sets, independent of the level of viscosity or viscoelasticity. The radius is found to be ± 4 μm, which is approximately half of a cell body diameter. The pitch of the motile cells seems to be dependent on fluid elasticity, as differences in pitch between motility in a Newtonian fluid and viscoelastic fluid are apparent. This change in pitch due to fluid elasticity is plotted in Figure 6.13. The median values for

the pitch ranges between minus 60 to minus 10 μm, which are approximately 6 and 1 cell body diameters, respectively. The minus sign indicates a left handed chirality of the helical motion, which is observed for most cells in both cell cultures. More than 94% of the motile cells show left handed chirality, and this showed to be independent of the fluid elasticity.

Data set	Radius [μm]			Pitch [μm]			Chirality [%]	
Percentile	25%	50%	75%	25%	50%	75%	+	-
Baseline	3.6	4.9	6.3	-57	-47	-35	1.9	98.1
PAM 20 ppm	2.4	3.3	4.6	-69	-53	-37	2.9	97.1
Ficoll 4.0% wt	3.1	4.1	5.2	-43	-27	-13	3.4	96.6
PAM 40 ppm	2.4	3.4	4.6	-59	-43	-24	4.1	95.9
Ficoll 5.5% wt	3.1	4.1	5.3	-34	-20	-8.0	3.5	96.5
PAM 60 ppm	3.4	4.5	5.7	-57	-44	-31	1.6	98.4
Ficoll 6.5% wt	2.7	3.6	4.7	-24	-13	-5.0	5.5	94.5
PAM 80 ppm	2.9	4.0	5.2	-60	-44	-29	2.7	97.3
Ficoll 8.0% wt	2.7	3.6	4.7	-24	-13	-6.0	5.5	94.5

Table 6.1: Overview of metrics of the helical motion of Culture 1 (radius, pitch, chirality).

Data set	Radius [μm]			Pitch [μm]			Chirality [%]	
Percentile	25%	50%	75%	25%	50%	75%	+	-
Baseline 1	2.7	3.5	4.4	-45	-36	-24	1.4	98.6
Baseline 2	2.4	3.2	4.1	-43	-38	-26	2.3	97.7
Baseline 3	2.3	3.1	4.0	-44	-37	-26	2.0	98.0
PAM 20 ppm	3.1	4.2	5.5	-50	-39	-26	3.2	96.8
Ficoll 4.0% wt	3.4	4.4	5.6	-42	-27	-11	3.3	96.7
PAM 40 ppm	3.0	4.1	5.4	-49	-37	-25	1.5	98.5
Ficoll 5.5% wt	3.1	4.0	5.2	-39	-26	-12	2.6	97.4
PAM 60 ppm	3.3	4.3	5.6	-48	-36	-24	1.6	98.4
Ficoll 6.5% wt	2.7	3.5	4.3	-24	-15	-6	4.2	95.8

Table 6.2: Overview of metrics of the helical motion of Culture 2 (radius, pitch, chirality).

Figure 6.13 provides an overview of the pitch of the motile cells as a function of viscosity for both viscoelastic and Newtonian samples. The median pitch as a function of the updated Deborah number will be provided in Section 6.5.

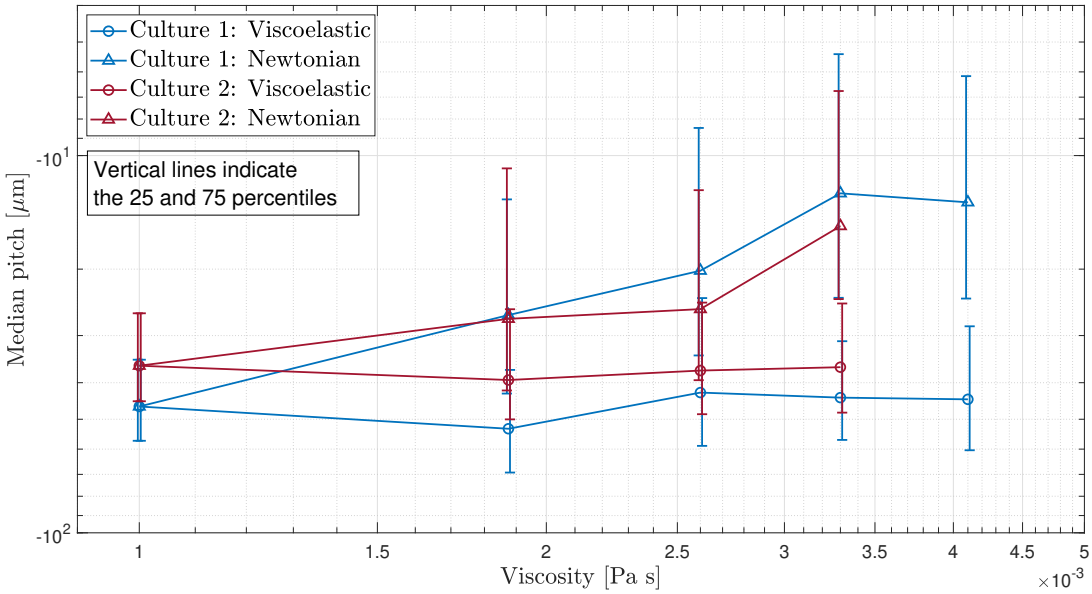

Figure 6.13: Median pitch of the helical motion as a function of viscosity with 25$^{\text{th}}$ and 75$^{\text{th}}$ percentiles.

6.4 Beating frequency analysis

The beating frequency is analysed from the forward and backward motion of the *C. reinhardtii* cell using 2D data with high frame rates. In the work of Qin et al. [17], the orientation of the cell body was observed during the measurements, making it possible to distinguish forward and backward motions and extract the beating frequency. In our study, the cell locations are detected with the modified tracking algorithm without information on the orientation of the cell body. The information provided by the modified 2D tracking algorithm consists of the algae location and the resulting velocities on each time step. The magnitude of the velocity vector is used to perform signal analysis on, as the velocity signal showed periodicity which can be linked back to the beating frequency. The cell has a velocity both in the forward en backward motion, resulting in a large and a small peaks in the velocity signal which can be seen in Figure 6.15 (top). Figure 6.14 shows a cell that becomes motile or reorientates itself into the 2D image plane, as shown by the increasing amplitude of the signal. Figure 6.15 shows a cell that is already motile in the image plane. Roughly 10 trajectories are considered per data set to determine the beating frequencies.

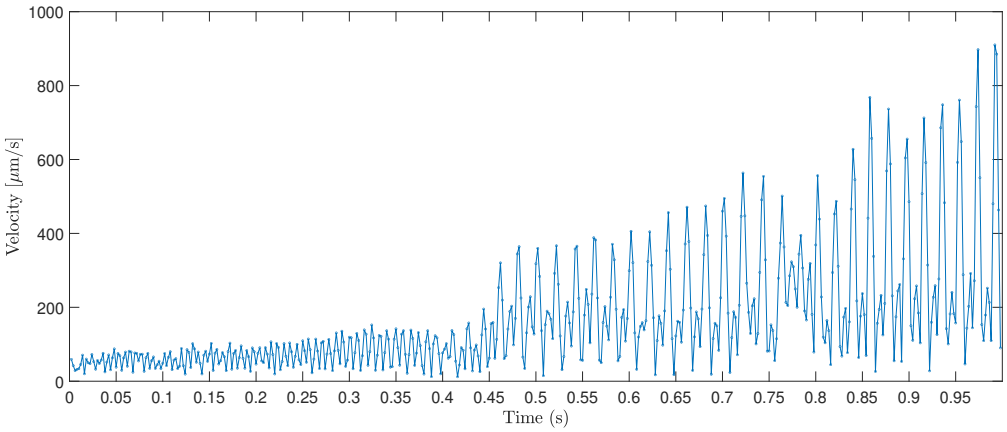

Figure 6.14: Magnitude of velocity signal for a cell that becomes motile or rotates into the 2D plane.

In the frequency domain, besides beating frequency, also zero frequency (not shown in figure) and the second harmonic is present. The second frequency peak occurs, among others because the magnitude of the velocity signal is taken. From the graph in the frequency domain, we extract the first dominant frequency for all samples of different viscosity and viscoelasticity. In the Appendix A.3, more examples of velocity signals and frequency spectra of cells can be found.

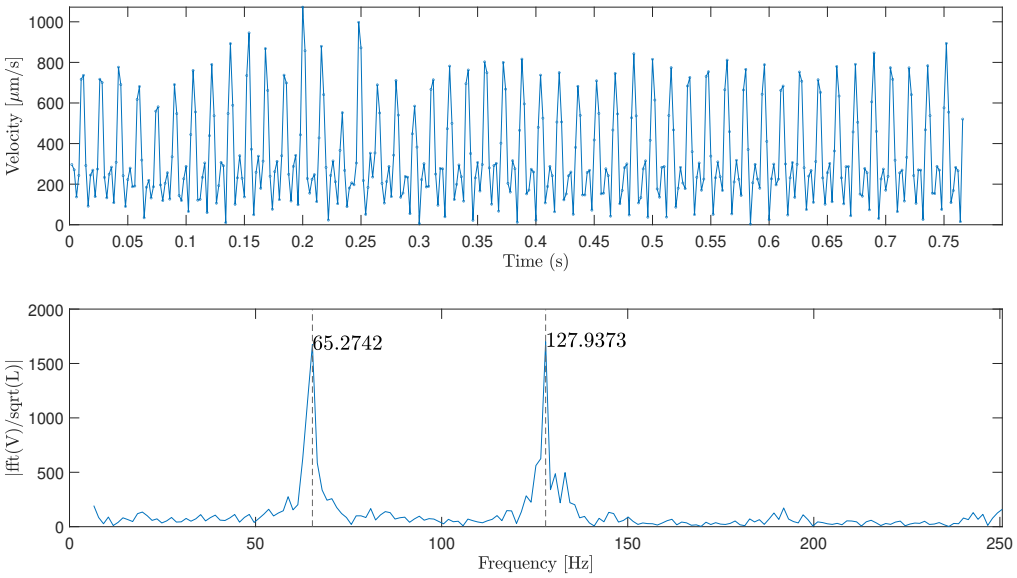

Figure 6.15: Magnitude of the velocity signal for a cell that is motile (top) with the frequency spectrum (bottom) in the baseline of Tris minimal.

For each data set, the average dominant beating frequency is plotted against the viscosity of the sample. Here, we distinguish the beating frequency in Newtonian and Viscoelastic samples, with the beating frequency in Tris minimal as a baseline.

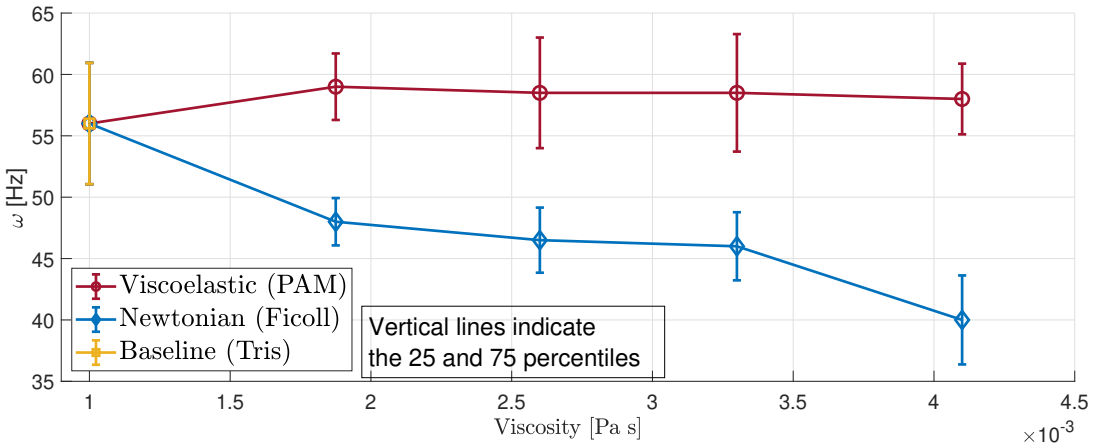

Figure 6.16: Beating frequency of the *C. reinhardtii* as a function of viscosity.

With the resulting beating frequencies for viscoelastic samples, the Deborah numbers calculated from literature can be updated. An updated overview of the rheological information related to Deborah numbers is given in Table 6.3. Deborah number is calculated with $\mathrm{De} = \omega\lambda$.

Data set	PAM [ppm]	λ [s]	ω [Hz]	De [-]
Baseline	0	0	56.2±4.9	0
1	20	0.02	59.0±2.7	1.2±0.05
2	40	0.06	57.5±4.5	3.5±0.27
3	60	0.09	59.3±4.8	5.3±0.43
4	80	0.12	58.0±2.9	7.0±0.35

Table 6.3: Updated Deborah numbers with analysed beating frequencies.

6.5 Motility results with updated Deborah number

The results obtained from the motility analyses can now be plotted as a function of the updated Deborah numbers. Figure 6.17 provides the normalized beating frequency, where ω_V denotes the beating frequency of the *C. reinhardtii* in a viscoelastic fluid and ω_N the beating frequency in a Newtonian fluid. Figure 6.17 shows a noticeable increase in normalized beating frequency with increasing Deborah numbers. The beating frequency for the baseline data set in Tris minimal is shown in yellow, at a De = 0 (Newtonian).

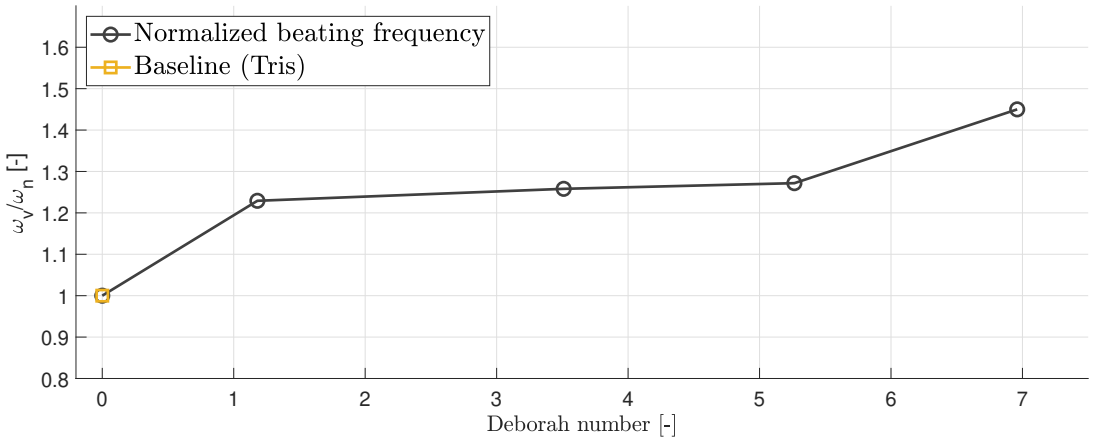

Figure 6.17: Beating frequency of the *C. reinhardtii* as a function of the Deborah number.

Figure 6.18 shows the normalized velocity of the *C. reinhardtii* cells for both Culture 1 and Culture 2, where V_V denotes the velocity of the *C. reinhardtii* in a viscoelastic fluid and V_N the velocity in a Newtonian fluid. An sudden increase of normalized velocity is noted at De = 1 (slightly viscoelastic), indicating an increase in velocity even at the lowest concentration of PAM and thus the lowest elasticity level. This velocity slightly increases with higher Deborah number for Culture 1, but not as extensive as the increase from De = 0 to De = 1 . For Culture 2, this velocity increase from De = 0 to De = 1 is less noticeable. However, for Culture 2 the velocity increases more for higher values of Deborah.

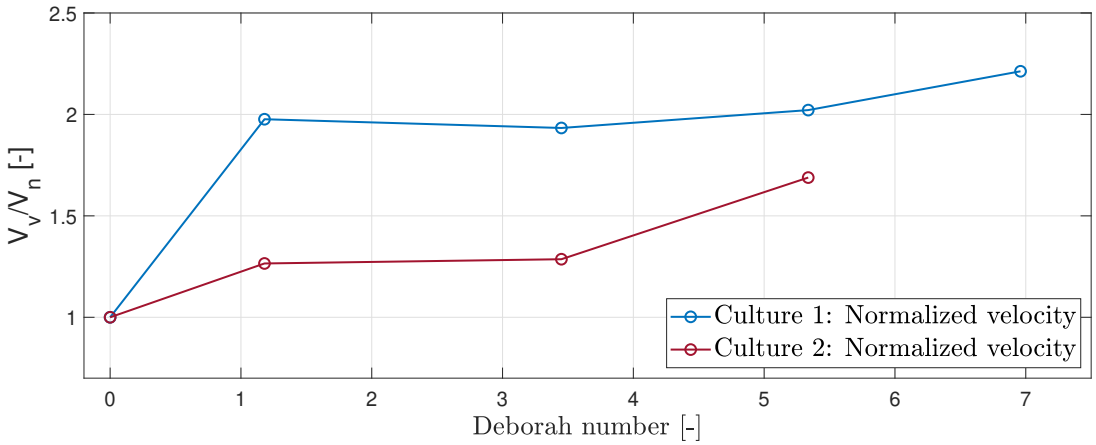

Figure 6.18: Median velocities of the trajectories as a function of the Deborah number.

Figure 6.19 provides the normalized pitch as function of the updated Deborah number, where P_V denotes the pitch of the *C. reinhardtii* in a viscoelastic fluid and P_N the pitch in a Newtonian fluid. Similar increases in pitch with an increasing Deborah number were found for both Culture 1 and Culture 2.

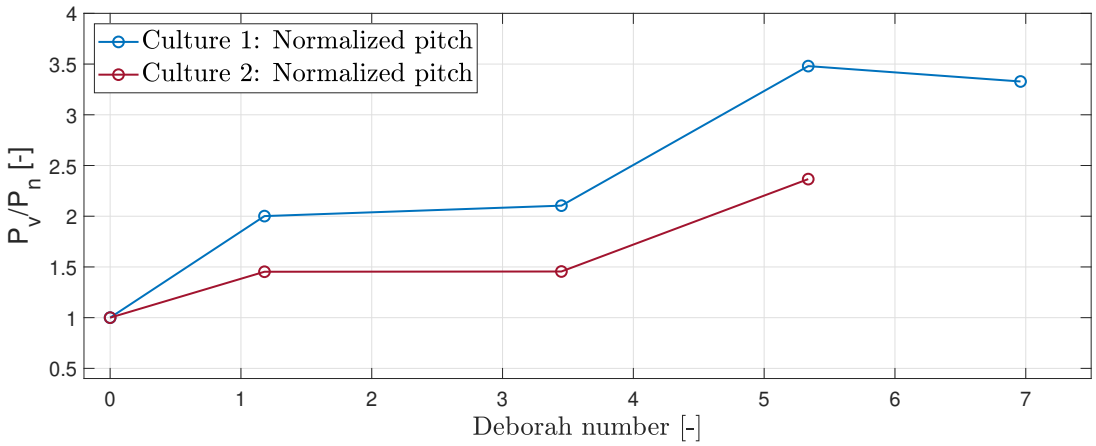

Figure 6.19: Median pitch of the helical motion as a function of the Deborah number.

7 | Discussion & Conclusion

In this research we analysed velocities of motile *C. reinhardtii* cells in a 3D environment, in viscoelastic and Newtonian fluids of various levels of viscosity and elasticity. This research distinguishes from published literature by combining motility research in an unconstricted 3D environment with viscoelastic fluids. The results of our experiments show that the velocity of *C. reinhardtii* reduces in a Newtonian fluid when viscosity increases, whereas the velocity in a viscoelastic fluid is hardly influenced by increasing fluid elasticity and viscosity levels. Similar trends were found for the magnitude of the pitch, describing the helical motion. The beating frequency of the motile cells, analysed using an inverted microscope, shows a reduction in Newtonian fluids at higher viscosities whereas a slight increase is observed in a viscoelastic fluid independent of the viscosity.

Comparing velocity and beating frequency
Both the velocity and the beating frequency of motile *C. reinhardtii* were observed by separate measurements for cells originating from Culture 1, submerged in fluids of various levels of viscosity and elasticity. The results of our study shows that the change in velocity in a Newtonian fluid can for a large part be explained by the change in beating frequency, when comparing the red circles in Figure 7.1 (left) and Figure 7.2 (left). In a viscoelastic fluid, the beating frequency increases slightly (Figure 7.2 middle), but remains constant for values of Deborah larger than 1, which could partially explain the fact that no decrease in velocity is observed. At a Deborah number of 1, the relaxation time of the fluid is equal to the time a motile cell takes to perform one beat. At De < 1, the fluid around the cell has time to relax before the next beat starts. For values of De > 1, the elastic stresses within the fluid will not be dissipated yet.

The differences between velocities and beating frequencies found in Newtonian and viscoelastic fluids, could be explained by a difference in swimming efficiency for the gaits found in both types of fluids respectively. Li et al. [32] simulated the Newtonian and viscoelastic swimming gait of *C. reinhardtii* cells in Newtonian and viscoelastic fluids. They showed that elastic properties of a fluid modifies the stroke kinematics of cells in a way that the efficiency of the swimming gait increases [32]. The higher swimming efficiency can prove to be beneficial at higher viscosities, where more viscous drag is present. In the numerical study of Li et al., it was found that velocities are higher in Newtonian fluids, but these high velocities could only be reached under the circumstances that much more power (up to 150% as shown in Figure 2.3 left). Assuming that our cells use the maximum power in each rheologically distinct fluid, it is to be expected that the velocity will reduce more when viscosity increases in a Newtonian fluid than in a viscoelastic fluid, as the power required to maintain the same velocities may not be available. That the maximum power is reached in Newtonian fluid with high viscosities is also supported by our findings that the beating frequency goes down at higher viscosities, only in the Newtonian fluids. Moreover, Li et al. reported a coasting effect when elasticity was present. They showed that the elastic memory effect, resulted in coasting of the cells, i.e. forwards movement of

the cell even when the flagella stop moving. This would increase the average velocity of cells in a viscoelastic fluids, whereas the phenomenon would not be present in Newtonian fluids.

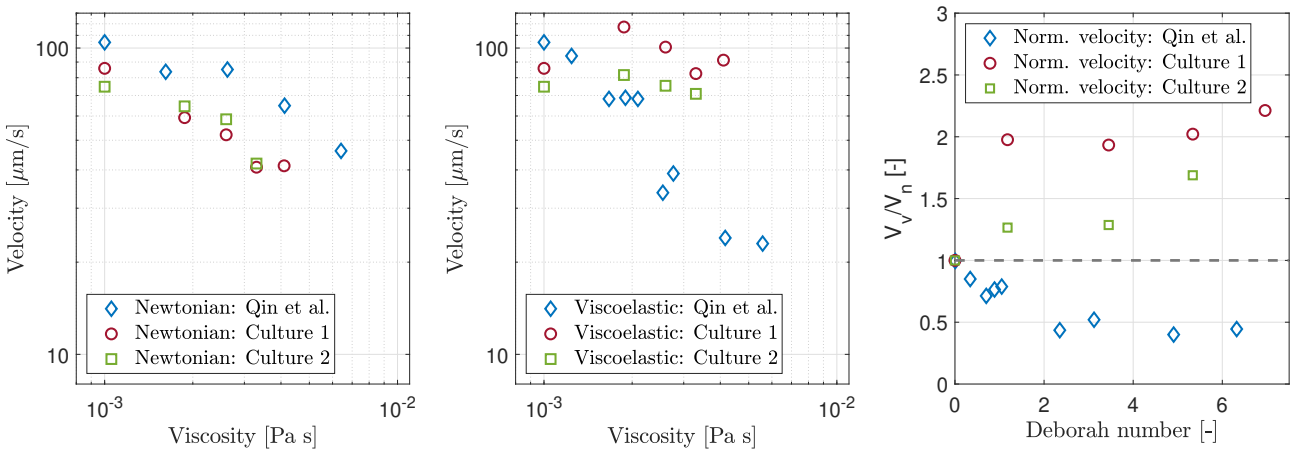

Figure 7.1: Comparison of the velocities found in this study with the velocities found by Qin et al. [17]. Newtonian (left), Viscoelastic (middle), Normalized (right).

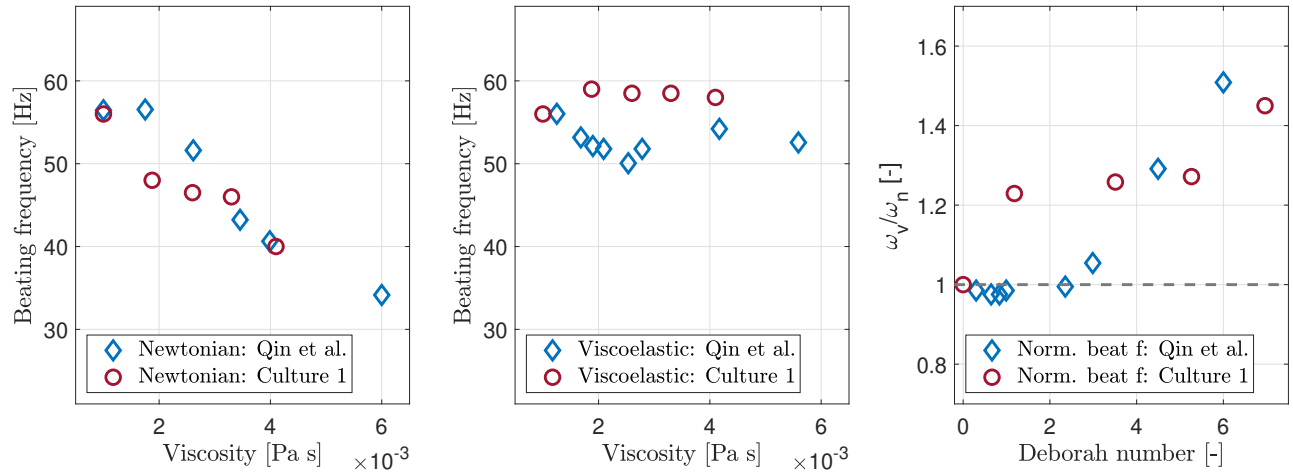

Figure 7.2: Comparison of the beating frequencies found in this study with the beating frequencies found by Qin et al. [17].
Newtonian (left), Viscoelastic (middle), Normalized (right).

Comparing velocity and beating frequency to findings in literature

As indicated in Section 2.3, Qin et al. [17] performed similar measurements, but limited the motility of the cells to a quasi-2D plane. Our findings, that velocity in viscoelastic fluid is higher than in Newtonian fluid with higher viscosities is not in agreement with the finding of Qin et al. as shown in Figure 7.1. Qin et al. found a reducing velocity in both viscoelastic and Newtonian fluids for increasing viscosities with a larger reduction in viscoelastic fluids. In their study, the difference in velocities cannot be explained by a change in beating frequency. They show a reduction in velocities for viscoelastic fluids

whereas the beating frequency is hardly influenced (blue diamonds in Figures 7.1 middle and 7.2 middle). They argue that due to elastic effects the displacement during the power stroke and recovery stroke are both enhanced, but a larger increase is observed in the recovery stroke, resulting in a decreasing net displacement of the cell per beat. To find the origin of the discrepancy between the results, differences between experimental conditions are analysed.
Some experimental differences are for example:

- **2D versus 3D confinement**. Qin et al. investigated the behaviour of *C. reinhardtii* in a quasi-2D environment using a thin liquid layer. This layer has a width approximately 20 μm which is roughly twice the cell body size. The natural behavior of freely swimming microorganisms is truly 3D, as described by Crenshaw [24]. In the study of Qin et al. motile cells swim constantly in proximity of an air-liquid interface, acting as a confinement. This quasi 2D plane limits this motility, possibly restricting flagellar movement. As indicated by Sudha [34], velocities of motile *C. reinhardtii* cells reduces when entering a contact region (defined as 20 μm). In our study the cells are free to move in 3D space and their behaviour showed to have different characteristics. We observed a similar velocity decrease in Newtonian fluids of increasing viscosity. However, we did not find similar results when elastic properties were present in the fluid. The presence of these polymers could influence the motility either directly or the viscoelastic fluids behave differently near liquid-air interfaces. When there is flow, induced by the cells or thermal convection, polymers might tend to go more to the center of the film, creating a region of higher polymer concentration and mostly Tris at the interface. The thickness of this Tris layer might be dependent on viscosity. This could create a different apparent viscosity in the middle layer then expected on the basis of concentrations. Pullers microorganisms, such as *C. reinhardtii*, tend to reorientate themselves away from solid confinements [54]. Li et al. [55] mentioned that this reorientation effect is hindered in viscoelastic fluids due to a polymeric torque. This effect may also be of influence at a liquid-air interface.

- **Individual tracks** In the study of Qin et al., individual tracks have been carefully selected and observed. Only motile cells, that performed a regular stroke pattern where both flagella beat synchronously within specific velocity ranges, were selected, resulting in a sample size of roughly N≈10-20. Each selected cell was then observed for multiple beating sequences ($\pm$1s), over which the characteristic metrics are averaged. In our case, motile algae were selected on more general characteristics, as all cells with velocity higher than 25 μm/s are tracked for at least 10 s, of which a bigger sample size of N≈2000 cells is considered. The outcome of both studies could be different due to the differences between observation time and sample size.

- **Surfactant**. In the study performed by Qin et al., a surfactant (Tween-20) was used to give the fluid a lower surface tension to create the thin film (a bubble). Surfactants have a similarity to the phospholipid (hydrophile) molecules of the membrane lipid bilayer [56]. By adsorbing at the cell membrane, surfactants can

disrupt the normal structure of the lipid bilayer and reduce the surface tension. Tween-20 is a surfactant which is generally a gentle surfactant, which does not affect protein activity and is effective in increasing the solubility [56]. Tweens are routinely used to increase permeability of cell membranes. Hence, although the surfactant has especially an effect on the surface tension of a fluid, and thus influencing the liquid-air interface, it is also possible that it affects the interaction of the fluid with the cell body. This interaction might have a larger influence in a Newtonian fluid than in a viscoelastic fluid due to the presence of large polymers which are less sensitive to surfactant. If that is the case than this could explain the reduced velocity at high viscosities in Newtonian fluids in the study of Qin et al.

- **Healthiness of cells**. In our solution we found many non-motile cells or cells that we do not consider properly motile. Hence, we excluded many cell trajectories (approx. 80% of the trajectories), indicated in Figure 6.2 by the reducing number of considered cells (N) when segmentation criteria increases. This shows that many cells do not show very active motility. This might have influenced our results. For example, our cells might already work on maximum power and could be wrongly excluded from the analysis.

- **Solvent**. Qin et al. used water as a solvent, whereas our polymers are dissolved in Tris. Tris is a solution with nutrients and a buffer for a more stable pH. We do not know if this absence of nutrients has effect on the motility of available power of the motile cells. It is expected that the presence of Tris did not affect the rheological properties of the solution.

More research is needed to determine the effect of different experimental conditions such as quasi 2D, solvent, surfactant and healthiness on the motility behavior of the cells.

Recommendations for future work

To get more insight in the role of the above mentioned aspects, the following experiments are advised:

- Proceed on rheological work by introducing methods that are able to measure low levels of elastic properties at low viscosity and low levels of elasticity. Using tools which have a larger surface area could increase the signal-to-noise ratio which allows for more accuracy at lower concentrations of PAM.

- Conduct experiments in viscoelastic and Newtonian fluids in both a 2D and a 3D experimental setup, using motile cells extracted from the same cell culture to make sure that differences in culturing conditions does not play an important role. The influence of the air-liquid interface on the motile behaviour of the cells in viscoelastic fluids could provide new insights. Use the methods proposed by [17] of introducing a surfactant to create a quasi-2D plane. The influence of this surfactant on the rheological properties of the materials should be measured to see if this could be the origin of the differences.

- Analyse the interactions of motile cells with solid confinements in viscoelastic fluids. This will extend the work of Sudha [34], and Buchner et al. [49]. Solid confinements could provide different behaviours of the cells in viscoelastic fluids than air-liquid interfaces.
- Measure cell body orientation. When observing the beating frequency, observing the cell body orientation could provide more insights on the forward and backwards motion. Similar to the work by Qin et al. [17], the forwards and backwards motion can be observed for various levels of viscoelasticity. Observing possible behavioural changes without the limitations of a 2D confinement could show different results.

Conclusion

We measured the influence of Newtonian and viscoelasticity fluid on the motile behaviour of *Chlamydomonas Reinhardtii*. An in-house 3D microscopic setup, consisting of 4 LaVision sCMOS cameras was used to observe the unconstricted 3D motility of the cells in fluids of various levels of viscosity. We observed a constant velocity, pitch and beating frequency independent of the Deborah number, whereas a decreasing velocity, pitch and beating frequency was found in Newtonian fluids of equal viscosity. The radius of the helical motion showed to be independent of viscoelasticity or viscosity. Our results in a viscoelastic fluid differ from results of a quasi 2D study found in literature, whereas the results in a Newtonian fluid are comparable. This shows that experimental conditions are crucial when investigating behaviour of motile microorganisms, which makes the comparisons of results found by different experimental setups extremely difficult.

Bibliography

[1] Bhat, S., Jun, D., Paul, B., & Dahms, T. (2012). Viscoelasticity in biological systems: A special focus on microbes. *Viscoelasticity—From Theory to Biological Applications.: InTech*, 123–156.

[2] Harris, E. H. (2001). Chlamydomonas as a model organism. *Annual review of plant biology*, *52*(1), 363–406.

[3] Hall-Stoodley, L., Costerton, J. W., & Stoodley, P. (2004). Bacterial biofilms: From the natural environment to infectious diseases. *Nature reviews microbiology*, *2*(2), 95–108.

[4] Celli, J. P., Turner, B. S., Afdhal, N. H., Keates, S., Ghiran, I., Kelly, C. P., Ewoldt, R. H., McKinley, G. H., So, P., Erramilli, S. et al. (2009). Helicobacter pylori moves through mucus by reducing mucin viscoelasticity. *Proceedings of the National Academy of Sciences*, *106*(34), 14321–14326.

[5] Fauci, L. J., & Dillon, R. (2006). Biofluidmechanics of reproduction. *Annu. Rev. Fluid Mech.*, *38*, 371–394.

[6] Suarez, S. S., & Pacey, A. (2006). Sperm transport in the female reproductive tract. *Human reproduction update*, *12*(1), 23–37.

[7] Peyer, K. E., Zhang, L., & Nelson, B. J. (2013). Bio-inspired magnetic swimming microrobots for biomedical applications. *Nanoscale*, *5*(4), 1259–1272.

[8] Huang, H.-W., Sakar, M. S., Petruska, A. J., Pané, S., & Nelson, B. J. (2016). Soft micromachines with programmable motility and morphology. *Nature communications*, *7*(1), 1–10.

[9] Dreyfus, R., Baudry, J., Roper, M. L., Fermigier, M., Stone, H. A., & Bibette, J. (2005). Microscopic artificial swimmers. *Nature*, *437*(7060), 862–865.

[10] Ghosh, A., & Fischer, P. (2009). Controlled propulsion of artificial magnetic nanostructured propellers. *Nano letters*, *9*(6), 2243–2245.

[11] Griesbeck, C., Kobl, I., & Heitzer, M. (2006). Chlamydomonas reinhardtii. *Molecular biotechnology*, *34*(2), 213–223.

[12] Franklin, S. E., & Mayfield, S. P. (2004). Prospects for molecular farming in the green alga chlamydomonas reinhardtii. *Current opinion in plant biology*, *7*(2), 159–165.

[13] Kosourov, S., Tsygankov, A., Seibert, M., & Ghirardi, M. L. (2002). Sustained hydrogen photoproduction by chlamydomonas reinhardtii: Effects of culture parameters. *Biotechnology and bioengineering*, *78*(7), 731–740.

[14] Patteson, A., Gopinath, A., Goulian, M., & Arratia, P. (2015). Running and tumbling with e. coli in polymeric solutions. *Scientific reports*, *5*, 15761.

[15] Gabelle, J.-C., Jourdier, E., Licht, R., Ben Chaabane, F., Henaut, I., Morchain, J., & Augier, F. (2012). Impact of rheology on the mass transfer coefficient during the growth phase of trichoderma reesei in stirred bioreactors. *Chemical Engineering Science*, *75*, 408–417. https://doi.org/https://doi.org/10.1016/j.ces.2012.03.053

[16] Lauga, E. (2009). Life at high deborah number. *EPL (Europhysics Letters)*, *86*(6), 64001.

[17] Qin, B., Gopinath, A., Yang, J., Gollub, J. P., & Arratia, P. E. (2015). Flagellar kinematics and swimming of algal cells in viscoelastic fluids. *Scientific reports*, *5*, 9190.

[18] Demott, R. P., & Suarez, S. S. (1992). Hyperactivated sperm progress in the mouse oviduct. *Biology of reproduction*, *46*(5), 779–785.

[19] Lauga, E. (2007). Propulsion in a viscoelastic fluid. *Physics of Fluids*, *19*(8), 083104.

[20] Ojakian, G., & Katz, D. (1973). A simple technique for the measurement of swimming speed of chlamydomonas. *Experimental Cell Research*, *81*(2), 487–491.

[21] Ronkin, R. (1959). Motility and power dissipation in flagellated cells, especially chlamydomonas. *The Biological Bulletin*, *116*(2), 285–293.

[22] Drescher, K., Goldstein, R. E., Michel, N., Polin, M., & Tuval, I. (2010). Direct measurement of the flow field around swimming microorganisms. *Physical Review Letters*, *105*(16), 168101.

[23] Guasto, J. S., Johnson, K. A., & Gollub, J. P. (2010). Oscillatory flows induced by microorganisms swimming in two dimensions. *Physical review letters*, *105*(16), 168102.

[24] Crenshaw, H. C. (1996). A new look at locomotion in microorganisms: Rotating and translating. *American Zoologist*, *36*(6), 608–618.

[25] Allen, R. D. (1981). Motility. *The Journal of cell biology*, *91*(3), 148s–155s.

[26] Silflow, C. D., & Lefebvre, P. A. (2001). Assembly and motility of eukaryotic cilia and flagella. lessons from chlamydomonas reinhardtii. *Plant physiology*, *127*(4), 1500–1507.

[27] Lauga, E., & Powers, T. R. (2009). The hydrodynamics of swimming microorganisms. *Reports on Progress in Physics*, *72*(9), 096601.

[28] Purcell, E. M. (1977). Life at low reynolds number. *American journal of physics*, *45*(1), 3–11.

[29] Polin, M., Tuval, I., Drescher, K., Gollub, J. P., & Goldstein, R. E. (2009). Chlamydomonas swims with two "gears" in a eukaryotic version of run-and-tumble locomotion. *Science*, *325*(5939), 487–490.

[30] De Corato, M., Greco, F., & Maffettone, P. (2015). Locomotion of a microorganism in weakly viscoelastic liquids. *Physical Review E*, *92*(5), 053008.

[31] Crenshaw, H. C., Ciampaglio, C. N., & McHenry, M. (2000). Analysis of the three-dimensional trajectories of organisms: Estimates of velocity, curvature and torsion from positional information. *Journal of Experimental Biology*, *203*(6), 961–982.

[32] Li, C., Qin, B., Gopinath, A., Arratia, P. E., Thomases, B., & Guy, R. D. (2017). Flagellar swimming in viscoelastic fluids: Role of fluid elastic stress revealed by simulations based on experimental data. *Journal of The Royal Society Interface*, *14*(135), 20170289.

[33] Muller, K. (2016). Collective swimming dynamics of motile micro-algae. cell-wall and cell-cell interactions.

[34] Sudha, A. (2019). Influence of viscoelasticity on the kinematics and hydrodynamic interactions of c.reinhardtii.

[35] Tanner, R. I. (2000). *Engineering rheology* (Vol. 52). OUP Oxford.

[36] Schramm, G. et al. (1994). *A practical approach to rheology and rheometry*. Haake Karlsruhe.

[37] Poole, R. (2012). The deborah and weissenberg numbers. *Rheology Bulletin*, *53*(2), 32–39.

[38] Internal structures of samples and shear-thinning behavior :: Anton paar wiki. (n.d.). https://wiki.anton-paar.com/en/internal-structures-of-samples-and-shear-thinning-behavior/

[39] Baird, D. G. (2011). *Flow behavior of viscoelastic fluids*. https://doi.org/10.1036/1097-8542.YB110147

[40] Paar, A. (2020). *Internal structures of samples and shear-thinning behavior*. Retrieved September 30, 2020, from https://wiki.anton-paar.com/nl-en/internal-structures-of-samples-and-shear-thinning-behavior/

[41] Heemskerk, J., Rosmalen, R., Janssen-Van, R., Holtslag, R., & Teeuw, D. (1984). Quantification of viscoelastic effects of polyacrylamide solutions. *SPE Enhanced Oil Recovery Symposium*.

[42] Rheometer. (n.d.). https://www.anton-paar.com/nl-en/products/group/rheometer/

[43] Qian, B., Jiang, H., Gagnon, D. A., Breuer, K. S., & Powers, T. R. (2009). Minimal model for synchronization induced by hydrodynamic interactions. *Physical Review E*, *80*(6), 061919.

[44] Amplitude sweeps :: Anton paar wiki. (n.d.). https://wiki.anton-paar.com/nl-en/amplitude-sweeps/

[45] Mezger, T. (2006). *The rheology handbook*. Vincentz Network. https://books.google.nl/books?id=W-0gAAAACAAJ

[46] Quaranta, G., Aubin-Tam, M.-E., & Tam, D. (2015). Hydrodynamics versus intracellular coupling in the synchronization of eukaryotic flagella. *Physical review letters*, *115*(23), 238101.

[47] Fábregas, J., Vázquez, V., Cabezas, B., & Otero, A. (1993). Tris not only controls the ph in microalgal cultures, but also feeds bacteria. *Journal of applied phycology*, *5*(5), 543–545.

[48] Kim, H., Westerweel, J., & Elsinga, G. E. (2012). Comparison of tomo-piv and 3d-ptv for microfluidic flows. *Measurement Science and Technology*, *24*(2), 024007.

[49] Buchner, A.-J., Muller, K., Mehmood, J., & Tam, D. (2021). Hopping trajectories due to long-range interactions determine surface accumulation of microalgae. *Proceedings of the National Academy of Sciences*, *118*(20).

[50] Kim, H., Große, S., Elsinga, G. E., & Westerweel, J. (2011). Full 3d-3c velocity measurement inside a liquid immersion droplet. *Experiments in fluids*, *51*(2), 395–405.

[51] Sweryda-Krawiec, B., Devaraj, H., Jacob, G., & Hickman, J. J. (2004). A new interpretation of serum albumin surface passivation. *Langmuir*, *20*(6), 2054–2056.

[52] Adrian, L., Adrian, R. J., & Westerweel, J. (2011). *Particle image velocimetry*. Cambridge university press.

[53] Crenshaw, H. C. (1989). Kinematics of helical motion of microorganisms capable of motion with four degrees of freedom. *Biophysical journal*, *56*(5), 1029–1035.

[54] Yazdi, S., Ardekani, A. M., & Borhan, A. (2014). Locomotion of microorganisms near a no-slip boundary in a viscoelastic fluid. *Physical review E*, *90*(4), 043002.

[55] Li, G.-J., Karimi, A., & Ardekani, A. M. (2014). Effect of solid boundaries on swimming dynamics of microorganisms in a viscoelastic fluid. *Rheologica acta*, *53*(12), 911–926.

[56] Johnson, M. (2021). Detergents: Triton x-100, tween-20, and more. https://www.labome.com/method/Detergents-Triton-X-100-Tween-20-and-More.html

A | Appendix

A.1 Velocity histograms for all data sets

This appendix provides velocity histograms of all experimental recordings of Culture 1 and culture 2 (Baseline Tris, Viscoelastic, and Newtonian). N represents the total number of trajectories that are observed during the recording.

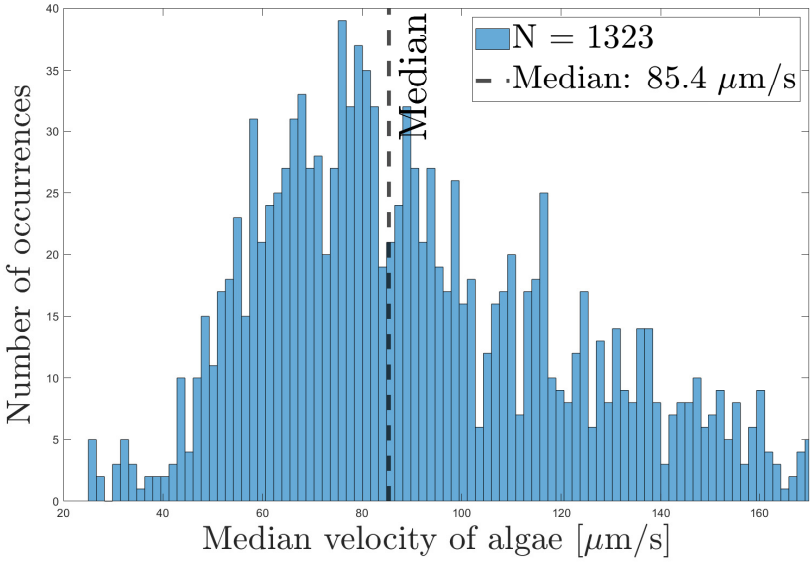

Figure A.1: Velocity histogram for Baseline Tris (Culture 1).

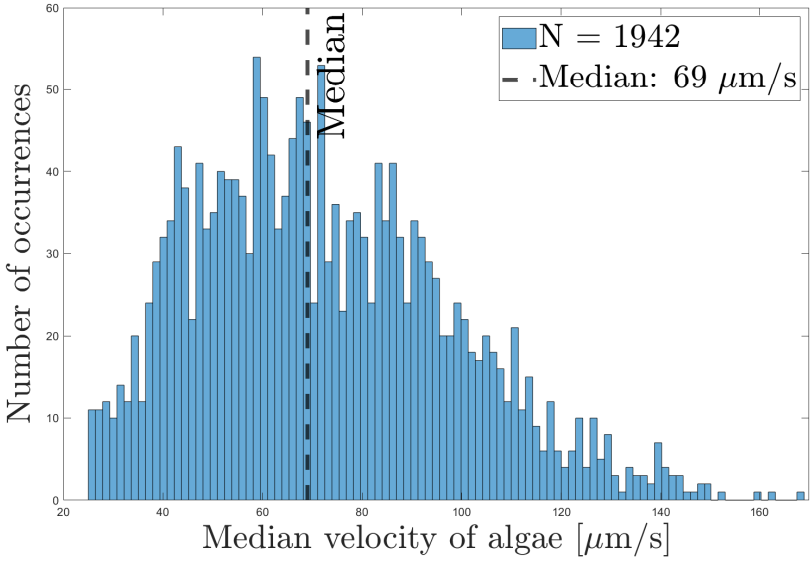

Figure A.2: Velocity histogram for Baseline 1 Tris (Culture 2).

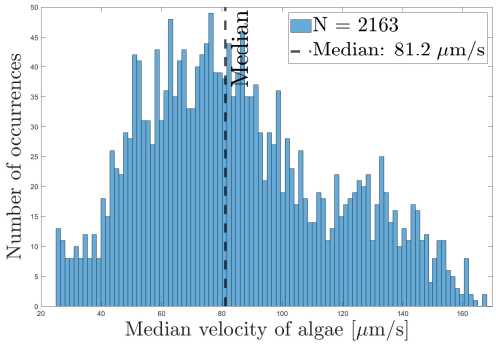

(a) Data set 1: Viscoelastic (PAM 20 ppm).

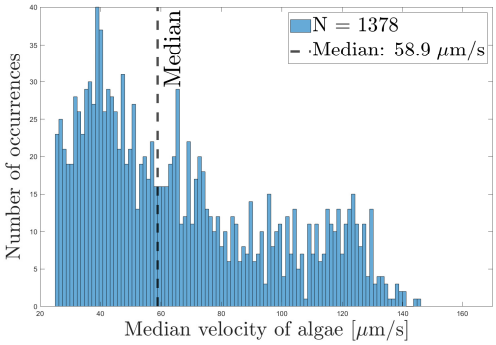

(b) Data set 1: Newtonian (Ficoll 4%).

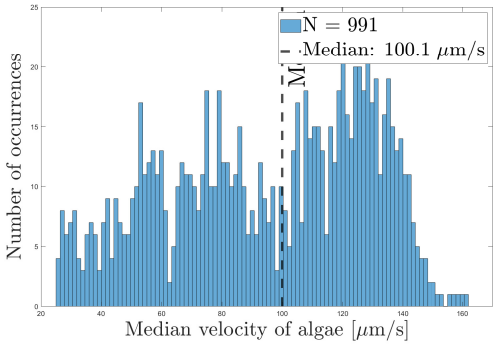

(c) Data set 2: Viscoelastic (PAM 40ppm).

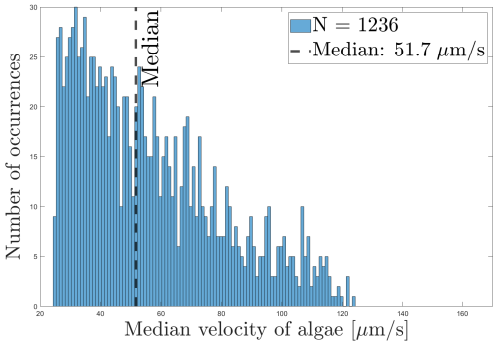

(d) Data set 2: Newtonian (Ficoll 5.5%).

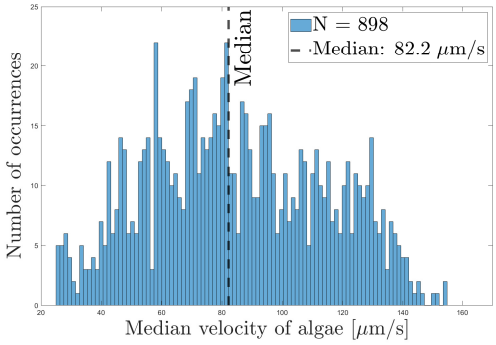

(e) Data set 3: Viscoelastic (PAM 60ppm).

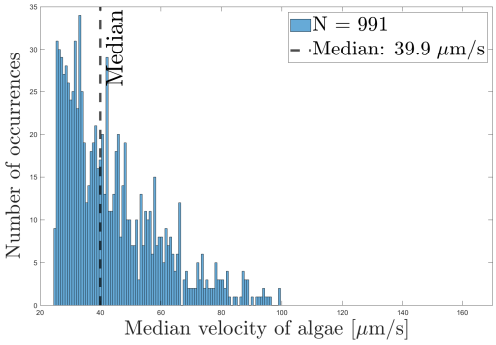

(f) Data set 3: Newtonian (Ficoll 6.5%).

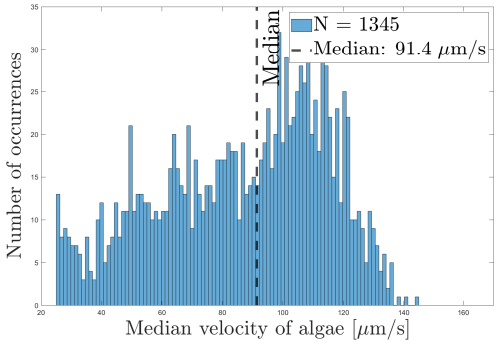

(g) Data set 4: Viscoelastic (PAM 80ppm).

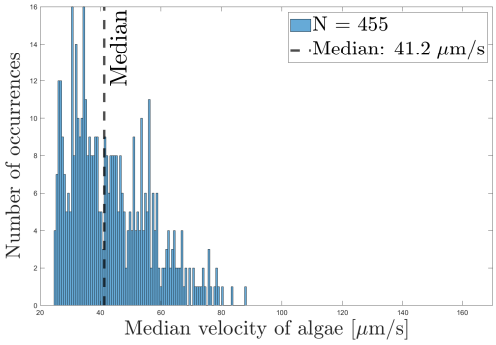

(h) Data set 4: Newtonian (Ficoll 8%).

Figure A.3: Velocity histograms for Culture 1 (February 23rd).

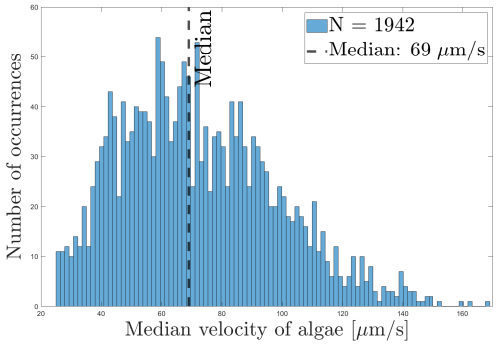

(a) Baseline 2 (Tris).

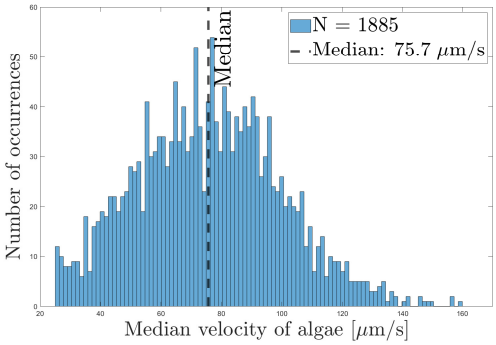

(b) Baseline 3 (Tris).

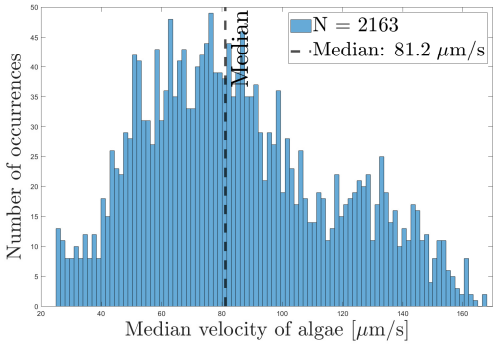

(c) Data set 1: Viscoelastic (PAM 20ppm).

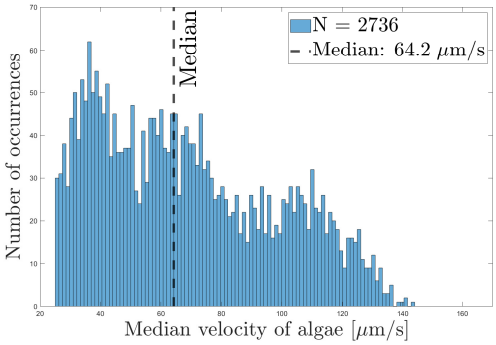

(d) Data set 1: Newtonian (Ficoll 4%).

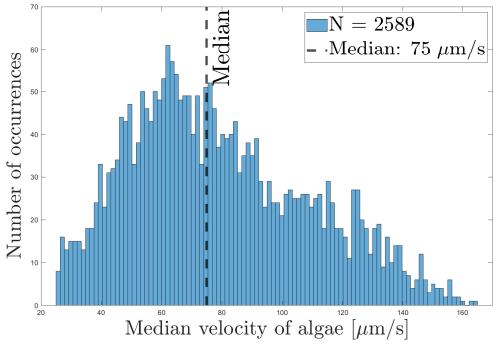

(e) Data set 2: Viscoelastic (PAM 40ppm).

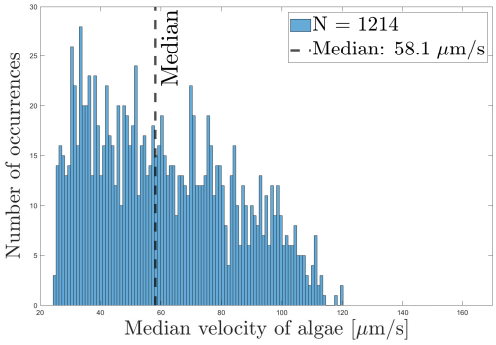

(f) Data set 2: Newtonian (Ficoll 5.5%).

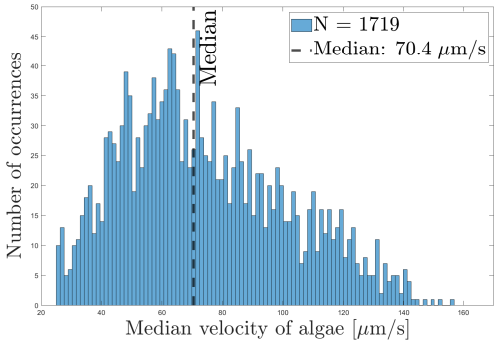

(g) Data set 3: Viscoelastic (PAM 60ppm).

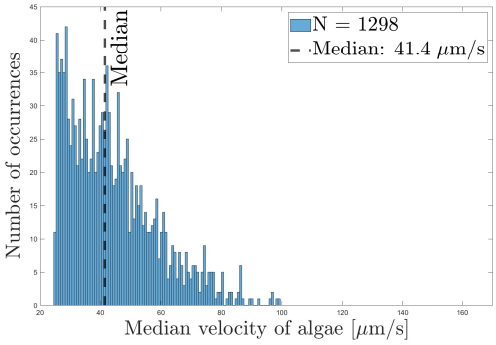

(h) Data set 3: Newtonian (Ficoll 6.5%).

Figure A.4: Velocity histograms for Culture 2 (February 26$^{\text{th}}$).

A.2 Joint distributions of helical motion for all data sets

This appendix provides joint histograms of the metrics describing the helical motion, Culture 1 (Figures A.5, A.6, and A.7) and Culture 2 (Figure A.8, A.9, and A.10).

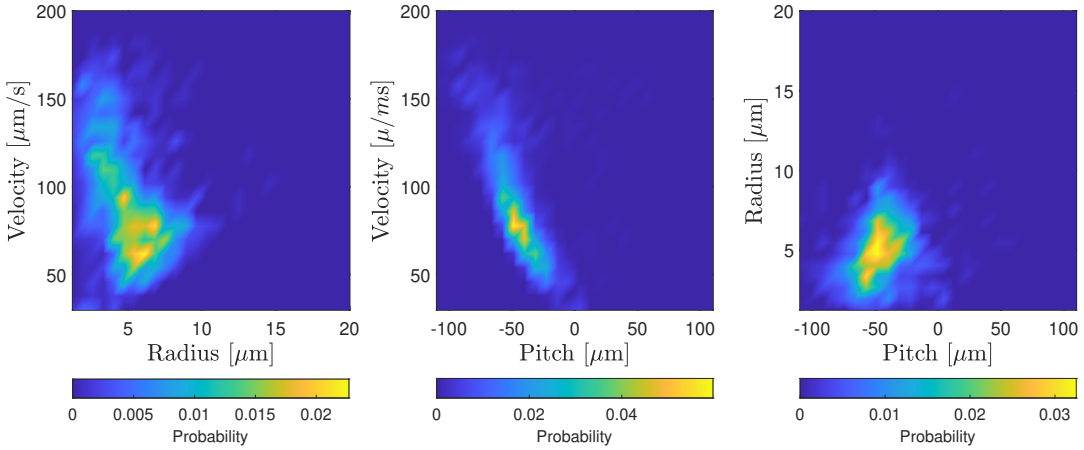

(a) Baseline: Joint histograms of velocity, pitch, and radius in Tris.

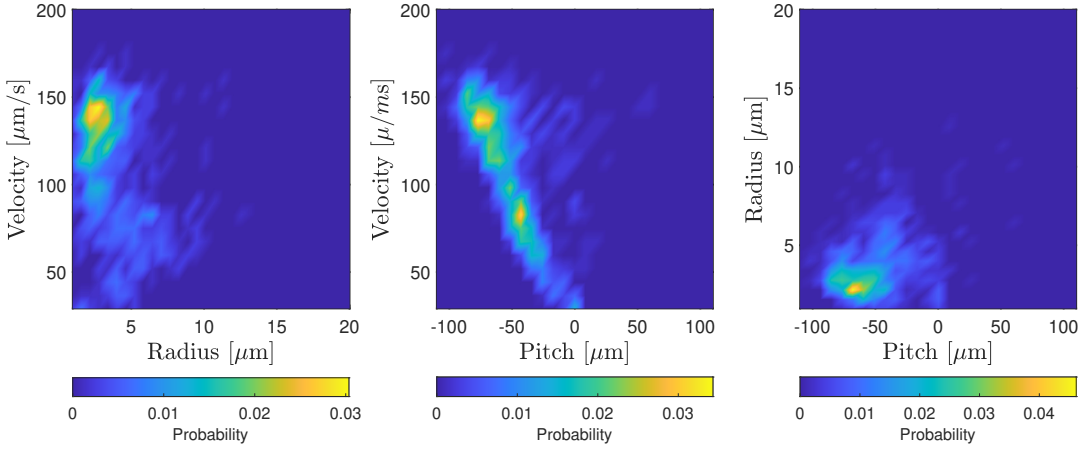

(b) Data set 1: Joint histograms of velocity, pitch, and radius in viscoelastic.

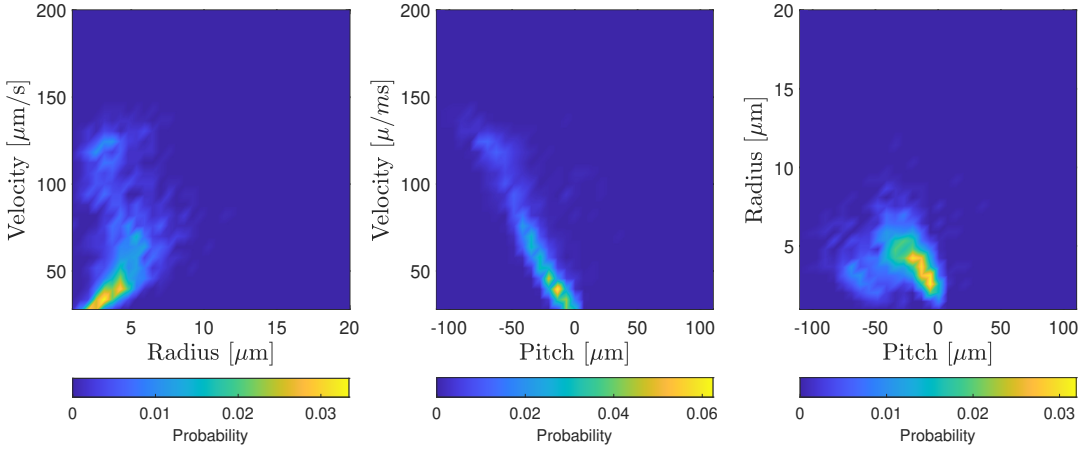

(c) Data set 1: Joint histograms of velocity, pitch, and radius in Newtonian.

Figure A.5: Joint histograms for the metrics describing the helical motion (1). (Culture 1)

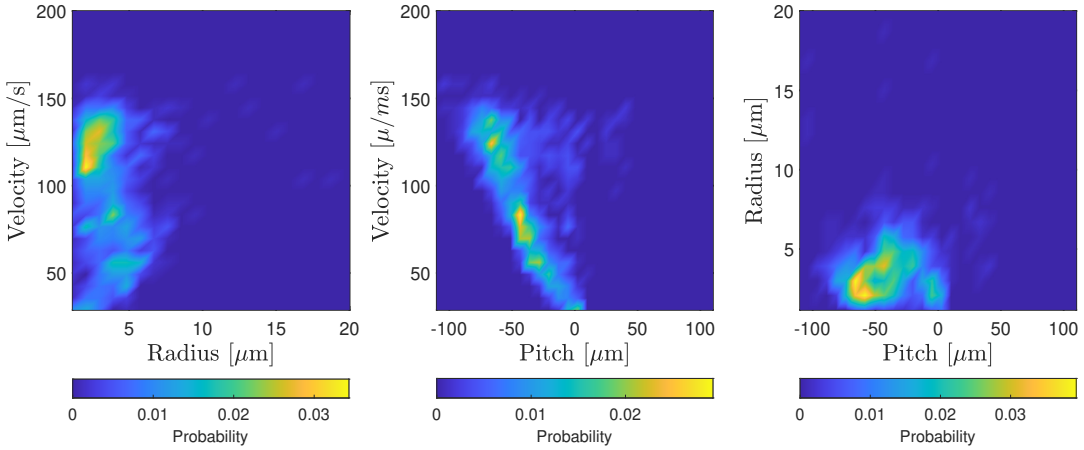

(a) Data set 2: Joint histograms of velocity, pitch, and radius in viscoelastic.

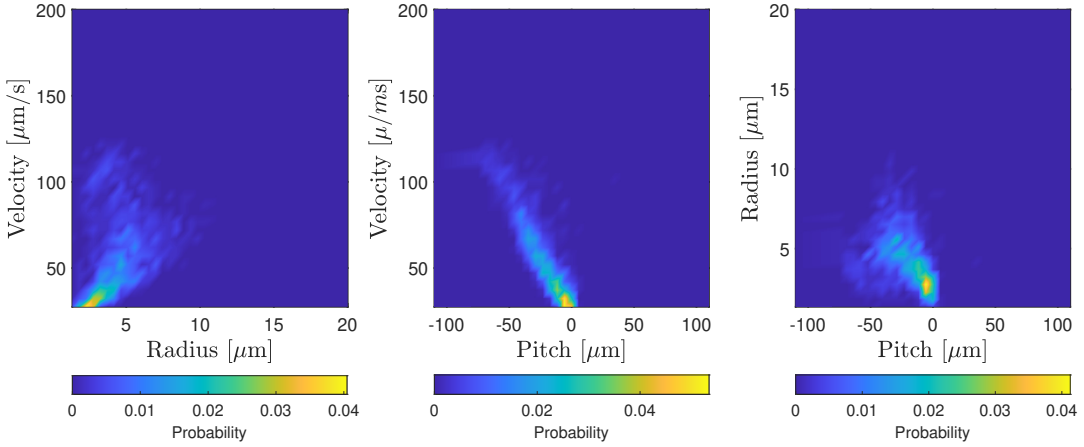

(b) Data set 2: Joint histograms of velocity, pitch, and radius in Newtonian.

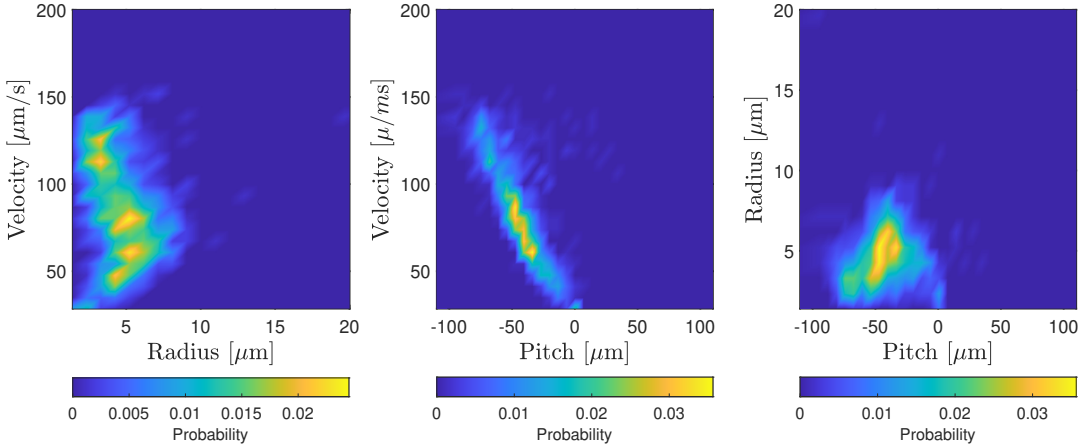

(c) Data set 3: Joint histograms of velocity, pitch, and radius viscoelastic.

Figure A.6: Joint histograms for the metrics describing the helical motion (2). (Culture 1)

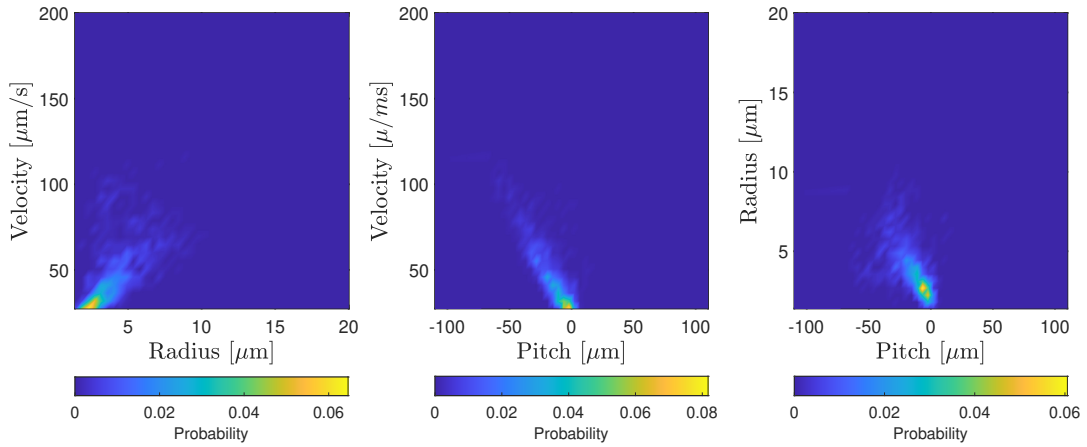

(a) Data set 3: Joint histograms of velocity, pitch, and radius in Newtonian.

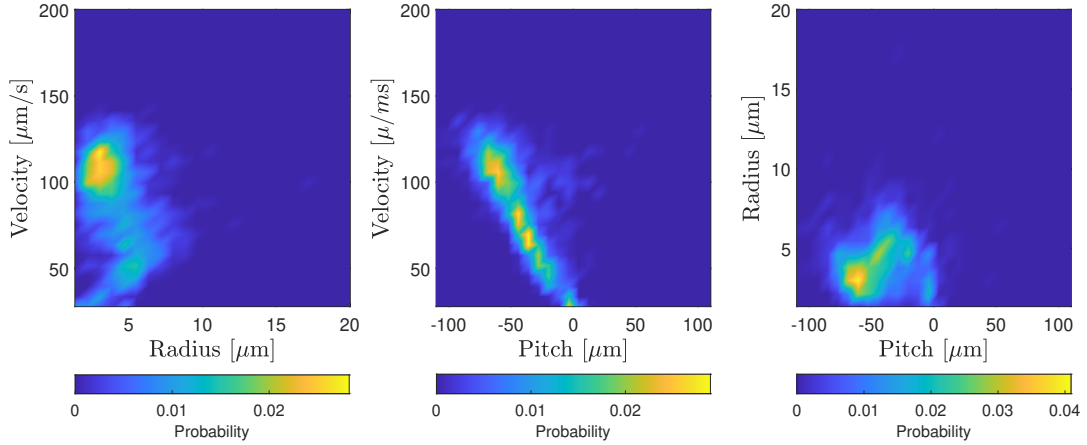

(b) Data set 4: Joint histograms of velocity, pitch, and radius in viscoelastic.

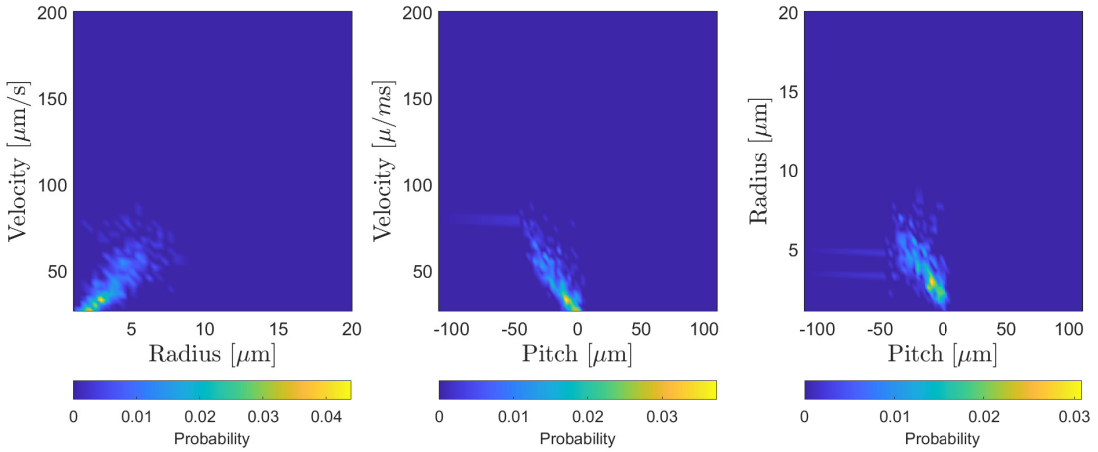

(c) Data set 4: Joint histograms of velocity, pitch, and radius in Newtonian.

Figure A.7: Joint histograms for the metrics describing the helical motion (3). (Culture 1)

Culture 2:

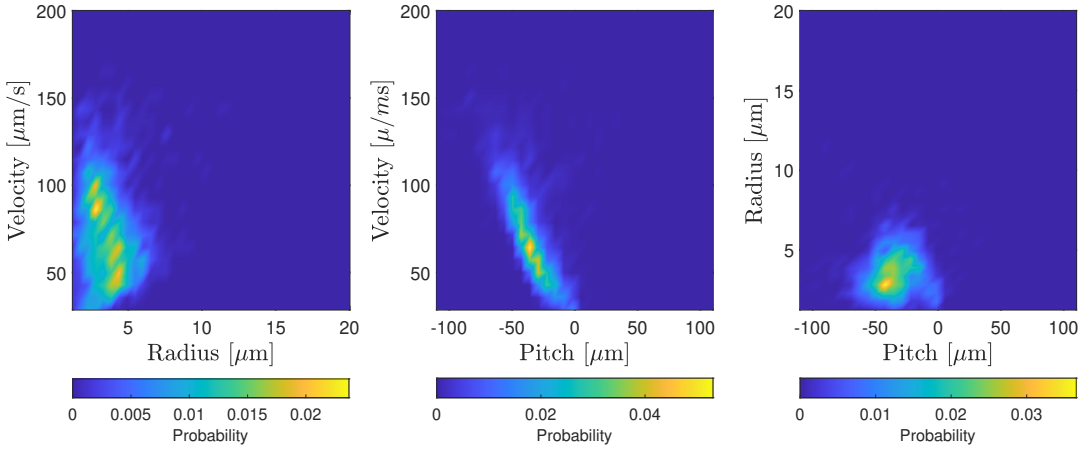

(a) Baseline: Joint histograms of velocity, pitch, and radius in Tris.

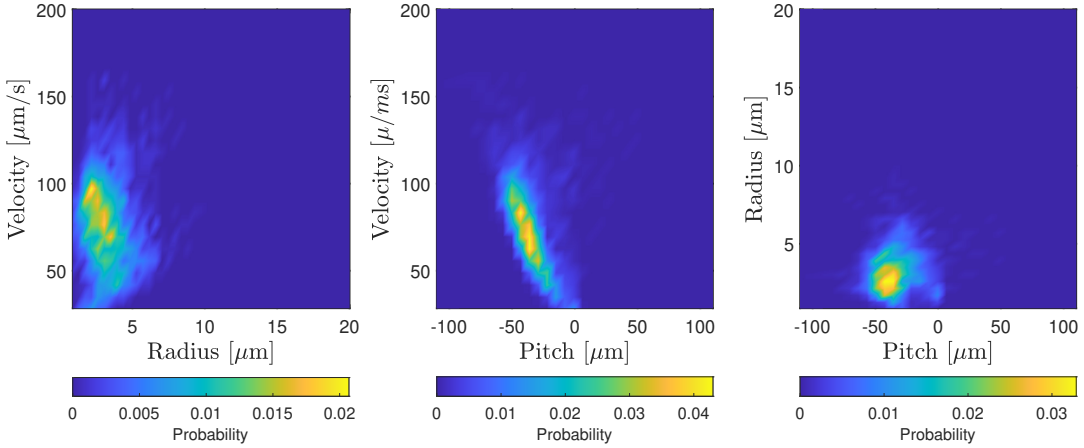

(b) Baseline: Joint histograms of velocity, pitch, and radius in Tris.

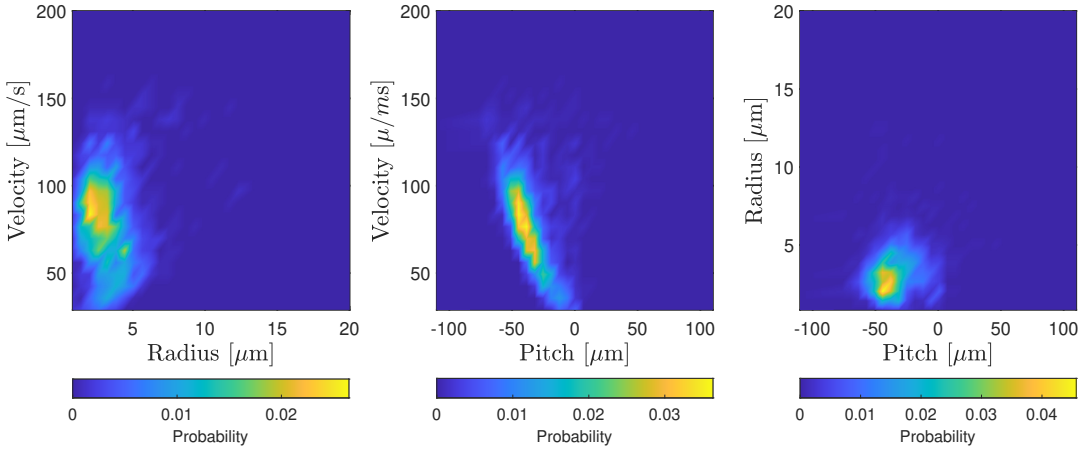

(c) Baseline: Joint histograms of velocity, pitch, and radius in Tris.

Figure A.8: Joint histograms for the metrics describing the helical motion (1). (Culture 2)

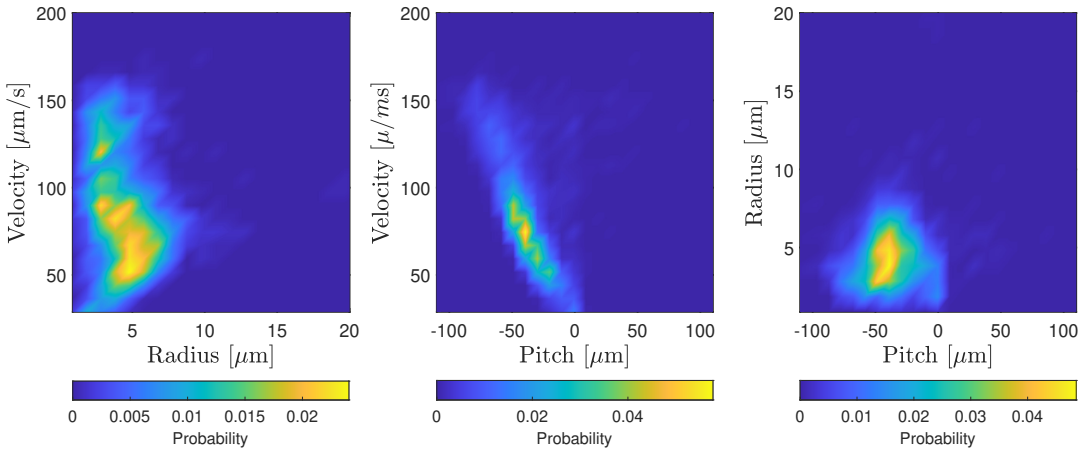

(a) Data set 1: Joint histograms of velocity, pitch, and radius in viscoelastic (Culture 2).

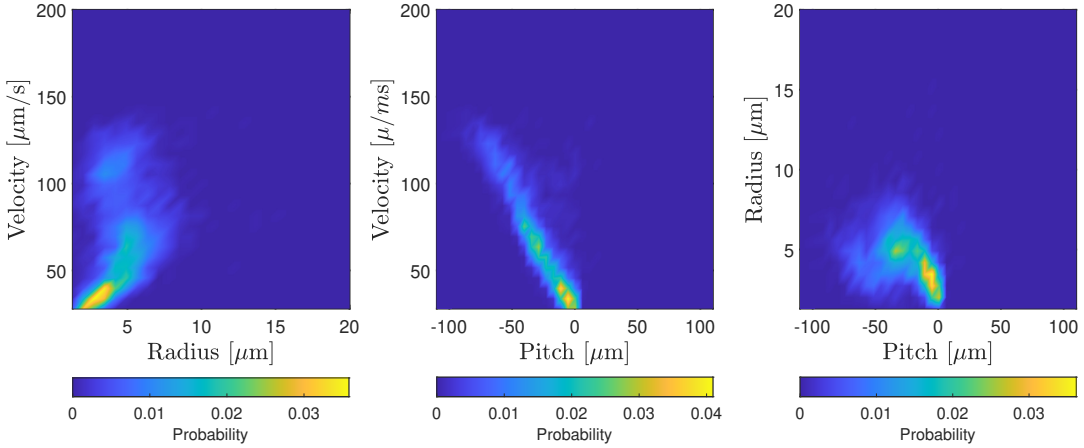

(b) Data set 1: Joint histograms of velocity, pitch, and radius in Newtonian.

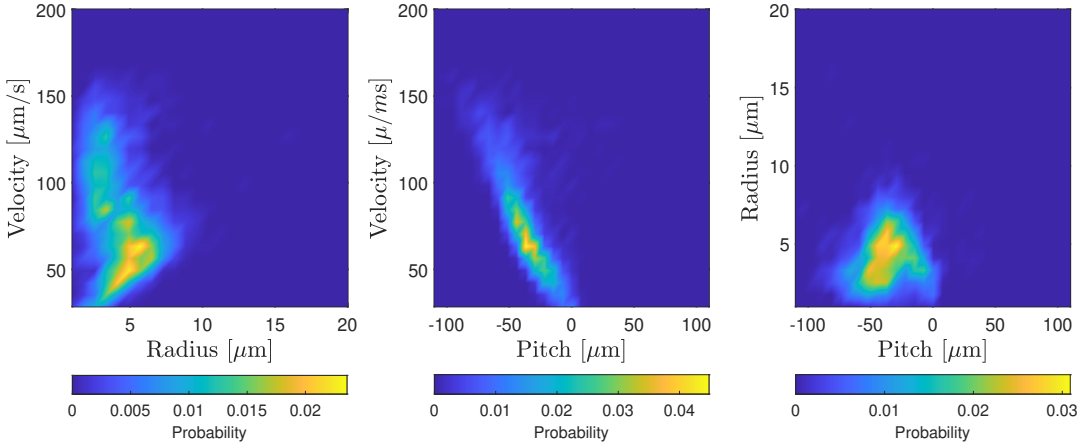

(c) Data set 2: Joint histograms of velocity, pitch, and radius in viscoelastic.

Figure A.9: Joint histograms for the metrics describing the helical motion (2). (Culture 2)

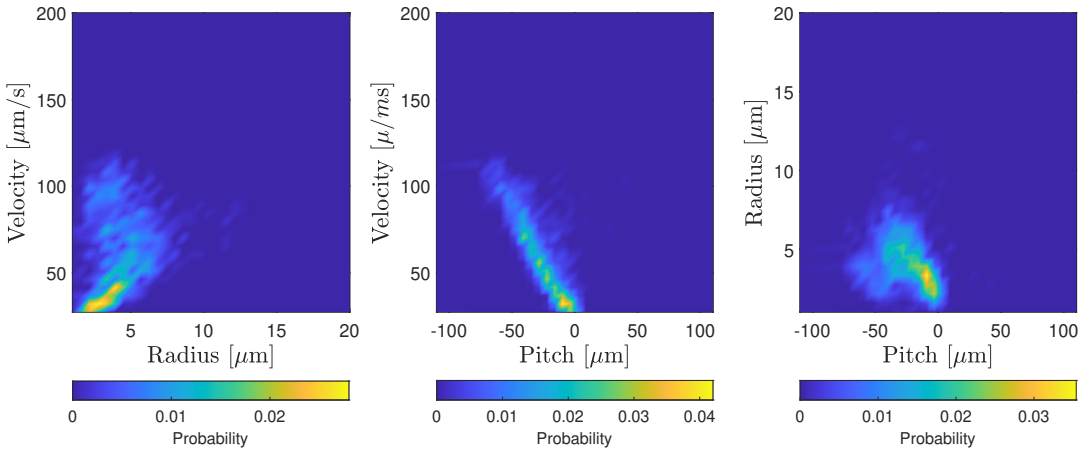

(a) Data set 2: Joint histograms of velocity, pitch, and radius in Newtonian.

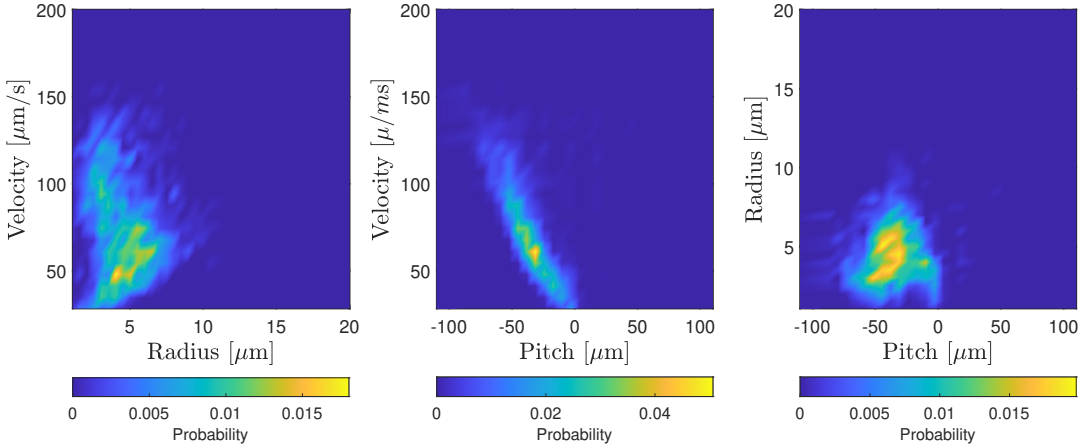

(b) Data set 3: Joint histograms of velocity, pitch, and radius in.

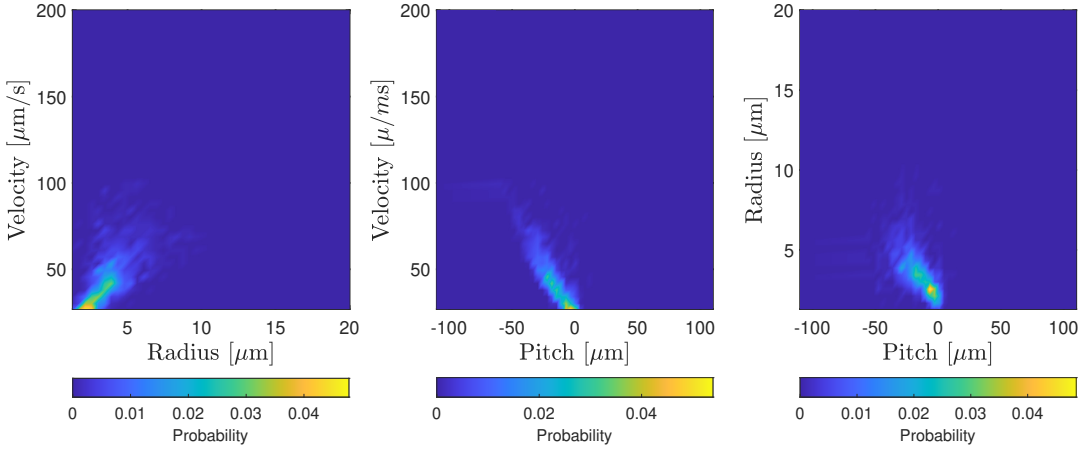

(c) Data set 3: Joint histograms of velocity, pitch, and radius in Newtonian.

Figure A.10: Joint histograms for the metrics describing the helical motion (3). (Culture 2)

A.3 Beating frequency plots for all data sets

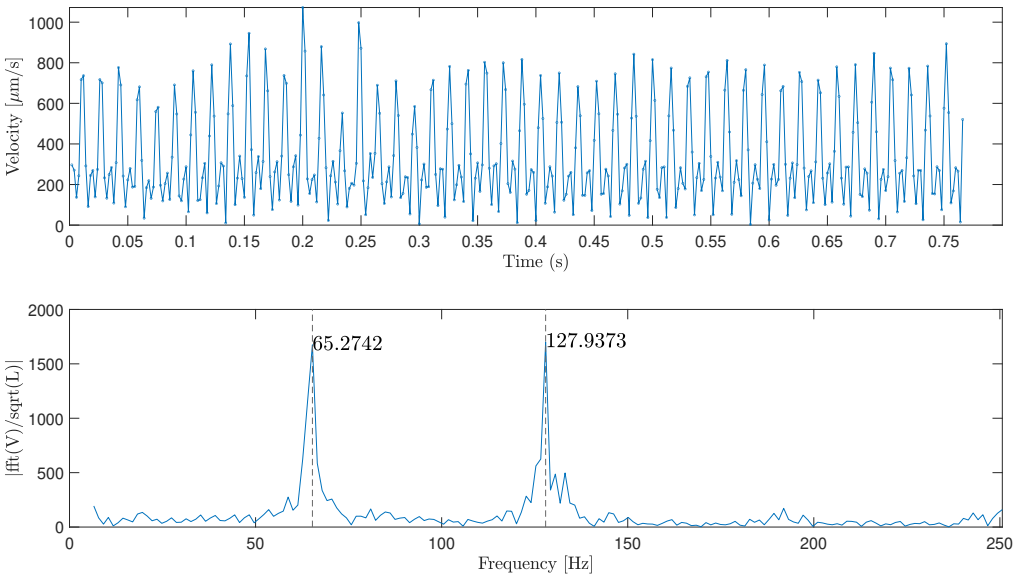

Figure A.11: Magnitude of the velocity signal for a cell that is motile (top) with the frequency spectrum (bottom) in the baseline of Tris minimal.

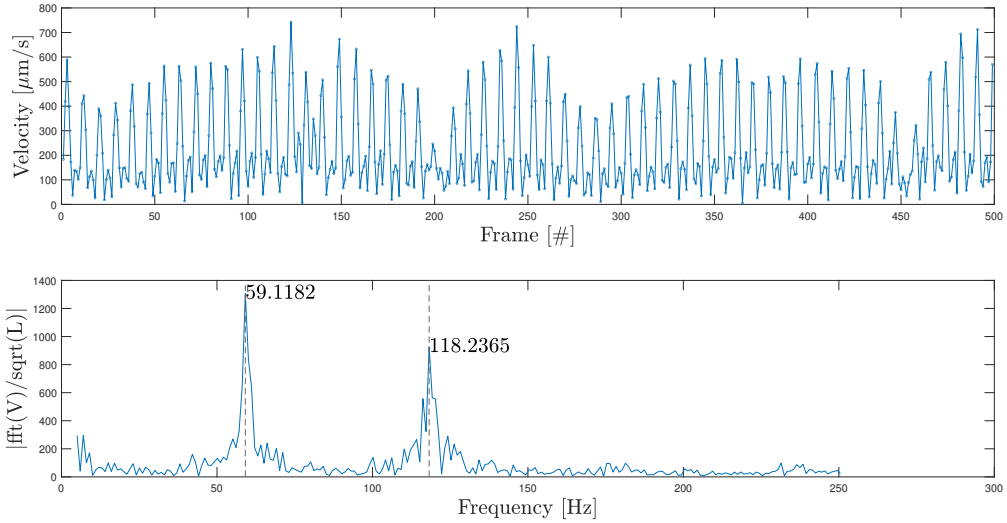

Figure A.12: Magnitude of the velocity signal for a cell that is motile (top) with the frequency spectrum (bottom) in PAM 20 ppm.

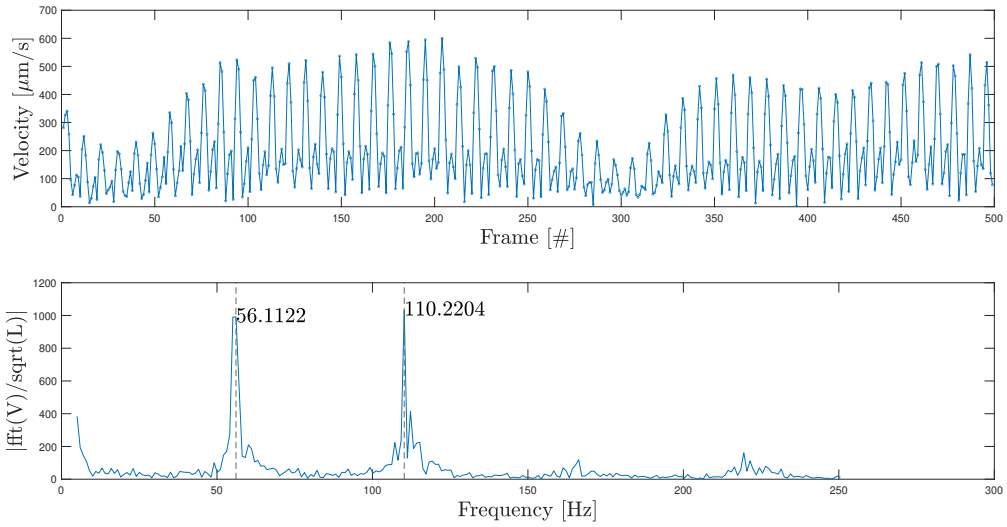

Figure A.13: Magnitude of the velocity signal for a cell that is motile (top) with the frequency spectrum (bottom) in PAM 40 ppm.

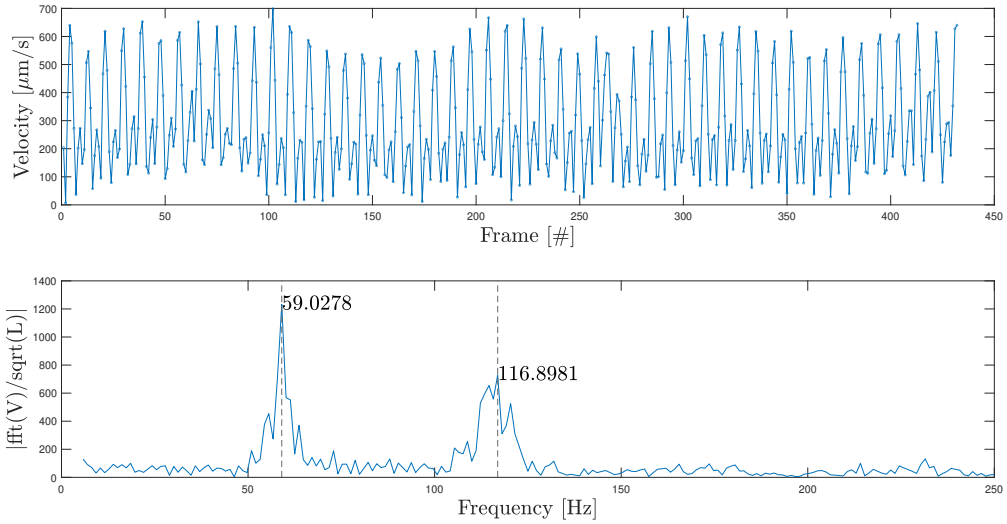

Figure A.14: Magnitude of the velocity signal for a cell that is motile (top) with the frequency spectrum (bottom) in PAM 60 ppm.

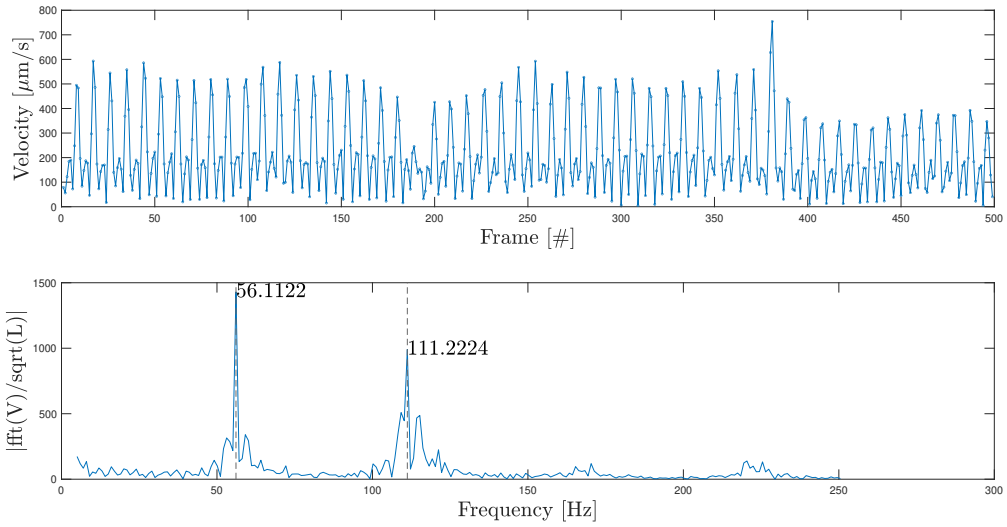

Figure A.15: Magnitude of the velocity signal for a cell that is motile (top) with the frequency spectrum (bottom) in PAM 80 ppm.

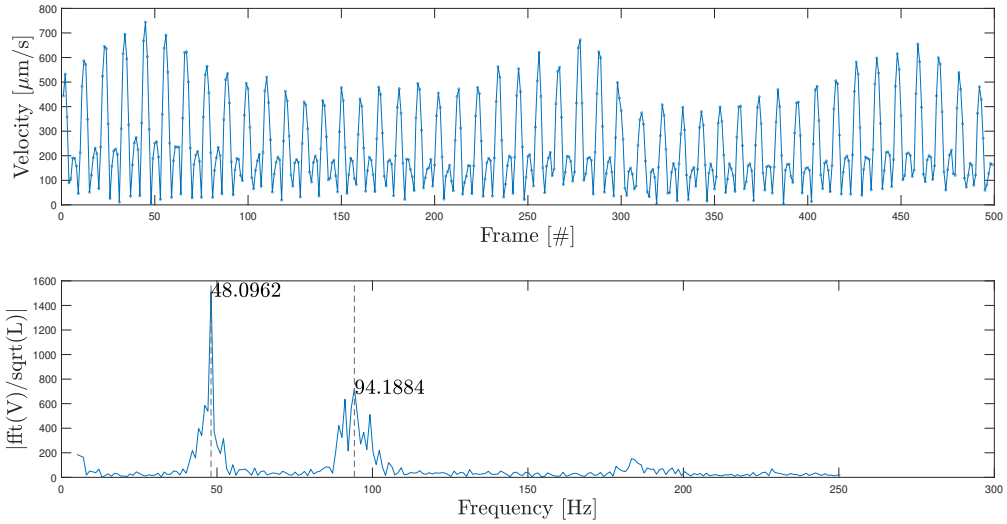

Figure A.16: Magnitude of the velocity signal for a cell that is motile (top) with the frequency spectrum (bottom) in Ficoll 4.0% wt.

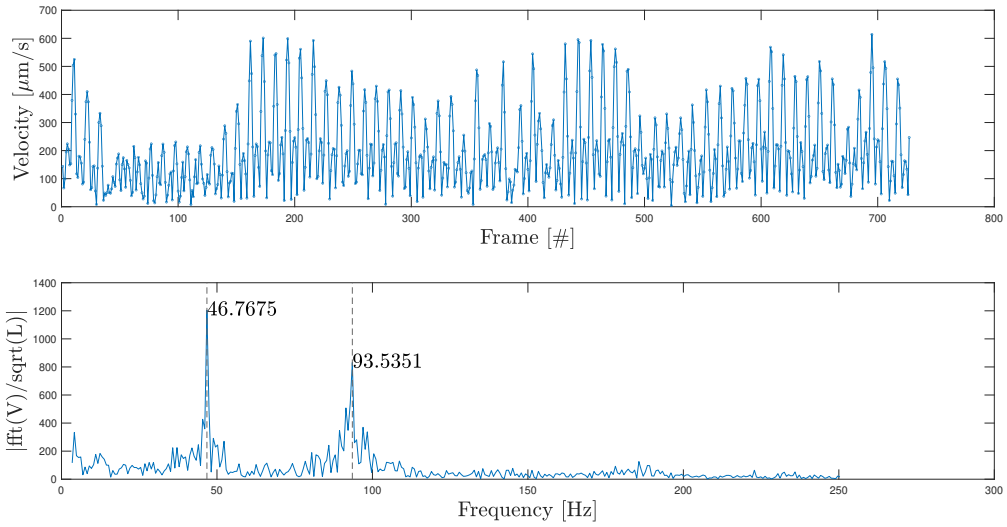

Figure A.17: Magnitude of the velocity signal for a cell that is motile (top) with the frequency spectrum (bottom) in Ficoll 5.5% wt.

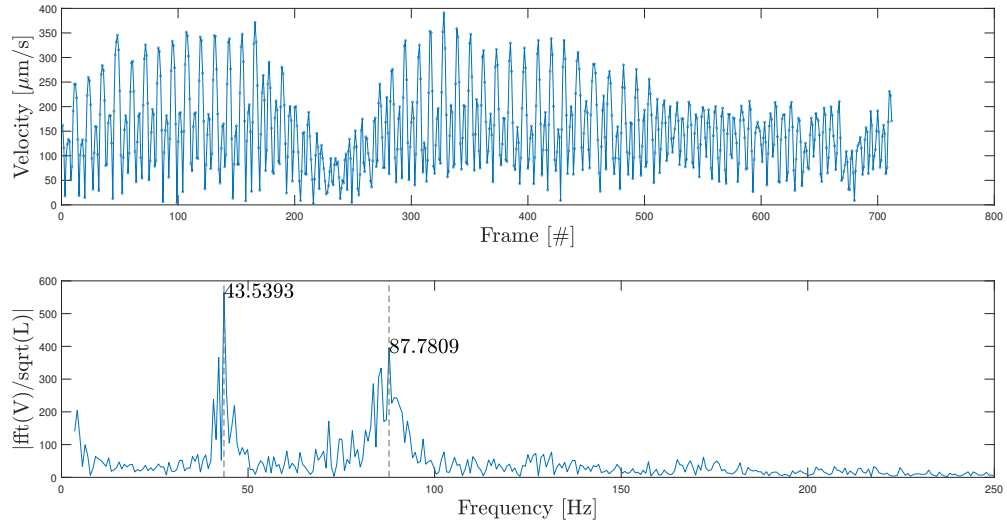

Figure A.18: Magnitude of the velocity signal for a cell that is motile (top) with the frequency spectrum (bottom) in Ficoll 6.5% wt.

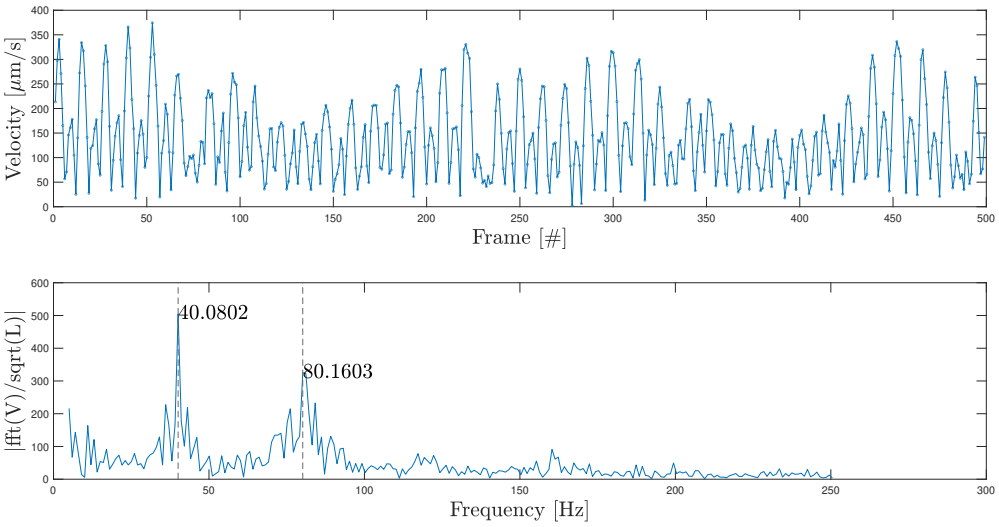

Figure A.19: Magnitude of the velocity signal for a cell that is motile (top) with the frequency spectrum (bottom) in Ficoll 8.0% wt.